UNIVERSITÄT ULM

INSTITUT FÜR THEORETISCHE PHYSIK

Tabletop Tests of Quantum Gravity

Dissertation to obtain the degree Dr. rer. nat. of the Faculty of Natural Sciences

of the University of Ulm

submitted by

Shreya Prasanna Kumar

from Bangalore, India

Ulm, June 2020

Dissertation

Title: Tabletop Tests of Quantum Gravity

Day of promotion: 25 November 2020

Dean of Faculty: Prof. Dr. Thorsten Bernhardt

First reviewer: Prof. Dr. Martin B. Plenio

Second reviewer: Prof. Dr. Fedor Jelezko

Abstract

Models of quantum gravity imply a fundamental revision of our description of position and momentum. This revision manifests in modifications of the canonical commutation relations. Experimental tests of such modifications remain an outstanding challenge. In recent years, tabletop experiments to test for quantum gravity have been proposed. This thesis address two main challenges to such experiments.

The first contribution is related to the recent proposal to use cavity-optomechanical systems to test for these deformations [Nat. Phys. 8, 393-397 (2012)]. Improving the achievable precision of such devices represents a major challenge that we address with our present work. More specifically, we develop sophisticated paths in phase-space of such optomechanical systems to obtain significantly improved accuracy and precision under contributions from higher-order corrections to the optomechanical Hamiltonian. An accurate estimate of the required number of experimental runs is presented based on a rigorous error analysis that accounts for uncertainty in mean photon number, which can arise from classical fluctuations or from quantum shot noise in measurements. Furthermore, we propose a method to increase precision by using squeezed states of light. Finally, we demonstrate the robustness of our scheme to experimental imperfection, thereby improving the prospects of carrying out tests of quantum gravity with near-future optomechanical

technology.

The second contribution is based on the fact that the deformations in the canonical commutator scale with the mass of test particles, which motivates experiments using macroscopic composite particles. Here we consider a challenge to such tests, namely that quantum gravity corrections of canonical commutation relations are expected to be suppressed with increasing number of constituent particles. Since the precise scaling of this suppression is unknown, it needs to be bounded experimentally and explicitly incorporated into rigorous analyses of quantum gravity tests. We analyse this scaling based on concrete experiments involving macroscopic pendula and provide tight bounds that exceed those of current experiments based on quantum mechanical oscillators. Furthermore, we discuss possible experiments that promise even stronger bounds.

Thus, the work in this thesis brings rigorous and well-controlled tests of quantum gravity closer to reality.

Acknowledgements

First and foremost, I thank Prof. Dr. Martin Plenio for being a great supervisor. I appreciate him giving me the opportunity to work on the many interesting problems that made into this thesis. I have learnt so much from the many stimulating discussions with him, especially how to think analytically and attack problems from many different perspectives. Apart from the scientific side, I thank him also for being kind and supportive and always being enthusiastically present for discussions. He really brings out the best in his students!

I am also grateful to both Martin Plenio and Susana Huelga for cultivating a very positive and helpful working environment in the group. I will fondly remember the enthusiastic discussions, both academic and beyond, with many group members during my time at Ulm. Thank you to Mark Mitchison for many fruitful discussion on Bose Einstein condensates, which I really enjoyed working with him on. I also thank my friends and colleagues Mehdi Abdi, Meisam Aghtar, Jorge Casanova, Felipe Caycedo, Qiong Chen, Francesco Cosco, Sandro Donadi, Benjamin Desef, Dario Egloff, Pelayo Fernandez Acebal, Jan Haase, Milan Holzäpfel, Myung-Joong Hwang, Theodore Illias, Alexandre Le Boité, Andreas Lemmer, Korbinian Kottmann, Oliver Marty, Fabio Mascherpa, Andrea Mattioni, Alexander Nüßeler, Ricardo Puebla Antunes, Ewa Pasgreta, Julen Simon Pedernales, Joachim Rosskopf, Mor Schwartz, Ilai Schwarz, Andrea Smirne, Alejandro Somoza Marquez, Kirill

Streltsov, Marit Steiner, Thomas Theurer, Benedikt Tratzmiller, Zhenyu Wang and Raphael Weber for fun discussions and a pleasant working environment. Special thanks are in order to Gerlinde Walliser, for being the superhero of this group, and for always going above and beyond what was needed!

And finally, the PhD would not have been possible without the support and warmth of my family. I thank Ish for not only his unwavering love and support, but also for fun physics discussions through the highs and lows of the PhD. I am also grateful to Amma and Appa for instilling in me the love for learning and always being there for me. Thank you to Mama and Papa for the constant support and inspiration and for cheering me onwards and upwards. This thesis could not have been possible without you all!

Contents

List of Figures

List of Tables

Thesis content previously published

The results presented in this thesis are published in peer-reviewed journals or are under peer-review. The relevant articles or pre-prints are:

[1] S. P. Kumar and M. B. Plenio, Quantum-optical tests of Planck-scale physics, *Phys. Rev. A*, 97(6), 63855, 2018.

[2] S. P. Kumar and M. B. Plenio, On quantum gravity tests with composite particles, *Nat. Commun.*, 11(1), 3900, 2020.

The following portions are based on Ref. [1] with minor grammatical and structural modifications: large portions of Chapter 1, Section 2.1 of Chapter 2, all of Chapters 3 and 4 and some parts of Chapter 7.

The portions based on Ref. [2] with similar grammatical and structural modifications are: large portions of Chapter 1, Sections 2.2 and 2.3 of Chapter 2, all of Chapters 5 and 6 and some parts of Chapter 7.

Chapter 1

Introduction

One of the most important open problems in physics is the unification of quantum mechanics and gravity [5]. However, quantising gravity is not straightforward and despite continuous efforts in promising lines of research like string theory and loop quantum gravity, no clear-cut theory has emerged. One of the major challenges to developing such a theory is the lack of experimental evidence. This thesis contributes towards addressing this challenge.

Since there is no one widely-accepted theory, many phenomenological models of quantum gravity have been proposed. One feature of these models is the existence of a minimum length scale of the order of Planck length [6]. Detecting the existence of such a minimal length scale is one of the main goals of the field, but has so far eluded experimental verification. Direct detection of the Planck length, $1.6 \times 10^{-35}\,\mathrm{m}$, is infeasible with current and foreseeable technology because the effects of quantum gravity are expected to become directly relevant only at energies of the order of Planck energy which is $E_p = 1.2 \times 10^{19}\,\mathrm{GeV}$. This is 15 orders of magnitude larger than the energy scales achievable in the Large Hadron Collider today. Hence, it seems unlikely that these energy scales will be achieved in the near future and we must resort to indirect methods. So in order to experimentally probe quantum

gravity, we must rely on indirect tests of signatures of Planck length.

One class of indirect tests of a minimal length scale relies on observing distant astronomical events for cosmological consequences of these effects [7,8]. For instance, quantum gravity predicts that the velocity of photons depends on their energies. Thus, photons travelling from distant gamma ray bursts over cosmological distances will incur a detectable spread in their arrival times. This approach, however, suffers from challenges as it includes model-dependent assumptions, for example about the evolution of the objects that emit them and about the perturbations due to billions of light years of interstellar medium traversed by the gamma-rays. This lack of control of the experimental conditions is compounded by the limitations to possible improvements to the precision of such experiments due to limitations on the distance to observable gamma-ray bursts and the maximal energy of the gamma-rays. This motivates looking for an alternative route to detecting Planck-scale effects, which allow, at least in principle, for improving the sensitivity of the experiment with advancing technology.

1.1 Minimal length scale by means of deformed commutators

One such route involves using table-top experiments that can be controlled precisely, for example, those based on optical, optomechanical and matter-wave devices [3, 4, 9–11]. The underlying concept on which several such experiments rely upon is that the canonical commutation relations of position and momentum are deformed as a consequence of a variety of formulations of quantum gravity [6, 12–15]. These deformations are a phenomenological approach to modelling the existence of a minimum length scale in quantum gravity and different models of quantum gravity

involve different forms of modification of the commutator [16–18]. One such paradigmatic model is [16]

$$[x, p] = i\hbar \left(1 + \frac{\beta_0}{(M_p c)^2} p^2\right), \tag{1.1}$$

where $M_p = 2.176435 \times 10^{-8}\,\mathrm{kg}$ and $c = 299792458\,\mathrm{m/s}$ are the Planck mass and speed of light respectively. β_0 is a dimensionless parameter which is expected to be of the order of unity if the minimal length scale is of the order of Planck length, but it is not fixed by theory. Measuring or placing bounds on this parameter is thus the open experimental challenge that is the focus of these table-top experiments.

To get a heuristic idea on how quantum gravity implies a deformation in the canonical commutator like in Eq. (1.1), we perform a thought experiment following the argument in Ref. [19] which is based on Ref. [20]. We consider the usual argument that is used to motivate Heisenberg uncertainty principle but modify it to include the effects of gravity. Consider an experiment where we try to measure the position of an electron using photons of wavelength λ reflected off it into a lens. The resolution of the position measurement is limited by diffraction and therefore

$$\Delta x \sim \frac{\lambda}{\sin\theta}. \tag{1.2}$$

The accuracy in position can be improved by using higher frequency photons. But, according to Heisenberg, the photons impart some of their momenta onto the electron, and the uncertainty in the $x-$component of the momentum is

$$\Delta p \sim \frac{\hbar}{\lambda} \sin\theta. \tag{1.3}$$

With this, we have the Heisenberg uncertainty principle

$$\Delta x \Delta p \sim \hbar. \tag{1.4}$$

According to the HUP, the uncertainty in x can be made arbitrarily small if we allow for an arbitrarily large uncertainty in momentum and there is no minimum length scale. So, in principle, if we build a powerful enough microscope, we could resolve distances within the Planck length.

However, the equation changes if we also account for gravity. The photon not only transfers some of its momentum to the electron, but also exerts gravitational force on it. This gravitational force leads to an additional change in the position of the electron, which should be accounted for. To calculate this additional change in position, we assume that the photon interacts over some distance r. The acceleration experienced by the electron is proportional to $E/c^2 = h/\lambda c$ and is

$$a \sim \frac{Gh}{r^2 \lambda c}. \tag{1.5}$$

Therefore, over the time-scale of interaction $t = r/c$, the distance moved by the electron is of the order of $l \sim Gh/\lambda c^3$, which on projecting along the x axis is

$$\Delta x_{\text{grav}} \sim \frac{Gh}{\lambda c^3} \sin\theta. \tag{1.6}$$

Writing it in terms of Δp, we obtain

$$\Delta x_{\text{grav}} \sim \frac{G\Delta p}{c^3}. \tag{1.7}$$

Putting together the uncertainty in position from Heisenberg uncertainty principle and from gravitational effects, we obtain

$$\Delta x \gtrsim \max\left(\frac{\hbar}{\Delta p}, \frac{G\Delta p}{c^3}\right) \gtrsim \sqrt{\frac{\hbar G}{c^3}}. \tag{1.8}$$

The last relation uses the AM-GM inequality and the quantity $\sqrt{\frac{\hbar G}{c^3}}$ is defined as the Planck length. Hence, we see that accounting for gravitational effects enforces the existence of a minimal length scale beyond which no system can be probed.

Eq. (1.8) can be rewritten as a generalised uncertainty principle by simply adding the two terms with an arbitrary weighting constant β_0 to obtain

$$\Delta x \Delta p \gtrsim \hbar + \beta_0 \frac{G(\Delta p)^2}{c^3} = \hbar \left(1 + \beta_0 \left(\frac{\Delta p}{M_p c}\right)^2\right) \tag{1.9}$$

where in the last step, we have rewritten in terms of the Planck mass. This uncertainty principle can be seen as a result of a deformed commutator of the form

$$[x, p] = i\hbar \left(1 + \frac{\beta_0}{(M_p c)^2} p^2\right). \tag{1.10}$$

This argument may seem hand-wavy and a result of using Newtonian physics to calculate the scattering of the photon off the electron, but other arguments using general relativity [20], string theory [21] and calculating the horizon of a black hole [12, 13] all yield similar results.

Other models of quantum gravity yield slightly different forms of commutator deformations. One such model [17] leads to the form

$$[x, p]_{\mu_0} = i\hbar \left(1 + 2\mu_0 \frac{(p/c)^2 + m^2}{M_p^2}\right)^{\frac{1}{2}} \tag{1.11}$$

where the strength of the correction to canonical commutator is given by constant μ_0. Notice that this deformation depends on the mass m of the particle. In the limit $m \ll p/c \lesssim M_p$, the commutator reduces to the β_0 commutator of Eq. (1.1). So, in existing and current analyses, we consider the other limit where $p/c \ll m \lesssim M_p$ in which case the commutator reduces to

$$[x, p]_{\mu_0} = i\hbar \left(1 + \mu_0 \frac{m^2}{M_p^2}\right). \tag{1.12}$$

Another recently proposed model [18] of quantum gravity leads to the deformation

$$[x, p]_{\gamma_0} = i\hbar \left(1 - \gamma_0 \frac{p}{M_p c} + \gamma_0^2 \left(\frac{p}{M_p c}\right)^2\right) \tag{1.13}$$

with quantum gravity parameter γ_0. We consider the limit $\gamma_0 \ll 1$ or $p/c \ll M_p$, where the commutator reduces to

$$[x,p]_{\gamma_0} = i\hbar\left(1 - \gamma_0 \frac{p}{M_p c}\right). \tag{1.14}$$

This thesis deals with experiments that aim to measure the values of the parameters β_0, μ_0 and γ_0 or at least place an upper bound on them.

1.2 Tests of deformed commutators

One approach to bounding the value of parameters like β_0 is to use single particle systems, for example, using measurements of Landau levels, of the Lamb shift, or of electron tunnelling through a potential barrier [22]. However, the best bound obtained with these methods is $\beta_0 < 10^{20}$, which is far from the expected $\beta_0 \sim 1$ [19]. To improve the bounds significantly, recent experimental proposals suggest using massive composite systems rather than elementary particles. These experiments aim to exploit the fact that the quantum gravity signal is enhanced with larger momenta, which result from larger system mass. Experiments and proposals in this direction include those based on the change in resonant frequency of a harmonic oscillator [4, 11, 23], the change in broadening times of large molecular wave-packets [24], and optomechanical schemes [3, 9].

The first part of the thesis is based on using an optomechanical scheme to test for quantum gravity signatures based on the work by Pikovski *et al.* [3]. The scheme in Ref. [3] proposes to measure the canonical commutator of a massive object directly in order to bound the parameters β_0, γ_0 and μ_0. Using laser pulses, the state of the mechanical resonator is taken through a loop in phase space causing the commutator of the position and momentum operator of the mechanical

oscillator to be mapped to the phase of the outgoing light. The commutator is measured and the contribution from regular quantum mechanics is subtracted to estimate the quantum gravity parameter. This proposal is promising in exploring an entirely new parameter space at the intersection of quantum mechanics and gravity. Furthermore, technological progress and advanced experimental protocols have the potential to improve sensitivity by many orders of magnitude.

In Ref. [1] and in this thesis, we show that despite the novel idea in the use of optomechanics to probe quantum gravity, there are some challenges in the analysis of this proposal that make it difficult to realise experimentally. The contributions from the higher order corrections to the cavity Hamiltonian are much larger than the quantum gravity signal and need to be taken into account to avoid false positives. The precision of the estimated parameters is reduced because of uncertainty in the incident-light mean photon number, which can arise from classical fluctuations or from quantum shot noise in measurement. We address these issues by taking higher order terms into account and suggesting different, more complicated paths in phase space so that the imprecision arising from photon number uncertainty is minimised. We also suggest using squeezed states of light to further improve precision.

Another major challenge in the proposal of Refs. [3, 9] and many other proposals [4, 11, 23] that use macroscopic objects to test for quantum gravity is that the implications of using multi-particle systems to probe quantum gravity are not clear. This is because the deformations of the canonical commutation relations like Eq. (1.1) have been derived for point particles and not for centre of mass (COM) modes of multi-particle objects [25]. The deformations for the COM modes are expected to decrease with the number of constituent particles in the test object [25,26], but the exact expression for this suppression is not known and therefore

needs to be bounded by experiment. Even if the scaling with particle number of this suppression was known, the question of what constitutes a fundamental particle remains open. This scaling of quantum-gravity deformations with the number of particles is a direct consequence of the so-called soccer-ball problem [27–29].

In Ref. [2] and in this thesis, we argue that the inclusion and hence estimation of the suppression of the quantum gravity parameter is essential for the rigorous interpretation of any experiment that uses composite test objects. To this end, we introduce a phenomenological parameter α_0 to account for this unknown scaling law and the canonical commutator deformation now reads as

$$[x,p] = i\hbar\left(1 + \frac{\beta_0}{N^{\alpha_0}(M_p c)^2}p^2\right) \tag{1.15}$$

where N is the number of constituent particles in the test object. We propose to assess any such experiment by the exclusion area in a two-dimensional parameter space spanned by α_0 and β_0 and carry out such an analysis for three experiments. While the precise value of α_0 is unknown, it is commonly accepted that it needs to be positive [25, 26]. We shall see that the best bounds that can be calculated from recent experiments based on micro- and nano-scale quantum harmonic oscillators [4, 11] are in fact negative for $\beta_0 = 1$ (and in fact any $\beta_0 < 10^6$).

Here we show that measured data of a macroscopic pendulum reveals the first positive bound on α_0 for any value of $\beta_0 > 10^{-3}$ based on a careful analytical examination of the effect of deformations of the canonical commutation relations (Eq. (1.15)) on the time period of a pendulum. Specifically, we obtain $\alpha_0 > 0.12$ for a value of $\beta_0 = 1$, which is expected in various models of quantum gravity. The reason for this significant enhancement of the bound over those obtained from micro- and nano-scale quantum harmonic oscillators can be traced back to the

low achievable momenta in those experiments which in turn lead to very weak deformations of the canonical commutation relations, for example, in the second term in Eq. (1.15). We argue that our bound on α_0 can be improved further by moving a pendulum to a vacuum set-up with optimised low damping suspension or by moving to diamagnetically levitated systems which exhibit extremely low damping rates [30, 31] on earth and promise even better values when located in a space probe.

While performing the calculations of the time period of a pendulum when the canonical commutators are deformed, we unify two different methods to calculate the same. Our results pertaining to the time period are derived using the method of deformed Poisson brackets [32–34]. We also put this method on a more rigorous footing by connecting it to the calculations based on deformed commutators [16, 35, 36] and show that the two results match. These two approaches have so far been considered independent [37], but we connect the two approaches and show that we obtain identical results. Finally, we show that the suppression of quantum gravity deformations is not just restricted to this one framework of oscillator frequency measurement. For instance, we consider the optomechanical system of Refs. [3, 9] and verify that broadly analogous considerations hold.

This thesis is organised as follows: In Chapter 2, we give relevant background for this thesis. In particular, we describe the methods to estimate quantum gravity parameters using the optomechanical scheme in Ref. [3] and by measuring the frequency of harmonic oscillators in Refs. [4, 11]. In Chapter 3, we show that the method used in Ref. [3] is not experimentally feasible and devise modifications to the method using new experimental schemes and different initial states. Furthermore, we check the effect of experimental imperfections and theoretical assumptions on

the suggested new schemes in Chapter 4. In Chapter 5, we extend the time period calculations of Refs. [4, 11], which deal with harmonic oscillators in the presence of deformed commutators, to those of a pendulum. These calculations use the framework of the two parameter deformations (β_0 and α_0) that we introduced in Ref. [2]. The time period calculations are performed using both deformed commutators and Poisson brackets and we show that the two approaches result in identical expressions. Using the expression for changes in the time period of a pendulum, we use experimental data to place bounds on the quantum gravity parameters in Chapter 6. We further suggest other experiments to substantially improve the bounds. Finally, we conclude the thesis with a summary and outlook in Chapter 7.

Chapter 2

Background

This chapter provides relevant background material that will be used in the rest of the thesis. In Section 2.1, we first describe the existing scheme [3] for testing quantum gravity effects via cavity optomechanics which we will analyse and improve in Chapters 3 and 4. We then describe the experiments performed to test for the same deformed commutators by measuring the frequency of harmonic oscillators in Section 2.2 and discuss this scheme further in Chapters 5 and 6. Finally, Section 2.3, we discuss generalised coherent states that are useful in the calculations of Chapter 5.

2.1 Optomechanical scheme by Pikovski *et al.*

In this section, we detail the experimental scheme of Ref. [3]. This scheme uses the optomechanical coupling between light and mechanical modes to imprint the canonical commutator of the mechanical mode, as in Eq. (1.1), onto the phase of light. By measuring the phase of light, we can make estimates of quantum gravity parameters like β_0.

We first introduce relevant notation and describe the Hamiltonian of the system

that couples the light and mechanical modes. We then detail the experimental scheme that causes the laser pulses to acquire a phase that depends on the commutator. We then perform the uncertainty analysis and list the suggested required experimental parameters.

2.1.1 The Hamiltonian

The Hamiltonian that couples the light and mechanical resonator is given by

$$H = \hbar\omega_m n_m + \hbar\frac{cn_0}{2(L+x)}a^\dagger a, \tag{2.1}$$

where n_m is the number operator of the mechanical modes, L is the length of the cavity at zero displacement, x is the position operator describing the displacement from the mean position of the mirror, the integer n_0 depends on the frequency of the light incident at the cavity and a and $a^\dagger$ are the annihilation and creation operators of light modes.

The Hamiltonian is approximated by expanding to first order in x as

$$H \approx \hbar\omega_m n_m + \hbar\omega_L a^\dagger a - \hbar\omega_L\frac{x}{L}a^\dagger a, \tag{2.2}$$

where

$$\omega_L = \frac{cn_0}{2L}. \tag{2.3}$$

Rewriting the Hamiltonian in terms of the dimensionless quadratures

$$\begin{aligned} X &= x\left(\frac{\hbar}{m\omega_m}\right)^{-\frac{1}{2}} \\ P &= p\left(\hbar m\omega_m\right)^{-\frac{1}{2}} \end{aligned} \tag{2.4}$$

where m is the mass of the mirror and ω_m is the frequency of the mirror, and defining

$$g_0 = \omega_L\left(\frac{\hbar}{m\omega_m L^2}\right)^{\frac{1}{2}} \tag{2.5}$$

we rewrite the Hamiltonian in a slightly more simplified notation as

$$H \approx \hbar\omega_m n_m + \hbar\omega_L a^\dagger a - \hbar g_0 X a^\dagger a. \tag{2.6}$$

In Section 3.1, we will show that the approximation Eq. (2.2) of truncating the Hamiltonian to only the first order is not valid under the conditions that are relevant to the detection of possible quantum gravitational corrections to the canonical commutation relations. Nonetheless, we demonstrate the implications of this assumption in the remainder of this section to describe the experimental scheme [3].

2.1.2 The scheme: measuring deformations in the commutator

The experimental scheme that is described in this section is based on the idea of pulsed optomechanics [38], i.e., the light that interacts with the mechanical resonator is only sent in short pulses. In the following calculations, we work in the interaction picture with respect to $H_0 = \hbar\omega_L a^\dagger a$. Hence, during these short pulses, the effective Hamiltonian is approximately

$$\begin{aligned} H_{\text{on}} &\approx -\hbar g_0 X a^\dagger a \\ &=: -\hbar g_0 X n \end{aligned} \tag{2.7}$$

where we have rewritten $n = a^\dagger a$. When there is no pulse, the Hamiltonian is only governed by the free evolution of the mechanical resonator, i.e.,

$$H_{\text{off}} = \hbar\omega_m n_m. \tag{2.8}$$

When laser light is sent in pulses, the effective unitary operator is approximately given by the time evolution due to H_{on} and H_{off} alternatively, i.e.,

$$U = \ldots \mathrm{e}^{i\theta n_m} \mathrm{e}^{i\lambda n X} \mathrm{e}^{i\theta n_m} \mathrm{e}^{i\lambda n X} \mathrm{e}^{i\theta n_m} \mathrm{e}^{i\lambda n X} \tag{2.9}$$

where θ and λ depend on the frequency of the mechanical oscillator, decay rate in the cavity, the duration between laser pulses and duration of laser pulses. Here, $\lambda \simeq g_0/\kappa$ with κ is the optical amplitude decay rate and $n = a^\dagger a$. λ depends on the finesse $\mathcal{F}$ of the cavity as $\lambda = 4\mathcal{F}x_0/\lambda_L$ where λ_L is the optical wavelength and $x_0 = \left(\frac{\hbar}{m\omega_m}\right)^{\frac{1}{2}}$.

This experimental scheme involves implementing the unitary operator

$$U = \mathrm{e}^{i\lambda n P}\mathrm{e}^{-i\lambda n X}\mathrm{e}^{-i\lambda n P}\mathrm{e}^{i\lambda n X} \tag{2.10}$$

which can be obtained from Eq. (2.9) with four pulses and choosing the duration between laser pulses such that $\theta = \pi/2$.

We now show that implementing this unitary operator leads to the outgoing light acquiring a phase that depends on the commutator of X and P. The deformed commutator in Eq. (1.1) can be rewritten in a simpler manner in terms of the dimensionless position and momentum operators (Eq. (2.4)) as

$$[X, P] = i\left(1 + \beta' P^2\right), \tag{2.11}$$

where $\beta' = \beta_0 \frac{\hbar\omega_m m}{M_p c}$. Using the new commutation rules, the unitary operator can be calculated up to first order in β' to obtain

$$U = \mathrm{e}^{-i\lambda^2 n^2}\mathrm{e}^{-i\beta'\left(\lambda^2 n^2 P^2 + \lambda^3 n^3 P + (1/3)\lambda^4 n^4\right)}. \tag{2.12}$$

The quantity that is measured during the experiment is the phase of the outgoing light. To estimate the phase, we calculate the mean optical field of the outgoing light, which is

$$\langle a \rangle = \mathrm{Tr}\left(aU\rho_m^{th} \otimes \rho_\ell^\alpha U^\dagger\right) \tag{2.13}$$

for initial mechanical and optical state ρ_m^{th} and ρ_ℓ^α respectively. The initial state of the mechanical oscillator is assumed to be the thermal state

$$\rho_m^{th} = \sum_{n_m=0}^{\infty} \frac{\bar{n}^{n_m}}{(1+\bar{n})^{1+n_m}} |n_m\rangle \langle n_m| \tag{2.14}$$

where $\bar{n}$ is the mean phonon number of the oscillator. The state of light is initially in a coherent state given by

$$\rho_\ell^\alpha = |\alpha\rangle \langle \alpha| = \mathrm{e}^{-|\alpha|^2} \sum_{n_\ell, k_\ell} \frac{\alpha^{n_\ell} \alpha^{*k_\ell}}{\sqrt{n_\ell! k_\ell!}} |n_\ell\rangle \langle k_\ell| \tag{2.15}$$

where $|n_\ell\rangle$ are the Fock states. The mean photon number of the coherent state $|\alpha\rangle$ is given by $N_p = |\alpha|^2$. For $N_p \gg 1$ and $\lambda^2 N_p^3 \gg \bar{n}$, the mean optical field can be calculated and is approximately

$$\langle a_\ell \rangle \approx \alpha \mathrm{e}^{-i\lambda^2 - N_p(1-\mathrm{e}^{-i2\lambda^2})} \mathrm{e}^{-i\Theta_\beta} \tag{2.16}$$

where Θ_β is given by

$$\Theta_\beta \approx \frac{4}{3} \beta' N_p^3 \lambda^4 \mathrm{e}^{-i6\lambda^2}. \tag{2.17}$$

The initial state of light is $|\alpha\rangle$, whose mean optical field is α. We see that after the pulse sequences and interaction with the mechanical oscillator, the light has picked up a phase Φ_T which is

$$\begin{aligned} \Phi_T &= \lambda^2 - iN_p(1 - \mathrm{e}^{-i2\lambda^2}) + \Theta_\beta \\ &\approx 2\lambda^2 N_p + \Theta_\beta. \end{aligned} \tag{2.18}$$

This approximation holds when the number of photons N_p is large. The first term $2\lambda^2 N_p$ occurs as a result of quantum mechanics alone (from the fact that the commutator $[x, p] = i\hbar$), but the terms Θ_β is as a result of the deformations in the commutator.

Similar calculations can be performed with the γ_0 and μ_0 commutators (Eq. (1.14), Eq. (1.12)), which can be rewritten in terms of the dimensionless variables as

$$[X, P] = i\,(1 - \gamma P) \quad \text{for} \quad \gamma = \gamma_0 \frac{\sqrt{\hbar m \omega}}{M_p c} \tag{2.19}$$

and

$$[X, P] = i\,(1 + \mu) \quad \text{for} \quad \mu = \mu_0 \frac{m^2}{M_p^2}. \tag{2.20}$$

These calculations lead to the phases

$$\Theta_\gamma \approx -\frac{3}{2}\gamma N_p^2 \lambda^3 \mathrm{e}^{-i4\lambda^2} \tag{2.21}$$

and

$$\Theta_\mu \approx 2\mu N_p \lambda^2 \mathrm{e}^{-i2\lambda^2}. \tag{2.22}$$

In order to estimate the contribution from quantum gravity, the total phase Φ_T is measured experimentally and the quantum mechanical contribution $\lambda^2 - iN_p(1 - \mathrm{e}^{-i2\lambda^2}) \approx 2\lambda^2 N_p$ is subtracted from the total phase to get $\Theta_{\beta/\gamma/\mu}$.

For convenience, the current analysis makes the assumption that a and $a^\dagger$ remain unchanged as a function of X and P as in usual quantum mechanics. The justification behind this assumption needs to be studied further.

2.1.3 Uncertainty analysis and required experimental parameters

Having calculated the phase that is acquired by light due to quantum gravity deformations, here we discuss the feasibility of such an experiment by calculating the uncertainty in the estimated parameters for some optimistic experimental parameters.

The precision to which the quantum gravity parameters are determined depends on the experimental parameters used and the number of times, N_r, the experiment

is performed. The values of μ_0, γ_0 and β_0 are expected to be of order 1 [19]. To have a precision of $\delta\mu_0 \sim 1$, $\delta\gamma_0 \sim 1$ and $\delta\beta_0 \sim 1$, the required number of runs of experiment is calculated. It is assumed that the uncertainty in the total measured phase Φ_T is proportional to the uncertainty in the quantum gravity parameters, i.e, the other terms contribute a negligible amount of uncertainty. We will show in Section 3.2 that this assumption is not always correct. The number of experimental runs N_r is calculated using the relation

$$\delta \langle \Phi_T \rangle = \frac{1}{2\sqrt{N_p N_r}} \tag{2.23}$$

and the results are listed in Table 2.1.

Parameters	μ equation	γ equation	β' equation
$\mathcal{F}$	10^5	2×10^5	4×10^5
m	10^{-11} kg	10^{-9} kg	10^{-7} kg
$\frac{\omega_m}{2\pi}$	10^5 Hz	10^5 Hz	10^5 Hz
λ_L	1064 nm	1064 nm	532 nm
N_p	10^8	5×10^{10}	10^{14}
$\delta \langle \Phi \rangle$	10^{-4}	10^{-8}	10^{-10}
N_r	1	10^5	10^6

Table 2.1: Experimental parameters as suggested in Table 2 of Ref. [3]. Reprinted by permission from Springer Nature and Copyright Clearance Center: I. Pikovski, M. R. Vanner, *et al.* Probing Planck- scale physics with quantum optics. *Nat. Phys.*, 8(5), 393, 2012.

In summary, the Pikovski *et al.* scheme measures the quantum gravity parameters by using optomechanics to output light whose phase is proportional to the quantum gravity parameters. The calculations of the phase of the outgoing light are performed assuming that the cavity Hamiltonian is truncated to first order in the displacement of the cavity's mirror. The experimental parameters required to perform this experiment are calculated assuming that the uncertainty in the mean

number of photons can be ignored. In Sections 3.1 and 3.2, we show that these assumptions are not valid and in Sections 3.3 and 3.4, we suggest modifications to the scheme and to the calculations to overcome these challenges.

2.2 Tests of deformations via measuring frequency of harmonic oscillators

In this section, we describe a second method to estimate the commutator deformation parameters, namely from the measurement of frequency of harmonic oscillators. Deformations in the canonical commutators lead to a shift in the resonant frequency of a harmonic oscillator that is directly dependent on the quantum gravity parameter. Experiments that measure the frequency of harmonic oscillators very precisely have been performed [4, 11] to place bounds on the quantum gravity parameters. Here, we detail the theory behind and the results of these experiments.

2.2.1 Theory: Effect of deformed commutator on harmonic oscillator

The derivation of the change in frequency in Refs. [4, 11] is as follows. We assume that under the deformed commutators, the Hamiltonian maintains the classical form

$$H = \frac{1}{2}m\omega^2 x^2 + \frac{p^2}{2m} \tag{2.24}$$

and the commutator is given by Eq. (1.1)

$$[x, p] = i\hbar\left(1 + \frac{\beta_0}{(M_p c)^2}p^2\right). \tag{2.25}$$

We also assume that the Heisenberg equation of motion i.e.,

$$\frac{\mathrm{d}A}{\mathrm{d}t} = \frac{1}{i\hbar}[A, H] \tag{2.26}$$

still holds despite the commutators being deformed.

One method to simplify calculations is to define a transformed momentum operator $\tilde{p}$ such that the commutator $[x, \tilde{p}]$ is restored to the value $i\hbar$ while still keeping the Heisenberg equation of motion intact. Such a transformation implies that the harmonic oscillator Hamiltonian has additional non-linear terms depending on the quantum gravity parameter β_0. To linear order in $\beta_0/(M_pc)^2$, the transformation is given by

$$\tilde{p} \approx p - \frac{\beta_0}{3(M_pc)^2}p^3 \tag{2.27}$$

due to which the Hamiltonian can be rewritten in terms of $\tilde{p}$ as

$$H \approx \frac{1}{2}m\omega^2x^2 + \frac{\tilde{p}^2}{2m} + \beta_0\frac{\tilde{p}^4}{3m(M_pc)^2}. \tag{2.28}$$

The equations of motion can be calculated for x and p using the Heisenberg equation of motion in Eq. (2.26) to obtain

$$\begin{aligned} \dot{x} &= \frac{\tilde{p}}{m}\left(1 + \frac{4\beta_0}{3(M_pc)^2}\tilde{p}^2\right) \\ \dot{\tilde{p}} &= -m\omega^2x \end{aligned} \tag{2.29}$$

which can then be solved for initial conditions $\tilde{p}(0) = m\omega A$ and $x(0) = 0$ to obtain the solution

$$x(t) = A\left\{\sin(\tilde{\omega}t) + \frac{\beta_0m^2\omega^2A^2}{8(M_pc)^2}\sin(3\tilde{\omega}t)\right\} \tag{2.30}$$

where

$$\tilde{\omega} = \left(1 + \beta_0\frac{m^2\omega^2A^2}{2(M_pc)^2}\right)\omega. \tag{2.31}$$

Hence, we see that not only is the oscillation frequency (Eq. (2.31)) modified due to deformed commutators, but the shape of the oscillation (third harmonics) (Eq. (2.30)) is also modified. By measuring the motion of a harmonic oscillator

very precisely, one can estimate the parameter β_0. Even if no definite value of β_0 can be determined, very precise measurements can help us place tight bounds on the value. We note that this approach is still based on classical mechanics because we have defined boundary conditions such that we know both the momentum and position at time $t = 0$ exactly, i.e., $\tilde{p}(0) = m\omega A$ and $x(0) = 0$. A fully quantum mechanical treatment can be performed by starting with the modified quantum Hamiltonian as in Ref. [16] as will be shown in Section 5.2.

2.2.2 Experimental bounds on parameters

Experiments were performed on three different oscillators with masses approximately 10^{-4}, 10^{-7} and 10^{-11}kg respectively in Ref. [4]. The parameter β_0 was estimated both from monitoring the dependence of the oscillator frequency and the third harmonic on the amplitude of oscillations. These two estimates of β_0 were calculated independently. Table 2.2 lists the results of the experiment. We note that the bound

Mass (kg)	β_0 bound from Eq. (2.31)	β_0 bound from Eq. (2.30)
3.3×10^{-5}	3×10^{7}	2×10^{11}
7.7×10^{-8}	5×10^{13}	2×10^{18}
2×10^{-11}	2×10^{19}	1×10^{26}

Table 2.2: Estimates of the quantum gravity parameter from measurements on three oscillators by from Table 1 of Ref. [4], CC BY 4.0, https://creativecommons.org/licenses/by/4.0/

is tighter when calculated from frequency change of the oscillator as compared to the bound from measuring the third harmonic. We also note that the more massive oscillators provide tighter bounds.

In Ref. [11], frequency measurement a harmonic oscillator was performed to place even tighter bounds on the parameter β_0. Using a massive sapphire split-bar

resonator of mass 0.3 kg, the bound obtained was $\beta_0 < 5 \times 10^6$, which is an order of magnitude improvement over the bound in Ref. [4]. The bounds can be improved by using different kinds of oscillators, for example, a bulk acoustic wave quartz resonator, whose frequencies can be estimated more precisely.

We also note that in deriving the bounds on the quantum gravity parameter in Refs. [4, 11], it has been assumed that the form of the deformed commutator in Eq. (1.1) holds even for multi-particle systems. We show later in this thesis that this assumption may not be valid.

2.3 Gazeau-Klauder states

In Section 2.2, we saw that the deformation in the commutators can be alternatively expressed as a modification in the harmonic oscillator Hamiltonian. However, the analysis was entirely classical. The modified quantum mechanical Hamiltonian is derived in Ref. [16], but it is not clear how to choose the initial state of the oscillator. To compare with classical results, a natural choice is a coherent state, but due to the modified Hamiltonian, our usual definition of coherent states no longer hold because the coherent state does not remain one after evolution under this Hamiltonian. Hence, in this section, we introduce generalised coherent states that are suited for this modified Hamiltonian. These states are the Gazeau-Klauder states which were introduced in Ref. [39]. Here, we describe them in detail, closely following the details in Ref. [39].

Since a coherent state $|\alpha\rangle$ is parametrised by one complex number, we generalise it slightly by considering states parametrised by two real parameters $|J, \gamma\rangle$. To ensure that $|J, \gamma\rangle$ behaves like a classical state, we demand that it satisfies the following conditions with respect to the given Hamiltonian H:

1. The continuity condition

$$(J', \gamma') \to (J, \gamma) \implies |J', \gamma'\rangle \to |J, \gamma\rangle \tag{2.32}$$

2. Resolution of identity

$$\int \mathrm{d}\mu(J, \gamma) \, |J, \gamma\rangle \langle J, \gamma| = \mathbb{1} \tag{2.33}$$

3. Temporal stability such that the time-evolved state is always a generalised coherent state

$$\mathrm{e}^{-iHt/\hbar} \, |J, \gamma\rangle = |J, \gamma + \omega t\rangle \tag{2.34}$$

4. The energy of the state only depends on J

$$\langle J, \gamma | H | J, \gamma \rangle = \hbar \omega J \tag{2.35}$$

The conditions Eqs. (2.34) and (2.35) are defined with respect to a Hamiltonian, and so coherent states do not satisfy them with respect to a modified Hamiltonian and we need these generalised states.

If the eigenvalues and eigenstates of the Hamiltonian are defined such that

$$H \, |n\rangle = \hbar \omega e_n \, |n\rangle \, , \tag{2.36}$$

we can verify that the definition of the generalised coherent state

$$|J, \gamma\rangle = \frac{1}{N(J)} \sum_n \frac{J^{n/2} \mathrm{e}^{-i\gamma e_n}}{\sqrt{\rho_n}} \, |n\rangle \tag{2.37}$$

where

$$\begin{aligned} \rho_n &= \prod_{k=1}^{n} e_k \\ N(J)^2 &= \sum_n \frac{J^n}{\rho_n} \end{aligned} \tag{2.38}$$

satisfies all the above properties.

As an example, we consider the harmonic oscillator Hamiltonian. Here, the eigenvalues are given by $H|n\rangle = \hbar\omega n|n\rangle$ (after ignoring the constants) and therefore

$$e_n = n. \tag{2.39}$$

We now find the generalised coherent state associated with this Hamiltonian. We find that

$$\begin{aligned} \rho_n &= \prod_{k=1}^{n} e_k = n! \\ N(J)^2 &= \sum_n \frac{J^n}{\rho_n} = \sum_n \frac{J^n}{n!} = \mathrm{e}^J \end{aligned} \tag{2.40}$$

and therefore, the state is

$$|J,\gamma\rangle = \mathrm{e}^{-J/2} \sum_n \frac{J^{n/2}\mathrm{e}^{-i\gamma n}}{\sqrt{n!}} |n\rangle . \tag{2.41}$$

Note that if we define the complex number α such that $\alpha = \sqrt{J}\mathrm{e}^{-i\gamma}$, then the state can be rewritten as

$$|J,\gamma\rangle = \mathrm{e}^{-\frac{|\alpha|^2}{2}} \sum_n \frac{\alpha^n}{\sqrt{n!}} |n\rangle \tag{2.42}$$

which is exactly the definition of a coherent state. Thus we see that the Gazeau-Klauder state reduces to the coherent state when the Hamiltonian is the harmonic oscillator Hamiltonian.

To summarise, in this chapter, we first described the proposal of Ref. [3] to estimate quantum gravity parameters based in optomechanics in Section 2.1. In Section 2.2, we described the experiments [4, 11] performed to estimate the parameters from frequency measurements of oscillators. Finally, we introduced generalised coherent states that are the most classical states under a Hamiltonian modified from deformed commutators.

Chapter 3

Results: Improved optomechanical scheme

In Section 2.1.3, we described an experimental scheme [3] using optomechanics that seemed to be able to very precisely measure the quantum gravity parameters. In this chapter, we show that high precision cannot be achieved with this scheme and suggest methods to overcome these challenges.

In Sections 3.1 and 3.2, we revisit the analysis of Ref. [3] to show that the scheme is not experimentally feasible. Specifically, in Section 3.1, we show that the higher order terms in the optomechanical Hamiltonian have a large contribution to the phase measured in the experiment. This large contribution significantly reduces the accuracy of the estimated quantum gravity parameters and hence cannot be ignored. In Section 3.2, we show that the precision of the estimated parameter is decreases by several orders of magnitude when the non-zero uncertainty in the mean photon number is accounted for. To have the same precision in the parameters as originally intended, we would need to repeat the experiment far more often than suggested originally, making the experiment infeasible.

To overcome these challenges, we suggest a modification to the scheme by using

a different sequence of pulses in Section 3.3. With the new sequence, we show that the experimental runs are brought down to being feasible again. We also show that the scheme can further be improved by using squeezed states of light in Section 3.4.

The calculations of Sections 3.1 to 3.4 are performed assuming the γ_0 model of deformed commutators. So, in Section 3.5, we perform the same calculations for the other models of deformed commutators.

3.1 Revisiting analysis: Accuracy

In this section, we show that the accuracy of the experimental scheme of Ref. [3] can be significantly improved by taking into account the higher order terms in the optomechanical Hamiltonian. Specifically, we calculate the additional phase incurred by the outgoing light due to these higher order terms and show that this additional phase is much larger than the quantum gravitational signal, thereby reducing the accuracy of the parameter estimates.

The optomechanical Hamiltonian is given by Eq. (2.1) which is

$$H = \hbar\omega_m n_m + \hbar\frac{cn_0}{2(L+x)}a^\dagger a. \tag{3.1}$$

Instead of truncating to linear order in x, we retain the higher order terms to obtain the Hamiltonian

$$H = \hbar\omega_m n_m + \hbar\omega_L a^\dagger a - \hbar g_0 X a^\dagger a + \hbar g_0 k X^2 a^\dagger a + \dots \tag{3.2}$$

where $k = \sqrt{\frac{\hbar}{m\omega_m L^2}}$. To make the notation easier, we define the quantities H_X and H_P as

$$\begin{aligned} H_X &= n\lambda_0\left(X - kX^2 + k^2X^3 - \dots\right) \\ H_P &= n\lambda_0\left(P - kP^2 + k^2P^3 - \dots\right). \end{aligned} \tag{3.3}$$

Following the same scheme of pulsed optomechanics as described in the background in Section 2.1.2, the four-displacement operator given by

$$U = \mathrm{e}^{iH_P}\mathrm{e}^{-iH_X}\mathrm{e}^{-iH_P}\mathrm{e}^{iH_X}. \tag{3.4}$$

While we focus on the nonlinearities of the form Eq. (3.2) for concreteness, our analysis can also be used for other forms of non-linearities in X in the Hamiltonian. For example, the accuracy might possibly be improved by considering corrections arising from the microscopic Hamiltonian by generalising the procedure adopted in Ref. [40] to higher powers of X than unity.

The effect of some specific anharmonic terms in the Hamiltonian, namely either X^3 or X^4 terms, on the phase has been studied in Ref. [41] but here we perform the analysis to obtain accurate estimates of the quantum gravity parameter.

To illustrate the effect of the higher order terms and for ease of calculation, we consider the Hamiltonian expanded up to third order in X and P. We evaluate U up to sixth order terms of the Baker-Campbell-Hausdorff (BCH) formula using Mathematica code [42]. Keeping only those terms that contribute to a phase larger than the minimum phase uncertainty, the operator is now given by

$$\begin{aligned} U = \exp\Big\{-i\Big[&\phi_{QG} + \lambda_0^2 n^2 - 2k\lambda_0^3 n^3 + 4k^2\lambda_0^4 n^4 \\ &+\sqrt{2}k\lambda_0^2 n^2\left((-1+i)a_m + (-1-i)a_m^\dagger\right) \\ &+\frac{7}{\sqrt{2}}k^2\lambda_0^3 n^3\left((1-i)a_m + (1+i)a_m^\dagger\right)\Big]\Big\} \end{aligned} \tag{3.5}$$

where

$$\phi_{QG} = \begin{cases} \frac{1}{3}\beta'\lambda_0^4 n^4 & \beta_0 \text{ case} \\ -\frac{1}{2}\gamma\lambda_0^3 n^3 & \gamma_0 \text{ case} \\ \mu\lambda_0^2 n^2 & \mu_0 \text{ case} \end{cases} \tag{3.6}$$

and a_m and $a_m^\dagger$ are the are the annihilation and creation operators of the modes of the mechanical resonator. The error due to this truncation in terms is discussed in Section 4.4.

We now calculate the phase acquired by light under the action of the above unitary operator on the system. Light is initially in a coherent state $|\alpha\rangle$ and the oscillator is initially in a thermal state ρ_m^{th}. Therefore, the mean optical field is given by

$$\langle a\rangle = \mathrm{Tr}\left(U^\dagger a U\,|\alpha\rangle\,\langle\alpha|\otimes\rho_m^{th}\right). \tag{3.7}$$

In the following subsection, we now evaluate the expression for mean optical field $\langle a\rangle$ to express it in the form

$$\langle a\rangle = \alpha' \mathrm{e}^{-i\Phi_T}. \tag{3.8}$$

Since initially the mean field is $\langle a\rangle_i = \alpha$, the phase acquired by the light is given by Φ_T.

3.1.1 Calculating the mean optical field

In this subsection, we detail the steps in calculating the phase acquired by the outgoing light from the pulse sequence that acts on the system. The main result of this section is the expression for phase, Eq. (3.53), which is obtained by evaluating the expression for mean field Eq. (3.7) starting from Eq. (3.5).

In the following calculations, since we are only interested in the largest contribution from the quantum gravity phase, we ignore the corrections to this phase arising from higher order terms of the Hamiltonian. To make the notation easier

to follow, we define the terms

$$w(n) = \lambda_0^2 n^2 - 2k\lambda_0^3 n^3 + 4k^2\lambda_0^4 n^4, \tag{3.9}$$

$$x = (-1-i)\sqrt{2}k\lambda_0^2, \tag{3.10}$$

$$y = (1+i)\frac{7}{\sqrt{2}}k^2\lambda_0^3. \tag{3.11}$$

so that the unitary operator in Eq. (3.5) can be written as

$$U = \mathrm{e}^{-iw(n)+\left(x^* n^2 + y^* n^3\right)a_m^\dagger - \left(x n^2 + y n^3\right)a_m}. \tag{3.12}$$

To evaluate $U^\dagger a U$ easily, we rewrite U as

$$U = \mathrm{e}^{-iw(n)}\mathrm{e}^{\left(x^* a_m^\dagger - x a_m\right)n^2 + \left(y^* a_m^\dagger - y a_m\right)n^3} \tag{3.13}$$

and using the Zassenhaus formula [43], split it into parts as

$$U = \mathrm{e}^{\left(x^* a_m^\dagger - x a_m\right)n^2}\mathrm{e}^{\left(y^* a_m^\dagger - y a_m\right)n^3}\mathrm{e}^{-\frac{1}{2}n^5(x^* y - x y^*)}\mathrm{e}^{-iw(n)}. \tag{3.14}$$

Therefore $U^\dagger a U$ is

$$\begin{aligned} U^\dagger a U = {} & \mathrm{e}^{iw(n)}\mathrm{e}^{\frac{1}{2}n^5(x^* y - x y^*)}\mathrm{e}^{-\left(y^* a_m^\dagger - y a_m\right)n^3} \\ & \times \mathrm{e}^{-\left(x^* a_m^\dagger - x a_m\right)n^2} a \mathrm{e}^{\left(x^* a_m^\dagger - x a_m\right)n^2} \\ & \times \mathrm{e}^{\left(y^* a_m^\dagger - y a_m\right)n^3}\mathrm{e}^{-\frac{1}{2}n^5(x^* y - x y^*)}\mathrm{e}^{-iw(n)}. \end{aligned} \tag{3.15}$$

In the following steps, we try to express $U^\dagger a U$ as Va where V is some operator.

We first evaluate $\mathrm{e}^{-\left(x^* a_m^\dagger - x a_m\right)n^2} a \mathrm{e}^{\left(x^* a_m^\dagger - x a_m\right)n^2}$ from the expression for $U^\dagger a U$ using the BCH formula

$$\mathrm{e}^X Y \mathrm{e}^{-X} = Y + [X,Y] + \frac{1}{2!}[X,[X,Y]] + \frac{1}{3!}[X,[X,[X,Y]]] + \ldots. \tag{3.16}$$

to obtain

$$\mathrm{e}^{-\left(x^* a_m^\dagger - x a_m\right) n^2} a \mathrm{e}^{\left(x^* a_m^\dagger - x a_m\right) n^2} = a - \left(x^* a_m^\dagger - x a_m\right) \left[n^2, a\right] + \frac{1}{2!} \left(x^* a_m^\dagger - x a_m\right)^2 \left[n^2, \left[n^2, a\right]\right] + \ldots . \quad (3.17)$$

Observing that

$$\left[n^2, a\right] = -\left(2n+1\right) a \quad (3.18)$$

and simplifying, we get

$$\mathrm{e}^{-\left(x^* a_m^\dagger - x a_m\right) n^2} a \mathrm{e}^{\left(x^* a_m^\dagger - x a_m\right) n^2} = \mathrm{e}^{\left(x^* a_m^\dagger - x a_m\right)(2n+1)} a. \quad (3.19)$$

Now $U^\dagger a U$ reads as follows:

$$U^\dagger a U = \mathrm{e}^{iw(n)} \mathrm{e}^{\frac{1}{2} n^5 (x^* y - x y^*)} \mathrm{e}^{-\left(y^* a_m^\dagger - y a_m\right) n^3} \mathrm{e}^{\left(x^* a_m^\dagger - x a_m\right)(2n+1)} \times a \mathrm{e}^{\left(y^* a_m^\dagger - y a_m\right) n^3} \mathrm{e}^{-\frac{1}{2} n^5 (x^* y - x y^*)} \mathrm{e}^{-iw(n)}. \quad (3.20)$$

To perform similar calculations for the y terms, we should first interchange the terms $\mathrm{e}^{-\left(y^* a_m^\dagger - y a_m\right) n^3}$ and $\mathrm{e}^{\left(x^* a_m^\dagger - x a_m\right)(2n+1)}$. Using the Zassenhaus formula again, we obtain

$$\mathrm{e}^{-\left(y^* a_m^\dagger - y a_m\right) n^3} \mathrm{e}^{\left(x^* a_m^\dagger - x a_m\right)(2n+1)} = \mathrm{e}^{\left(x^* a_m^\dagger - x a_m\right)(2n+1)} \mathrm{e}^{-\left(y^* a_m^\dagger - y a_m\right) n^3} \times \mathrm{e}^{(x^* y - x y^*)\left(2n^4 + n^3\right)}. \quad (3.21)$$

We now evaluate $\mathrm{e}^{-\left(y^* a_m^\dagger - y a_m\right) n^3} a \mathrm{e}^{\left(y^* a_m^\dagger - y a_m\right) n^3}$ similarly to Eq. (3.17) using the BCH formula to obtain

$$\mathrm{e}^{-\left(y^* a_m^\dagger - y a_m\right) n^3} a \mathrm{e}^{\left(y^* a_m^\dagger - y a_m\right) n^3} = a - \left(y^* a_m^\dagger - y a_m\right) \left[n^3, a\right] + \frac{1}{2!} \left(y^* a_m^\dagger - y a_m\right)^2 \left[n^3, \left[n^3, a\right]\right] + \ldots . \quad (3.22)$$

Using the formula

$$\left[n^3, a\right] = -\left(3n^2 + 3n + 1\right) a \tag{3.23}$$

and simplifying, we find

$$\mathrm{e}^{-\left(y^* a_m^\dagger - y a_m\right) n^3} a \mathrm{e}^{\left(y^* a_m^\dagger - y a_m\right) n^3} = \mathrm{e}^{\left(y^* a_m^\dagger - y a_m\right)\left(3n^2+3n+1\right)} a. \tag{3.24}$$

Now $U^\dagger a U$ is given by

$$\begin{aligned} U^\dagger a U =& \mathrm{e}^{(x^* y - x y^*)\left(2n^4+n^3\right)} \mathrm{e}^{iw(n)} \mathrm{e}^{\frac{1}{2} n^5 (x^* y - x y^*)} \mathrm{e}^{\left(x^* a_m^\dagger - x a_m\right)(2n+1)} \\ & \times \mathrm{e}^{\left(y^* a_m^\dagger - y a_m\right)\left(3n^2+3n+1\right)} a \mathrm{e}^{-\frac{1}{2} n^5 (x^* y - x y^*)} \mathrm{e}^{-iw(n)}. \end{aligned} \tag{3.25}$$

Once again, using similar techniques, we evaluate $\mathrm{e}^{\frac{1}{2} n^5 (x^* y - x y^*)} a \mathrm{e}^{-\frac{1}{2} n^5 (x^* y - x y^*)}$ and $\mathrm{e}^{iw(n)} a \mathrm{e}^{-iw(n)}$. Observing that

$$\left[n^5, a\right] = -\left(5n^4 + 10n^3 + 10n^2 + 5n + 1\right) a, \tag{3.26}$$

we simplify

$$\mathrm{e}^{\frac{1}{2} n^5 (x^* y - x y^*)} a \mathrm{e}^{-\frac{1}{2} n^5 (x^* y - x y^*)} = \mathrm{e}^{-\frac{1}{2}(x^* y - x y^*)\left(5n^4+10n^3+10n^2+5n+1\right)} a. \tag{3.27}$$

and substituting for $w(n)$ and observing that

$$\left[n^4, a\right] = -\left(4n^3 + 6n^2 + 4n + 1\right) a, \tag{3.28}$$

we obtain

$$\mathrm{e}^{iw(n)} a \mathrm{e}^{-iw(n)} = \mathrm{e}^{i2k\lambda_0^3\left(3n^2+3n+1\right)} \mathrm{e}^{-i\lambda_0^2(2n+1)} \mathrm{e}^{-i4k^2\lambda_0^4\left(4n^3+6n^2+4n+1\right)} a. \tag{3.29}$$

Now $U^\dagger a U$ is given by

$$\begin{aligned} U^\dagger a U =& \mathrm{e}^{(x^* y - x y^*)\left(2n^4+n^3\right)} \mathrm{e}^{\left(x^* a_m^\dagger - x a_m\right)(2n+1)} \mathrm{e}^{\left(y^* a_m^\dagger - y a_m\right)\left(3n^2+3n+1\right)} \\ & \times \mathrm{e}^{i2k\lambda_0^3\left(3n^2+3n+1\right)} \mathrm{e}^{-\frac{1}{2}(x^* y - x y^*)\left(5n^4+10n^3+10n^2+5n+1\right)} \\ & \times \mathrm{e}^{-i\lambda_0^2(2n+1)} \mathrm{e}^{-i4k^2\lambda_0^4\left(4n^3+6n^2+4n+1\right)} a. \end{aligned} \tag{3.30}$$

which can be simplified and re-written as

$$U^\dagger a U = \mathrm{e}^{-\frac{1}{2}(x^*y-xy^*)\left(n^4+8n^3+10n^2+5n+1\right)}\mathrm{e}^{i2k\lambda_0^3\left(3n^2+3n+1\right)}\mathrm{e}^{-i\lambda_0^2(2n+1)} \times \mathrm{e}^{-i4k^2\lambda_0^4\left(4n^3+6n^2+4n+1\right)}\mathrm{e}^{\left(x^*a_m^\dagger-xa_m\right)(2n+1)}\mathrm{e}^{\left(y^*a_m^\dagger-ya_m\right)\left(3n^2+3n+1\right)}a. \quad (3.31)$$

Having expressed $U^\dagger a U$ as Va, it is now easier to calculate the quantity of interest: the expectation value of the annihilation operator on light states. Note that $a\left|\alpha\right\rangle = \alpha\left|\alpha\right\rangle$. Writing Eq. (3.7) explicitly, $\langle a\rangle$ is

$$\begin{aligned}\langle a\rangle = \mathrm{Tr}\Big(&\mathrm{e}^{-\frac{1}{2}(x^*y-xy^*)\left(n^4+8n^3+10n^2+5n+1\right)}\mathrm{e}^{-i\lambda_0^2(2n+1)} \\ &\times \mathrm{e}^{i2k\lambda_0^3\left(3n^2+3n+1\right)}\mathrm{e}^{-i4k^2\lambda_0^4\left(4n^3+6n^2+4n+1\right)} \\ &\times \mathrm{e}^{\left(x^*a_m^\dagger-xa_m\right)(2n+1)}\mathrm{e}^{\left(y^*a_m^\dagger-ya_m\right)\left(3n^2+3n+1\right)} \\ &\times\alpha\left|\alpha\right\rangle\left\langle\alpha\right|\otimes\rho_m^{th}\Big).\end{aligned} \quad (3.32)$$

Writing the trace explicitly as a sum over Fock state expectation values, we have

$$\begin{aligned}\langle a\rangle = \sum_{m=0}^{\infty}\frac{\bar{n}^m}{(1+\bar{n})^{1+m}}&\left\langle\alpha,m\right|\alpha\mathrm{e}^{-i4k^2\lambda_0^4\left(4n^3+6n^2+4n+1\right)} \\ &\times \mathrm{e}^{-\frac{1}{2}(x^*y-xy^*)\left(n^4+8n^3+10n^2+5n+1\right)}\mathrm{e}^{-i\lambda_0^2(2n+1)} \\ &\times \mathrm{e}^{i2k\lambda_0^3\left(3n^2+3n+1\right)}\mathrm{e}^{\left(x^*a_m^\dagger-xa_m\right)(2n+1)} \\ &\times \mathrm{e}^{\left(y^*a_m^\dagger-ya_m\right)\left(3n^2+3n+1\right)}\left|\alpha,m\right\rangle.\end{aligned} \quad (3.33)$$

In the remainder of this subsection, we simplify the above expression. Inserting identities $\sum_{k=0}^{\infty}\left|k\right\rangle\left\langle k\right|$ and $\sum_{n=0}^{\infty}\left|n\right\rangle\left\langle n\right|$ in the Hilbert space of the light field, the

mean optical field can be rewritten as

$$\begin{aligned}\langle a\rangle = \sum_{m=0}^{\infty}\sum_{k,n=0}^{\infty} & \frac{\bar{n}^m}{(1+\bar{n})^{1+m}} \\ & \times \langle \alpha, m| \, \alpha \mathrm{e}^{-\frac{1}{2}(x^*y-xy^*)\left(n^4+8n^3+10n^2+5n+1\right)} \\ & \times \mathrm{e}^{-i4k^2\lambda_0^4\left(4n^3+6n^2+4n+1\right)} \mathrm{e}^{i2k\lambda_0^3\left(3n^2+3n+1\right)} \\ & \times \mathrm{e}^{-i\lambda_0^2(2n+1)} \, |k,m\rangle \, \langle k,m| \, \mathrm{e}^{\left(x^*a_m^\dagger - xa_m\right)(2n+1)} \\ & \times \mathrm{e}^{\left(y^*a_m^\dagger - ya_m\right)\left(3n^2+3n+1\right)} \, |n,m\rangle \, \langle n,m|\alpha,m\rangle \end{aligned} \tag{3.34}$$

and using the relationship $\langle k|n\rangle = \delta_{n,k}$, we obtain

$$\begin{aligned}\langle a\rangle = \sum_{m=0}^{\infty}\sum_{n=0}^{\infty} & \frac{\bar{n}^m}{(1+\bar{n})^{1+m}} \, \langle \alpha|n\rangle \, \mathrm{e}^{i2k\lambda_0^3\left(3n^2+3n+1\right)} \mathrm{e}^{-i\lambda_0^2(2n+1)} \alpha \\ & \times \mathrm{e}^{-\frac{1}{2}(x^*y-xy^*)\left(n^4+8n^3+10n^2+5n+1\right)} \mathrm{e}^{-i4k^2\lambda_0^4\left(4n^3+6n^2+4n+1\right)} \\ & \times \langle m| \, \mathrm{e}^{\left(x^*a_m^\dagger - xa_m\right)(2n+1)} \mathrm{e}^{\left(y^*a_m^\dagger - ya_m\right)\left(3n^2+3n+1\right)} \, |m\rangle \, \langle n|\alpha\rangle \, . \end{aligned} \tag{3.35}$$

This expression can be evaluated straight-forwardly except for the expression

$$\langle m| \, \mathrm{e}^{\left(x^*a_m^\dagger - xa_m\right)(2n+1)} \mathrm{e}^{\left(y^*a_m^\dagger - ya_m\right)\left(4n^3+6n^2+4n+1\right)} \, |m\rangle \tag{3.36}$$

which we now evaluate. To shorten the notation, we define the variables

$$\upsilon = y\left(3n^2+3n+1\right) \tag{3.37}$$

$$\chi = x\left(2n+1\right). \tag{3.38}$$

We denote the displaced Fock state $\mathrm{e}^{\left(\upsilon^* a_m^\dagger - \upsilon a_m\right)} \, |m\rangle$ as $|\upsilon^*, m\rangle$. By definition

$$\langle m| \, \mathrm{e}^{\left(\chi^* a_m^\dagger - \chi a_m\right)} \mathrm{e}^{\left(\upsilon^* a_m^\dagger - \upsilon a_m\right)} \, |m\rangle = \langle -\chi^*, m|\upsilon^*, m\rangle \, . \tag{3.39}$$

Using the formula for the overlap of two displaced Fock states from Ref. [44], we have

$$\langle -\chi^*, m|\upsilon^*, m\rangle = \langle -\chi^*|\upsilon^*\rangle \, m! \sum_{j=0}^{m} \frac{\left(\upsilon^*+\chi^*\right)^{m-j} \left(-\chi-\upsilon\right)^{m-j}}{j! \, (m-j)! \, (m-j)!} \tag{3.40}$$

where

$$\langle -\chi^* | \upsilon^* \rangle = \exp\left\{ -\chi\upsilon^* - \frac{1}{2}\left(|\chi|^2 + |\upsilon|^2 \right) \right\}. \tag{3.41}$$

We now sum over the mechanical modes in the expression for $\langle a \rangle$ in Eq. (3.35). The sum is given by

$$\begin{aligned} &\sum_{m=0}^{\infty} \frac{\bar{n}^m}{(1+\bar{n})^{1+m}} \langle -\chi^*, m | \upsilon^*, m \rangle \\ &\qquad = \langle -\chi^* | \upsilon^* \rangle \sum_{m=0}^{\infty} \sum_{j=0}^{m} \frac{\bar{n}^m}{(1+\bar{n})^{m+1}} m! (-1)^{m-j} \frac{|\chi+\upsilon|^{2(m-j)}}{j!\left[(m-j)!\right]^2} \end{aligned} \tag{3.42}$$

To evaluate the above expression, replace $m-j$ with k. This gives us

$$\begin{aligned} &\sum_{m=0}^{\infty} \frac{\bar{n}^m}{(1+\bar{n})^{1+m}} \langle -\chi^*, m | \upsilon^*, m \rangle \\ &\qquad = \langle -\chi^* | \upsilon^* \rangle \sum_{k=0}^{m} \sum_{m=k}^{\infty} \frac{\bar{n}^m}{(1+\bar{n})^{m+1}} m! (-1)^k \frac{|\chi+\upsilon|^{2k}}{(m-k)!\,(k!)^2} \\ &\qquad = \langle -\chi^* | \upsilon^* \rangle \sum_{k=0}^{m} (-1)^k \frac{|\chi+\upsilon|^{2k}}{k!} \sum_{m=k}^{\infty} \binom{m}{k} \frac{\bar{n}^m}{(1+\bar{n})^{m+1}} \\ &\qquad = \langle -\chi^* | \upsilon^* \rangle \sum_{k=0}^{m} (-1)^k \frac{|\chi+\upsilon|^{2k} \bar{n}^k}{k!} \\ &\qquad = \langle -\chi^* | \upsilon^* \rangle \, \mathrm{e}^{-|\chi+\upsilon|^2 \bar{n}} \\ &\qquad = \mathrm{e}^{-\chi\upsilon^* - \frac{1}{2}\left(|\chi|^2+|\upsilon|^2\right)} \mathrm{e}^{-|\chi+\upsilon|^2\bar{n}}. \end{aligned} \tag{3.43}$$

Rewriting the expression back in terms of the original variables x, y and n, we get

$$\begin{aligned} \mathrm{e}^{-\chi\upsilon^* - \frac{1}{2}\left(|\chi|^2+|\upsilon|^2\right)} \mathrm{e}^{-|\chi+\upsilon|^2\bar{n}} &= \mathrm{e}^{-xy^*(2n+1)\left(3n^2+3n+1\right)} \\ &\quad \times \mathrm{e}^{-\frac{1}{2}\left(|x|^2(2n+1)^2+|y|^2\left(3n^2+3n+1\right)^2\right)} \\ &\quad \times \mathrm{e}^{-\left|x(2n+1)+y\left(3n^2+3n+1\right)\right|^2 \bar{n}}. \end{aligned} \tag{3.44}$$

Also note that the other terms that are in the expression for $\langle a \rangle$ are given by

$$\langle \alpha | n \rangle \langle n | \alpha \rangle = \mathrm{e}^{-|\alpha|^2} \frac{|\alpha|^{2n}}{n!}. \tag{3.45}$$

Plugging the expressions Eqs. (3.44) and (3.45) back into the expression for $\langle a \rangle$ Eq. (3.35), we obtain

$$\begin{aligned}\langle a \rangle = \sum_{n=0}^{\infty} \alpha \mathrm{e}^{-|\alpha|^2} \frac{|\alpha|^{2n}}{n!} \mathrm{e}^{-\frac{1}{2}(x^* y - x y^*)\left(n^4+8n^3+10n^2+5n+1\right)} \\ \times \mathrm{e}^{-i\lambda_0^2(2n+1)} \mathrm{e}^{-i4k^2\lambda_0^4\left(4n^3+6n^2+4n+1\right)} \\ \times \mathrm{e}^{i2k\lambda_0^3\left(3n^2+3n+1\right)} \mathrm{e}^{-xy^*(2n+1)\left(3n^2+3n+1\right)} \\ \times \mathrm{e}^{-\frac{1}{2}\left(|x|^2(2n+1)^2+|y|^2\left(3n^2+3n+1\right)^2\right)} \\ \times \mathrm{e}^{-\left|x(2n+1)+y\left(3n^2+3n+1\right)\right|^2 \bar{n}}\end{aligned} \tag{3.46}$$

which is exact for the given expression for U in Eq. (3.5). This expression can be evaluated numerically for a more accurate estimation of the phase. However, to obtain a qualitative estimate, we evaluate it using the saddle point approximation (to leading order in N_p) and find

$$\begin{aligned}\langle a \rangle = \alpha \mathrm{e}^{-\frac{1}{2}\left(4|x|^2 N_p^2+9|y|^2 N_p^4\right)} \\ \times \mathrm{e}^{-\frac{1}{2}(x^* y - x y^*) N_p^4 - i2\lambda_0^2 N_p - i16k^2\lambda_0^4 N_p^3 + i6k\lambda_0^3 N_p^2} \\ \times \mathrm{e}^{\left(4|x|^2 N_p^2+9|y|^2 N_p^4+6(xy^*+x^*y)N_p^3\right)\bar{n}}.\end{aligned} \tag{3.47}$$

We note that this approximation may not be valid for all cases, for instance when the terms ignored by the approximation are much larger than the quantum gravity signal.

Expressing $\langle a \rangle$ in terms of an amplitude and phase

$$\langle a \rangle = \alpha' \mathrm{e}^{-i\Phi_{QM}}, \tag{3.48}$$

we find that the new amplitude is

$$\alpha' = \alpha \mathrm{e}^{-\frac{1}{2}\left(4|x|^2 N_p^2+9|y|^2 N_p^4\right)} \mathrm{e}^{\left(4|x|^2 N_p^2+9|y|^2 N_p^4+6(xy^*+x^*y)N_p^3\right)\bar{n}} \tag{3.49}$$

and the new phase is

$$\Phi_{QM} = \frac{1}{2i}\left(x^* y - x y^*\right) N_p^4 + 2\lambda_0^2 N_p + 16k^2\lambda_0^4 N_p^3 - 6k\lambda_0^3 N_p^2 \tag{3.50}$$

which on substituting with x and y from Eqs. (3.10) and (3.11) gives

$$\Phi_{QM} = 2\lambda_0^2 N_p - 6k\lambda_0^3 N_p^2 + 16k^2\lambda_0^4 N_p^3. \tag{3.51}$$

This is the phase that light acquires from the optomechanical Hamiltonian. Also including the contribution from the quantum gravitational deformed commutators, we find the total phase

$$\Phi_T = \Phi_{QG} + 2\lambda_0^2 N_p - 6k\lambda_0^3 N_p^2 + 16k^2\lambda_0^4 N_p^3. \tag{3.52}$$

and

$$\Phi_{QG} = \begin{cases} \frac{4}{3}\beta'\lambda_0^4 N_p^3 & \beta_0 \text{ case} \\ -\frac{3}{2}\gamma\lambda_0^3 N_p^2 & \gamma_0 \text{ case} \\ 2\mu\lambda_0^2 N_p & \mu_0 \text{ case,} \end{cases} \tag{3.53}$$

which differs from the phase obtained in Eq. (2.18).

The assumptions made in the calculation of the phase in this subsection and their validities are discussed in Section 4.4.

3.1.2 Contribution of the higher order terms

Comparing these results with those obtained in Eq. (2.18), we observe that we have the extra contribution $-6k\lambda_0^3 N_p^2 + 16k^2\lambda_0^4 N_p^3$. In Table 3.1, we evaluate the magnitude of this contribution for the experimental parameters suggested in Ref. [3] (Table 2.1) and compare it to the minimum uncertainty in the phase due to quantum mechanical fluctuations and the expected magnitude of the quantum gravity signal.

Description	Terms	μ_0 case	γ_0 case	β_0 case
Quantum gravity phase	Φ_{QG}	10^{-4}	4×10^{-9}	3×10^{-10}
Min. phase uncertainty	$\frac{1}{2\sqrt{N_p N_r}}$	5×10^{-7}	2×10^{-8}	5×10^{-10}
QM phase from [3]	$2\lambda_0^2 N_p$	4×10^2	10^4	10^6
From higher order terms	$-6k\lambda_0^3 N_p^2 + 16k^2\lambda_0^4 N_p^3$	0.2	45	7×10^5

Table 3.1: Magnitude of terms using the parameters suggested by Pikovski *et al.*. Note that the contribution from the higher order terms is much larger than both the signal due to quantum gravity and the minimum phase uncertainty. Reproduced from Ref [1].

We see that these extra terms are larger than both the minimum uncertainty and the quantum gravity signal and therefore cannot be ignored. Ignoring them leads to overestimation of the quantum gravity parameters.

In summary, higher order terms in the cavity Hamiltonian have to be considered while calculating the quantum gravity phase Φ_{QG} from the total phase Φ_T. This is done in Section 3.3.

3.2 Revisiting analysis: Precision

In this section, we show that the precision of the proposal of Ref. [3] is lowered in a more careful analysis. The precision calculation of Ref. [3] considers the uncertainty in the measurement of the total phase, $\Delta\Phi_T$, as can be seen in Eq. (2.23). However, the uncertainty in the average number of photons in each laser pulse, ΔN_p, is not considered. We show here that since the experiment requires very high precision, it is crucial to also account for uncertainty in the mean photon number.

The analysis of Ref. [3] assumes that the mean photon number is known precisely before the experiment measuring the phase and that it remains unchanged during the entire run of the experiment. However, on the one hand, the required

precision of the mean photon number will necessitate large experimental time for its measurement. On the other hand, even if an exceedingly precise measurement of the photon number is performed at the beginning of the experiment, lasers suffer from classical intensity fluctuations and drifts due to which the mean photon number becomes increasingly uncertain over time. Thus, the uncertainty in the mean photon number must be accounted for.

3.2.1 Noise models to account for photon number uncertainty

Here we consider two schemes to account for this uncertainty. In the first scheme, the intensity is measured repeatedly before each run of the experiment, for example by impinging the laser pulses on a low-reflectivity beamsplitter and performing intensity measurement on the reflected light, and the transmitted light is discarded (other methods for measuring mean-photon number will lead to a similar analysis). By repeatedly measuring the light intensity, the effects of classical intensity fluctuations are eliminated because the remaining pulses, which are used in the QG parameter estimation, will have photon number close to the measured preceding pulses. However, the mean photon number precision attained in these frequent measurements is limited by quantum shot noise, which we account for below. In the second scheme, the laser intensity is similarly measured once with very high precision in the beginning of the experiment such that the effect of the quantum noise is minimised as we explain below. The uncertainty in photon number is now dominated by classical fluctuation in photon number. The actual experimental method and the error model would depend strongly on the experimental considerations, for instance the time and experimental complexity required to perform each

kind of measurement in the lab and the amount of classical and quantum noise present. We now describe the schemes in detail.

Quantum-noise-limited scheme: Here we propose a scheme in which the mean photon number is estimated by measuring the photon number before each run of the phase measurement. Thus, the quantum gravity parameter estimation is performed before the mean photon number of the laser can fluctuate significantly. While now the classical fluctuations do not contribute to the mean photon number uncertainty, the measured mean photon number unavoidably suffers from quantum uncertainty. Specifically, if R measurements of the photon number are made, the error in the mean photon number ΔN_p due to quantum uncertainty is $\sqrt{N_p/R}$. For high-intensity pulses, the uncertainty from classical fluctuations is usually much larger than the quantum uncertainty even for a single ($R = 1$) photon-number measurement, in which case this model is useful as it provides a lower bound on the intensity fluctuations experienced in the experiment. In this analysis, we consider the case of $R = 1$ for simplicity.

Classical-noise-limited scheme: The second scheme to measure the laser intensity precisely (using feedback and a long measurement time) once before the experiment begins. For this single measurement performed in the beginning of the experiment, effectively $R \to \infty$ so there is no contribution from quantum noise, and we call this scheme classical-noise limited. We then perform the quantum gravity parameter estimation assuming that the mean photon number remains unchanged for the duration of the many runs of the experiment. In this case, the uncertainty in mean photon number arises from classical fluctuations of the form $\Delta N_p = \epsilon N_p$. The relative error from classical fluctuations in photon number for short, high-intensity pulses (as required in the experiment) is of the order of 10^{-3}

to 10^{-2} after stabilising the laser intensity. These values are calculated under the assumption that the relative error in laser intensity is $\epsilon = 10^{-4}$ over a few hours, which might be attainable in the near future for the short, high intensity pulses that are required in this experiment. The actual model would be something in between these two schemes described here.

3.2.2 Precision calculation of quantum gravity parameters

Here we present an analysis of the precision of the quantum gravity parameters under both these schemes. An outline of the calculations is as follows. We express the quantum gravity parameter as a function of the total measured phase and the average number of photons by substituting Eqs. (3.51) and (3.53) in

$$\Phi_{QG} = \Phi_T - \Phi_{QM} \tag{3.54}$$

and use standard techniques in error propagation [45] to determine the variance in the calculated parameter. The variance of the estimated quantum gravity parameter is expressed as a function of the variances and covariance of the measured quantities N_p and Φ_T. The calculations for the γ_0 model are detailed below.

We begin by rewriting the quantum gravity contribution to the phase Eq. (3.53) as

$$\Phi_{QG} = -\gamma_0 \kappa \lambda_0^3 N_p^2 \quad \text{where} \quad \kappa := \frac{3\sqrt{\hbar m \omega}}{2 M_p c}. \tag{3.55}$$

Expressing γ_0 in terms of Φ_T and N_p, we get

$$\gamma_0 = \frac{-1}{\kappa \lambda_0^3} \left(\frac{\Phi_T}{N_p^2} \right) + \frac{2}{\kappa \lambda_0 N_p} - \frac{6k}{\kappa} + \frac{16 k^2 \lambda_0 N_p}{\kappa} \tag{3.56}$$

and the variance in γ_0 is given by [45]

$$(\Delta\gamma_0)^2 = \left(\frac{1}{\kappa\lambda_0^3 N_p^2}\right)^2 (\Delta\Phi_T)^2 + \left(\frac{2\Phi_T}{\kappa\lambda_0^3 N_p^3} - \frac{2}{\kappa\lambda_0 N_p^2} + \frac{16k^2\lambda_0}{\kappa}\right)^2 (\Delta N_p)^2 \tag{3.57}$$

for one run of the experiment.

The incident light is in a coherent state but the outgoing light is not because its state gets distorted under the action of the four-displacement operator U. The standard deviation of Φ_T for such a distorted state is given by

$$\Delta\Phi_T \approx \sqrt{\frac{1}{4N_p} + \sin^2\left(\lambda_0^2 + 6k\lambda_0^3 N_p\right)} \tag{3.58}$$

whose calculations are detailed in Section 4.1. The value of error in photon number depends on the experimental scheme used, as described above. In the quantum-noise-limited scheme, the standard deviation in the the inferred photon number is given by $\Delta N_p = \sqrt{N_p}$ whereas in the classical-noise-limited scheme, the uncertainty in inferred photon number is given by $\Delta N_p = \epsilon N_p$. Since the phase and intensity measurements are performed on different pulses, the covariance is zero. We also note that for the experimental parameters suggested by Ref. [3] (Table 2.1), the effect of the distortion is negligible. However, we present it here for the sake of completeness.

The variance in γ_0 should ideally be calculated by measuring the values and variances of the total phase and number of photons. However, to numerically estimate the precision, we substitute the expression for Φ_T from Eq. (3.52) and assume that $\gamma_0 \sim 0$. For the experimental parameters in Table 2.1, we obtain the value of the variance $(\Delta\gamma_0)^2$ to be 10^{14} (5×10^{16}) in the quantum-noise-limited

(classical-noise-limited) scheme. Hence, in order to have $(\Delta\gamma_0)^2 \sim 1$, we need to perform the experiment $N_r = 10^{14}$ (5×10^{16}) times.

The number of experimental runs as predicted by Ref. [3] is $N_r = 10^5$. The difference arises because the first term of Eq. (3.57) (the uncertainty in phase) is considered by Ref. [3] in the calculation of variance (Eq. (2.23)) but the second term accounting for uncertainty in mean number of photons is ignored.

Similar calculations are performed for the β_0 and μ_0 cases (details in Section 3.5) and the required number of experimental runs is listed in Table 3.2.

Required number of runs	μ_0 case	γ_0 case	β_0 case
Suggested in Ref. [3]	1	10^5	10^6
Including $\Delta N_p = \sqrt{N_p}$	10^5	10^{14}	10^{19}
Including $\Delta N_p = \epsilon N_p$	10^5	5×10^{16}	10^{25}

Table 3.2: Required number of experimental runs in Pikovski *et al.* versus when accounting for uncertainty in number of photons ΔN_p (quantum- and classical-noise-limited schemes, with $\epsilon = 10^{-4}$) for different phenomenological models. Reproduced from Ref [1].

In summary, we see that the required number of experimental runs can be many orders of magnitude larger when the uncertainty in the number of photons is accounted for. This large increase in the number of experimental runs makes the experimental scheme no longer feasible for the same precision. Hence, we must modify the scheme for it to be feasible.

3.3 Improved phase space paths to reduce the experimental requirement

In this section, we suggest modifications to the proposal of Ref. [3] to make the scheme experimentally feasible by reducing the required number of experimental

runs. Specifically, we suggest different pulse sequences of the laser pulses, corresponding to a different path in phase space, to reduce the required number of experimental runs by many orders of magnitude. We also ensure that the calculated quantum gravity parameters are accurate by taking into account the higher order terms of the cavity Hamiltonian in these calculations.

The remainder of this section is organised as follows. We first describe the path in phase space that reduces the required number of runs. We then calculate the phase acquired by light due to the action of the unitary operator that effects this path. From the expression of the acquired phase, we calculate the variance in the estimated QG parameter and therefore the required number of runs for the same experimental parameters as before and show that the number of runs is many orders of magnitude smaller.

In all calculations in this section, we focus on the γ_0 commutator (Eq. (1.14)). Results from similar calculations in the β_0 and μ_0 (Eqs. (1.1) and (1.12)) commutators are described in Section 3.5.

3.3.1 Improved phase space paths

Examining the expression for the variance in γ_0 in Eq. (3.57), we notice that most of the contribution to the variance in the quantum gravity parameters comes from the quantum mechanical terms. So, reducing the quantum mechanical contribution can reduce the variance, and therefore the number of runs required to attain a set precision. Here, we use different pulse sequences to reduce the quantum mechanical contribution and hence the variance.

In order to come up with better pulse sequences, it is helpful to graphically

visualise the pulse sequence on Ref. [3]. The unitary operator in Eq. (2.10)

$$U = \mathrm{e}^{i\lambda nP}\mathrm{e}^{-i\lambda nX}\mathrm{e}^{-i\lambda nP}\mathrm{e}^{i\lambda nX} \tag{3.59}$$

can be interpreted as a series of displacement operators in the X, P phase space of the mechanical oscillators with the same amplitude of displacement, which results in coming back to the same point in phase space. This is represented by a square in Fig. 3.1. The solid circle represents the starting point and the hollow circle the ending point.

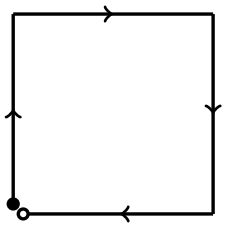

Figure 3.1: U: The loop in the X, P phase space of the mechanical oscillator as per the experimental scheme of Pikovski *et al.* Figure reproduced from Ref [1]. ©2018 APS

The new path to reduce the number of runs is composed of four such rectangular loops. Each of the loops is similar to that described by Eq. (2.10) and Fig. 3.1, but starts at a different point on the rectangle, sometimes even outside the rectangle. This four-loop path in phase space corresponds to the unitary operator

$$U_{\gamma_0} = U_1 U_2^\dagger U_3^\dagger U_4 \tag{3.60}$$

where the individual components are given by

$$\begin{aligned}
U_1 &= \mathrm{e}^{-2iH_X}\mathrm{e}^{-iH_P}\mathrm{e}^{iH_X}\mathrm{e}^{iH_P}\mathrm{e}^{iH_X} \\
U_2 &= \mathrm{e}^{-\frac{7}{3}iH_X}\mathrm{e}^{-iH_P}\mathrm{e}^{iH_X}\mathrm{e}^{iH_P}\mathrm{e}^{\frac{4}{3}iH_X} \\
U_3 &= \mathrm{e}^{\frac{2}{3}iH_P}\mathrm{e}^{-iH_X}\mathrm{e}^{-iH_P}\mathrm{e}^{iH_X}\mathrm{e}^{\frac{1}{3}iH_P} \\
U_4 &= \mathrm{e}^{iH_P}\mathrm{e}^{-iH_X}\mathrm{e}^{-iH_P}\mathrm{e}^{iH_X}.
\end{aligned} \tag{3.61}$$

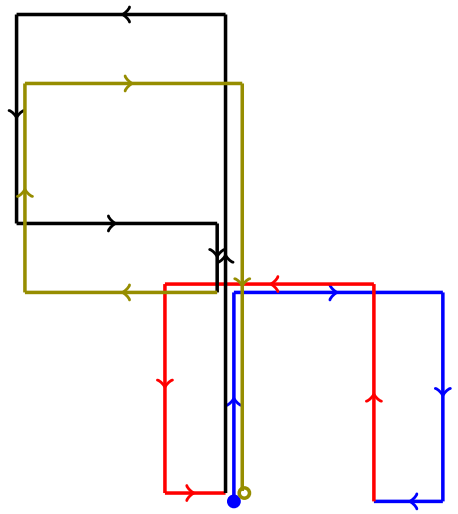

Figure 3.2: U_{γ_0}: The final shape of the path in phase space to remove QM contribution for the γ commutator. The system starts at the filled dot and ends at the unfilled dot. The paths are staggered for clarity, but actually overlap. Figure reproduced from Ref [1].

When the four loops are put together to obtain the composite loop, some parts of the path cancel and the final path is depicted in Fig. 3.2. Even though the individual operators are strictly not displacement operators because of the higher order corrections, we represent the path in such a figure for easier visualisation. However, we note that the higher order terms would lead to squeezing-like behaviour, which is not captured in this representation. The steps to arrive at such a path are detailed in the next subsection. Depending on the coherence time of the experimental setup, we can also design paths that are made of smaller or larger number of loops as described below.

Experimental realisation of a square path in phase space (Fig. 3.1) can be performed using a pulsed optomechanics setup described by Ref. [3]. Specifically, the transformation of Fig. 3.1 is implemented by alternating between phase-space translations along X and P axes using an optical loop to introduce time delays.

The composite rectangular paths in phase space (Fig. 3.2) of our proposal needs variable time delays, which can be realised by introducing an additional optical loop into the Ref. [3] setup. This additional loop is required to be connected to the original optical loop with fast switching, which can be implemented for instance by electro-optical modulation [46].

3.3.2 Arriving at the improved loops in phase space

The steps to arrive at the sophisticated path are outlined here. First, we consider unitary operators which describe arbitrary rectangular pulse sequences. Such unitary operators are given by U_X and U_P, where changing the values of a, b and c changes the dimensions of the loop and also determines the starting point. The operators are given by

$$U_X = \mathrm{e}^{-iaH_X}\mathrm{e}^{-icH_P}\mathrm{e}^{ibH_X}\mathrm{e}^{icH_P}\mathrm{e}^{-i(b-a)H_X} \tag{3.62}$$

and

$$U_P = \mathrm{e}^{iaH_P}\mathrm{e}^{-icH_X}\mathrm{e}^{-ibH_P}\mathrm{e}^{icH_X}\mathrm{e}^{i(b-a)H_P} \tag{3.63}$$

and are represented as loops in phase space in Figs. 3.3 and 3.4.

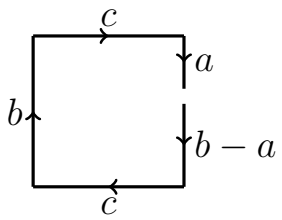

Figure 3.3: Shape of the path in phase space corresponding to U_X. Figure reproduced from Ref [1]. ©2018 APS

We then fix the number of loops that we want the sophisticated path to be made of. More paths can reduce the required number of runs, but they also increase

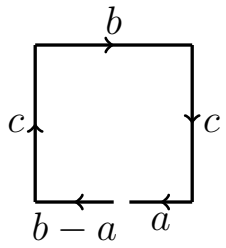

Figure 3.4: Shape of the path in phase space corresponding to U_P. Figure reproduced from Ref [1]. ©2018 APS

the required coherence time. Also, calculating the final phase of light can be more computationally intense with a larger number of loops. So, depending on the coherence time, the number of loops can be chosen. In this case, we choose four loops, two like U_X and two like U_P.

Once the loops are chosen, we express the final unitary operator as a single exponential of a sum of operators like in Eq. (3.5) instead of a product of exponentials using the BCH formula. This is done using Mathematica package [42]. The final simplified unitary operator is expressed as a function of the parameters $\{a_i, b_i, c_i\}; i = 1, 2, 3, 4$ for the four loops.

We order the resulting terms in order of descending magnitude of how much these terms contribute to the final phase of light. In this ordering, we assume that the ordering is the same if we directly substitute the experimental parameters in the operators (i.e., replacing the operator n with the average number of photons N_p).

Once the ordering is done, we choose values of the parameters $\{a_i, b_i, c_i\}$ such that the coefficients of the largest m quantum mechanical terms are zero, while the coefficient of the quantum gravity term is nonzero. We choose the largest m possible such that the solutions $\{a_i, b_i, c_i\}$ exist. This is how we determine a path in

phase space that can minimize the quantum mechanical contribution while keeping the quantum gravity contribution non-zero to arrive at Eq. (3.60).

3.3.3 Calculation of phase from the new paths

Here, we calculate the phase acquired by light due to the action of the unitary operator U_{γ_0} in Eq. (3.60).

We begin by first expressing U_{γ_0} as a single exponential by evaluating the BCH formula up to the sixth order. This is done using Mathematica code [42] to obtain the result

$$U_{\gamma_0} = \exp\left\{-i\left(\frac{1}{3}\gamma\lambda_0^3 n^3 - \frac{40}{3}k^3\lambda_0^5 n^5 + 24k^4\lambda_0^6 n^6 + \frac{\sqrt{2}}{3}k^2\lambda_0^3 n^3\left((-1-i)\,a - (1-i)\,a^\dagger\right)\right)\right\}. \tag{3.64}$$

Following similar calculations as in Section 3.1, we find that the mean optical field is given by the expression

$$\begin{aligned}\langle a\rangle = \sum_{n=0}^{\infty} \alpha \mathrm{e}^{-|\alpha|^2}\frac{|\alpha|^{2n}}{n!}\mathrm{e}^{-\frac{i}{3}\gamma\lambda_0^3\left(3n^2+3n+1\right)} \\ \times\, \mathrm{e}^{i\frac{40}{3}k^3\lambda_0^5\left(5n^4+10n^3+10n^2+5n+1\right)} \\ \times\, \mathrm{e}^{-i24k^4\lambda_0^6\left(6n^5+15n^4+20n^3+15n^2+6n+1\right)} \\ \times\, \mathrm{e}^{-\frac{4}{9}k^4\lambda_0^6\left(3n^2+3n+1\right)^2\left(\bar{n}+\frac{1}{2}\right)}\end{aligned} \tag{3.65}$$

which can be evaluated numerically if higher accuracy is required. Using the saddle point approximation like in Section 3.1.1, the phase acquired by the outgoing light is then evaluated to be

$$\Phi_T = \gamma\lambda_0^3 N_p^2 - \frac{200}{3}k^3\lambda_0^5 N_p^4 + 144k^4\lambda_0^6 N_p^5 + \frac{4840}{9}k^5\lambda_0^7 N_p^6. \tag{3.66}$$

In the calculation of the phase, several assumptions have been made. Details about these assumptions and a discussion regarding their validity are presented in Section 4.4.

3.3.4 Calculation of improved precision

The parameter γ_0 is estimated from the total measured phase by subtracting the rest of the terms (that arise from quantum mechanics alone). The variance in the estimated γ_0 for one run of the experiment is calculated below. If the experiment is performed N_r number of times, the variance reduces by a factor of N_r. We calculate the number of runs required to for the variance to be of order 1, i.e., $(\Delta\gamma_0)^2 \sim 1$.

Here we calculate the uncertainty in γ_0 assuming that we know λ_0 exactly, but neither the total measured phase Φ_T nor the average number of photons in the optical state N_p. The calculations and assumptions here are similar to those in Section 3.2.

In order to estimate the variance, we use Eq. (3.66), to express γ_0 as a function of the experimentally measured quantities Φ_T and N_p.

$$\gamma_0 = \frac{1}{\kappa\lambda_0^3}\left(\frac{\Phi_T}{N_p^2}\right) + \frac{200\lambda_0^2 k^3}{3\kappa}N_p^2 - \frac{144\lambda_0^3 k^4}{\kappa}N_p^3 - \frac{4840\lambda_0^4 k^5}{9\kappa}N_p^4. \tag{3.67}$$

where

$$\kappa := \frac{\sqrt{\hbar m\omega}}{M_p c}. \tag{3.68}$$

Using standard techniques in error propagation [45], we determine the uncertainty in γ_0 to be

$$\begin{aligned}(\Delta\gamma_0)^2 = &\left(\frac{1}{\kappa\lambda_0^3 N_p^2}\right)^2 (\Delta\Phi_T)^2 \\ &+ \left(-\frac{2\Phi_T}{\kappa\lambda_0^3 N_p^3} + \frac{400\lambda_0^2 k^3}{3\kappa}N_p - \frac{432\lambda_0^3 k^4}{\kappa}N_p^2\right)^2 (\Delta N_p)^2\end{aligned} \tag{3.69}$$

for one run of the experiment. The uncertainty in photon number is

$$\Delta N_p = \sqrt{N_p} \quad \text{or} \quad \Delta N_p = \epsilon N_p \tag{3.70}$$

depending on the experimental scheme used, as described in Section 3.2. We also note that the state of light after the action of the unitary operator is no longer coherent but distorted, albeit by a small quantity. However for the sake of completeness, we calculate the standard deviation of Φ_T for such a distorted state in Section 4.1 and is given by

$$\Delta\Phi_T \approx \sqrt{\frac{1}{4N_p} + \sin^2\left(360k^4\lambda_0^6 N_p^4 - \frac{400}{3}k^3\lambda_0^5 N_p^3\right)}. \tag{3.71}$$

Using this analysis, we estimate the value of the variance for experimental parameters suggested by Ref. [3] and obtain $(\Delta\gamma_0)^2 = 6 \times 10^5$ with either of the error models for ΔN_p estimation. The value is the same in both schemes because we have now successfully eliminated contribution from ΔN_p terms for these experimental parameters and all the contribution is from $\Delta\Phi_T$ terms. The number of experimental runs required to have $(\Delta\gamma_0)^2 = 1$ is

$$N_r = 6 \times 10^5, \tag{3.72}$$

as opposed to 10^{14} or 5×10^{16} runs required if we perform only the single loop. We also note that for the given experimental parameters, the effect of the distortion of the state is negligible but is presented here for completeness.

In summary, we can increase the sensitivity of the experiment to possible quantum gravity effects by using sophisticated paths in phase space. These changes significantly improve the prospects for realising tests of quantum gravity experimentally with near-future quantum technology.

3.4 Squeezed states to improve precision

In this section, we show that the precision in the estimated QG parameter can be further increased by using squeezed states of light.

We see from Eq. (3.69) that the variance in γ_0 depends both on $\Delta\Phi_T$ and ΔN_p. Plugging in the experimental parameters suggested by Ref. [3], we see that in the γ_0 case, the contribution from the $\Delta\Phi_T$ term is the largest. Therefore, we can perform the experiment using light squeezed in the phase Φ_T so that $\Delta\Phi_T$ is reduced at the expense of ΔN_p thereby improving precision. For different experimental parameters, if the contribution to the variance is larger from ΔN_p, then light squeezed in photon number improves precision.

To calculate the effect of squeezing quantitatively, we first recap and derive some results about the number and phase properties of squeezed light.

3.4.1 Number and phase statistics of squeezed states

First, we introduce some notation and an assumption regarding the state of light used. To understand how using squeezed states affects the uncertainty in the signal, we consider ideal squeezed states, which are defined as squeezed vacuum states which are displaced in phase space. The state is given by

$$|\alpha, r\rangle = D(\alpha)S(r)\,|0\rangle \tag{3.73}$$

where $S(r)$ is the squeezing operator with squeezing parameter r

$$S(r) = \exp\left(\frac{ra_m^2 - ra_m^{\dagger 2}}{2}\right) \tag{3.74}$$

and $D(\alpha)$ is the displacement operator displacement vector α

$$D(\alpha) = \exp\left(\alpha a_m^\dagger - \alpha^* a_m\right) \tag{3.75}$$

where $a_m^\dagger$ and a_m are the creation and annihilation operators respectively.

In calculating the uncertainties in the final measured phase of light due to it being in a squeezed state, we assume that the final state can be described by an ideal squeezed state with squeezing parameter r and displacement α. The final state that is measured can be described by an ideal squeezed state if the unitary operator only rotates the state and does not distort it as illustrated in Fig. 3.5.

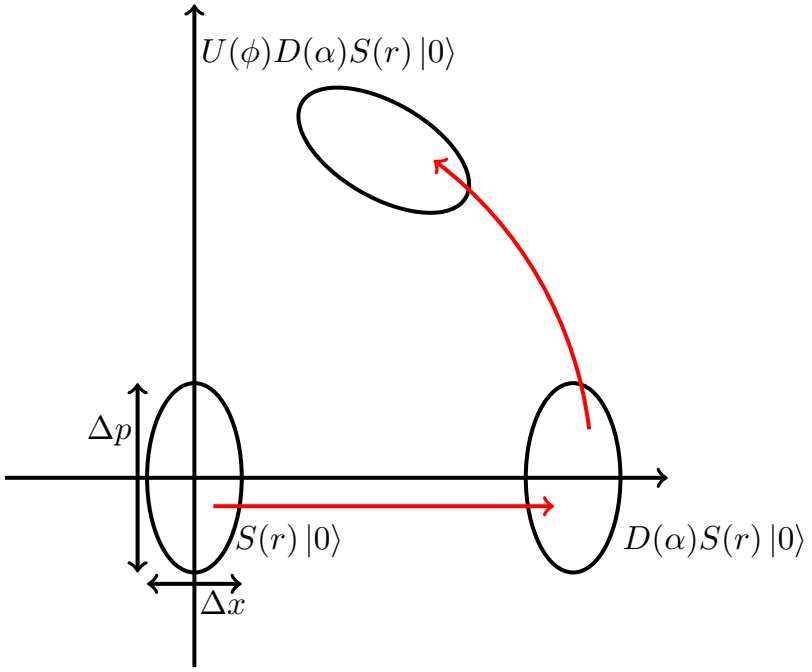

Figure 3.5: A rotated displaced squeezed state for real displacement vector α. Figure reproduced from Ref [1]. ©2018 APS

In the next subsections, we calculate the average photon number $N_p = \langle \hat{n} \rangle$, the uncertainty in the number of photons $\Delta N_p = \sqrt{\langle (\Delta \hat{n})^2 \rangle}$ and the uncertainty in the total phase $\Delta \Phi_T$ in terms of the squeezing parameter and displacement vector. In

order to calculate these quantities, we use the relations

$$D^\dagger(\alpha) a D(\alpha) = a + \alpha \tag{3.76}$$

$$D^\dagger(\alpha) a^\dagger D(\alpha) = a^\dagger + \alpha^*, \tag{3.77}$$

and

$$S^\dagger(r) a S(r) = a \cosh r - a^\dagger \sinh r \tag{3.78}$$

$$S^\dagger(r) a^\dagger S(r) = a^\dagger \cosh r - a \sinh r \tag{3.79}$$

which can be derived from the definitions Eq. (3.75) and Eq. (3.74).

Calculation of average photon number in a displaced squeezed state

The average photon number is given by

$$N_p = \langle \hat{n} \rangle \tag{3.80}$$

$$= \langle \alpha, r | a^\dagger a | \alpha, r \rangle \tag{3.81}$$

$$= \langle 0 | S^\dagger D^\dagger a^\dagger a D S | 0 \rangle \,. \tag{3.82}$$

We now evaluate $D^\dagger a^\dagger a D$ using Eq. (3.76) and Eq. (3.77) to obtain

$$D^\dagger a^\dagger a D = D^\dagger a^\dagger D D^\dagger a D \tag{3.83}$$

$$= \left(a^\dagger + \alpha^*\right)(a + \alpha) \tag{3.84}$$

$$= a^\dagger a + \alpha a^\dagger + \alpha^* a + |\alpha|^2. \tag{3.85}$$

Using Eq. (3.78) and Eq. (3.79), we see that

$$S^\dagger D^\dagger a^\dagger a D S = S^\dagger a^\dagger a S + \alpha S^\dagger a^\dagger S + \alpha^* S^\dagger a S + |\alpha|^2 S^\dagger S \tag{3.86}$$

$$\begin{aligned} &= \left(a^\dagger \cosh r - a \sinh r\right)\left(a \cosh r - a^\dagger \sinh r\right) \\ &\quad + \alpha \left(a^\dagger \cosh r - a \sinh r\right) \\ &\quad + \alpha^* \left(a \cosh r - a^\dagger \sinh r\right) + |\alpha|^2. \end{aligned} \tag{3.87}$$

The surviving terms in $\langle 0|S^\dagger D^\dagger a^\dagger a D S|0\rangle$ are

$$\langle 0|S^\dagger D^\dagger a^\dagger a D S|0\rangle = \langle 0|aa^\dagger|0\rangle \sinh^2 r + |\alpha|^2. \tag{3.88}$$

This gives

$$N_p = |\alpha|^2 + \sinh^2 r. \tag{3.89}$$

Calculation of spread in photon number in a displaced squeezed state

The uncertainty in the photon number is defined as

$$\Delta N_p = \sqrt{\langle (\Delta\hat{n})^2\rangle} \tag{3.90}$$

$$= \sqrt{\langle \hat{n}^2\rangle - \langle \hat{n}\rangle^2}. \tag{3.91}$$

We begin by evaluating $\langle \hat{n}^2\rangle$. Writing it explicitly, we have

$$\langle \hat{n}^2\rangle = \langle \alpha, r|a^\dagger a a^\dagger a|\alpha, r\rangle \tag{3.92}$$

$$= \langle 0|S^\dagger D^\dagger a^\dagger a a^\dagger a D S|0\rangle\,. \tag{3.93}$$

We evaluate $D^\dagger a^\dagger a a^\dagger a D$ using Eq. (3.85) to obtain

$$D^\dagger a^\dagger a a^\dagger a D = \left(a^\dagger a + \alpha a^\dagger + \alpha^* a + |\alpha|^2\right)^2. \tag{3.94}$$

Only terms with even number of operators in the above expression contribute to the calculation of $\langle \hat{n}^2\rangle$. Keeping only such contributing terms, we get

$$\begin{aligned}\langle \hat{n}^2\rangle =& \alpha^2 \langle 0|S^\dagger a^{\dagger 2} S|0\rangle + \alpha^{*2} \langle 0|S^\dagger a^2 S|0\rangle + |\alpha|^2 + |\alpha|^4 \\ &+ \langle 0|S^\dagger a^\dagger a a^\dagger a S|0\rangle + 4|\alpha|^2 \langle 0|S^\dagger a^\dagger a S|0\rangle\,.\end{aligned} \tag{3.95}$$

Using Eq. (3.78) and Eq. (3.79) and simplifying, we find

$$\begin{aligned}\langle \hat{n}^2\rangle =& 2\sinh^2 r \cosh^2 r + \sinh^4 r - \alpha^{*2} \sinh r \cosh r \\ &- \alpha^2 \sinh r \cosh r + 4|\alpha|^2 \sinh^2 r \\ &+ |\alpha|^2 + |\alpha|^4.\end{aligned} \tag{3.96}$$

To calculate $\langle\hat{n}\rangle^2$, recall that from Eq. (3.89) we have

$$\langle\hat{n}\rangle = |\alpha|^2 + \sinh^2 r. \tag{3.97}$$

We now calculate the variance in the photon number to be

$$\begin{aligned}\langle(\Delta\hat{n})^2\rangle &= \langle\hat{n}^2\rangle - \langle\hat{n}\rangle^2 &(3.98)\\ &= 2\sinh^2 r\cosh^2 r + \sinh^4 r - \alpha^{*2}\sinh r\cosh r \\ &\quad - \alpha^2\sinh r\cosh r + 4|\alpha|^2\sinh^2 r + |\alpha|^2 + |\alpha|^4 \\ &\quad - \left(|\alpha|^4 + \sinh^4 r + 2|\alpha|^2\sinh^2 r\right) &(3.99)\\ &= 2\sinh^2 r\cosh^2 r + |\alpha|^2 - \alpha^{*2}\sinh r\cosh r \\ &\quad - \alpha^2\sinh r\cosh r + 2|\alpha|^2\sinh^2 r. &(3.100)\end{aligned}$$

Writing $\alpha := |\alpha|e^{i\phi}$, we rewrite the above expression as

$$\begin{aligned}\langle(\Delta\hat{n})^2\rangle =& \frac{1}{2}\sinh^2 2r + |\alpha|^2\left(1 + 2\sinh^2 r\right. \\ & \left. -2\sinh r\cosh r\cos 2\phi\right)\end{aligned} \tag{3.101}$$

which can be rewritten as

$$\langle(\Delta\hat{n})^2\rangle = \frac{1}{2}\sinh^2 2r + |\alpha|^2\left(e^{2r}\sin^2\phi + e^{-2r}\cos^2\phi\right). \tag{3.102}$$

Therefore,

$$\Delta N_p = \sqrt{\frac{1}{2}\sinh^2 2r + |\alpha|^2\left(e^{2r}\sin^2\phi + e^{-2r}\cos^2\phi\right)} \tag{3.103}$$

which matches the expression of [47]. We consider real displacements. Thus, we set $\phi = 0$ and obtain

$$\Delta N_p = \sqrt{\frac{1}{2}\sinh^2 2r + |\alpha|^2 e^{-2r}}, \tag{3.104}$$

which, after substituting Eq. (3.89), is

$$(\Delta N_p)^2 = \frac{1}{2}\sinh^2 2r + \left(N_p - \sinh^2 r\right)e^{-2r}. \tag{3.105}$$

Calculation of uncertainty in measuring total phase for squeezed light

The uncertainty in measuring the total phase Φ_T is the spread in the coherent state in the tangential direction (along Φ) divided by the length of the vector, $|\alpha|$. Since a global phase and displacement does not alter the squeezing, we can instead consider a squeezed vacuum state to measure the spread in the P quadrature. The P quadrature is given by

$$P = \left(a - a^\dagger\right)/2i \tag{3.106}$$

and the spread in the state is given by

$$\Delta P = \sqrt{\langle P^2\rangle - \langle P\rangle^2}. \tag{3.107}$$

The mean of the P quadrature is zero, as can be seen from Eq. (3.78) and Eq. (3.79). Explicitly,

$$\langle P\rangle = \left(\langle 0|S^\dagger a S|0\rangle - \langle 0|S^\dagger a^\dagger S|0\rangle\right)/2i \tag{3.108}$$

$$= 0. \tag{3.109}$$

We now calculate $\langle P^2\rangle$ as

$$\langle P^2\rangle = \frac{1}{4}\langle 0|S^\dagger\left(1 + 2a^\dagger a - a^2 - a^{\dagger 2}\right)S|0\rangle \tag{3.110}$$

$$= \frac{1}{4}\left(1 + 2\sinh^2 r + 2\sinh r\cosh r\right) \tag{3.111}$$

$$= \frac{1}{4}\mathrm{e}^{2r}. \tag{3.112}$$

Therefore,

$$\Delta P = \frac{1}{2}\mathrm{e}^{r}. \tag{3.113}$$

Putting it all together we get,

$$\Delta\Phi_T = \frac{1}{2|\alpha|}\mathrm{e}^{r} \tag{3.114}$$

which, on substituting from Eq. (3.89) gives

$$\Delta\Phi_T = \frac{\mathrm{e}^r}{2\sqrt{N_p - \sinh^2 r}} \tag{3.115}$$

which remains positive by virtue of Eq. (3.89). This is the uncertainty in Φ_T when only one measurement is made.

3.4.2 Precision improvement due to squeezed light

In this experimental proposal, large values of N_p are required. For large values, the uncertainties in number of photons (Eq. (3.105)) and phase (Eq. (3.115)) can be approximated to

$$(\Delta N_p)^2 \approx N_p \mathrm{e}^{-2r}. \tag{3.116}$$

and

$$(\Delta\Phi_T)^2 \approx \frac{\mathrm{e}^{2r}}{4N_p} \tag{3.117}$$

respectively. Substituting these values of uncertainties in Eq. (3.69), we note that the precision $(\Delta\gamma_0)^2$, or equivalently the number of experimental runs N_r, depends on the squeezing parameter r. The dependence of the number of experimental runs required is plotted as a function of the squeezing parameter in Fig. 3.6 for the experimental parameters as suggested by Ref. [3] (Table 2.1).

We see that the best precision is obtained for a squeezing parameter of r $r = -2.3$ at which the required number of runs is $N_r = 2 \times 10^4$. This is an order of magnitude improvement over using coherent light, as seen in Eq. (3.72).

Similar calculations for the β_0 and μ_0 cases are presented in Section 3.5. In these cases, the contribution to $\Delta\beta_0$ and $\Delta\mu_0$ is dominated by the ΔN_p contribution, in which case it is useful to use light squeezed in photon number.

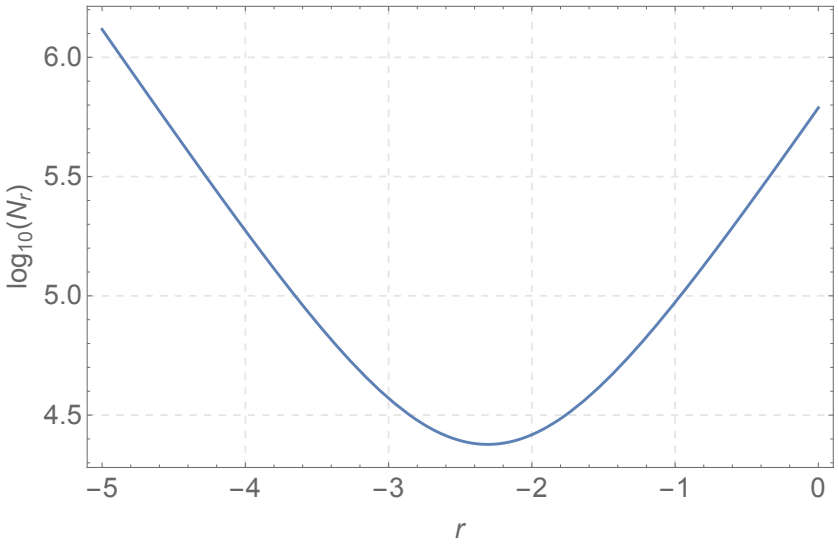

Figure 3.6: Logarithm of the required number of runs, $\log_{10}(N_r)$, as a function of the squeezing parameter r for fixed experimental parameters. Figure reproduced from Ref [1]. ©2018 APS

3.5 Calculation details for the β_0 and μ_0 case

In all the sections in this chapter so far, we have explicitly performed calculations only for the γ_0 commutator. In this chapter, we present the results for the β_0 and μ_0 commutators. Since the methods are identical to the previous sections, the details are not described here.

3.5.1 Experimental requirement after accounting for higher order terms and photon number uncertainty

In this subsection, we discuss the experimental requirement if we use the scheme of Ref. [3] using the β_0 and μ_0 deformed commutators. We do this by considering the higher order terms of the cavity Hamiltonian as described in Section 3.1 and accounting for the uncertainty in photon number as described in Section 3.2.

β_0 case

Here, the quantum gravity signal is given by

$$\Phi_{QG} = \beta_0 \kappa' \lambda_0^4 N_p^3 \quad \text{for} \quad \kappa' := \frac{4\hbar m\omega}{3M_p c}. \tag{3.118}$$

The expression for β_0 now reads

$$\beta_0 = \frac{1}{\kappa'\lambda_0^4}\left(\frac{\Phi_T}{N_p^3}\right) - \frac{2}{\kappa'\lambda_0^2 N_p^2} + \frac{6k}{\kappa'\lambda_0 N_p} - \frac{16k^2}{\kappa'} \tag{3.119}$$

and its standard deviation is given by

$$\begin{aligned}(\Delta\beta_0)^2 = &\left(\frac{1}{\kappa'\lambda_0^4 N_p^3}\right)^2 (\Delta\Phi_T)^2 + \left(-\frac{3\Phi_T}{\kappa'\lambda_0^4 N_p^4}\right. \\ &\left. + \frac{4}{\kappa'\lambda_0^2 N_p^3} - \frac{6k}{\kappa'\lambda_0 N_p^2}\right)^2 (\Delta N_p)^2\end{aligned} \tag{3.120}$$

for one run of the experiment. To estimate the precision, we substitute for Φ_T and evaluate $(\Delta\beta_0)^2$ for $\beta_0 \sim 0$. We obtain that for a precision of $(\Delta\beta_0)^2 \sim 1$, we need to perform the experiment $N_r = 10^{19}$ (10^{25}) times in the quantum-noise-limited (classical-noise-limited) scheme, which is much less feasible than the 10^6 required experimental runs claimed in Ref. [3].

μ_0 case

The quantum gravity signal is rewritten as

$$\Phi_{QG} = \mu_0 \kappa'' \lambda_0^2 N_p \quad \text{for} \quad \kappa'' := 2\frac{m^2}{M_p^2}. \tag{3.121}$$

The expression for μ_0 is given by

$$\mu_0 = \frac{1}{\kappa''\lambda_0^2}\left(\frac{\Phi_T}{N_p}\right) - \frac{2}{\kappa''} + \frac{6k\lambda_0 N_p}{\kappa''} - \frac{16k^2\lambda_0^2 N_p^2}{\kappa''}. \tag{3.122}$$

and its variance is

$$(\Delta\mu_0)^2 = \left(\frac{1}{\kappa''\lambda_0^2 N_p}\right)^2 (\Delta\Phi_T)^2 + \left(-\frac{\Phi_T}{\kappa''\lambda_0^2 N_p^2} + \frac{6k\lambda_0}{\kappa''} - \frac{32k^2\lambda_0^2 N_p}{\kappa''}\right)^2 (\Delta N_p)^2 \tag{3.123}$$

for one run of the experiment. Substituting for Φ_T, and assuming $\mu_0 \sim 0$, the variance is $(\Delta\mu_0)^2 = 10^5$ in both schemes. So, to have $(\Delta\mu_0)^2 \sim 1$, we need to perform the experiment $N_r = 10^5$ times as opposed to $O(1)$ times [3].

3.5.2 Improved schemes in β_0 and μ_0 cases

In this subsection, we present results for β_0 and μ_0 cases using improved paths in phase space similar to those of Section 3.3 for the γ_0 case and using squeezed light as described in Section 3.4. Specifically, we calculate the expected phase and the required number of experimental runs for the β_0 and μ_0 using unitary operators similar to that detailed in Section 3.1.1.

β_0 case

Here we present the analysis for the β_0 case. In this case, we suggest two possible solutions $U_{\beta_0,1}$ and $U_{\beta_0,2}$ with different advantages and disadvantages. The first solution is described below.

First solution – This path in phase space is identical to the path suggested for the γ_0 case. We perform similar calculations as in the γ_0 case to evaluate $U_{\beta_0,1}$ which implements the path in Fig. 3.2. Each of the individual loops was evaluated to sixth order in the BCH formula and the composition of the four loops was

evaluated to third order in BCH formula to obtain the phase

$$\Phi_T = -\frac{40}{9}\beta\lambda_0^4 N_p^3 - \frac{200}{3}k^3\lambda_0^5 N_p^4 + 144k^4\lambda_0^6 N_p^5 + \frac{1624}{3}k^5\lambda_0^7 N_p^6 - \frac{99680}{27}k^6\lambda_0^8 N_p^7 - 3116k^7\lambda_0^9 N_p^8 + \dots. \tag{3.124}$$

The advantage of this solution is that the total number of runs required decreases by a few orders of magnitude. However, a major disadvantage of this four-loop path is that the assumptions made in the above evaluation of $U_{\beta_0,1}$ (and the acquired phase thereof) are not controlled. In more detail, increasing the BCH order from 5 to 6 while evaluating the composition of the four loops leads to an additional contribution to the phase that is larger than the quantum gravity signal. Thus, there is no evidence that the phase obtained from the BCH approximations for higher than 6 orders is insignificant. In summary, the four-loop path is infeasible for estimating β_0 requires overcoming potential issues with the convergence of the expected phase. Instead, we suggest a different solution.

Second solution – This path in phase space is composed of only one rectangular loop like the original [3] but starting at a different vertex of the rectangle. The path is given by $U_{\beta_0,2}$.

$$U_{\beta_0,2} = \mathrm{e}^{-iH_X}\mathrm{e}^{-iH_P}\mathrm{e}^{iH_X}\mathrm{e}^{iH_P} \tag{3.125}$$

The path is depicted in Fig. 3.7.

Performing calculations similar to those in Eq. (3.7)–Eq. (3.53), we calculate the phase of the measured light Φ_T to be

$$\Phi_T = \frac{4}{3}\beta\lambda_0^4 N_p^3 + 2\lambda_0^2 N_p - 2k^3\lambda_0^5 N_p^4 + 35k^4\lambda_0^6 N_p^5 - 4k^5\lambda_0^7 N_p^6. \tag{3.126}$$

Since the shape of the loop remains the same as in the original case, the largest contribution to the quantum mechanical phase remains the same. However, the

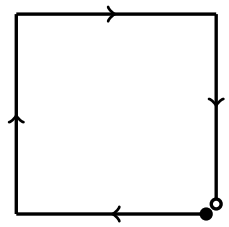

Figure 3.7: $U_{\beta_0,2}$: The shape of the path that reduces some of the QM contribution for the β_0 commutator. Figure reproduced from Ref [1]. ©2018 APS

second-largest term is reduced by 2 orders of magnitude by starting from the different vertex in the loop, which simplifies the phase calculations substantially.

Now we estimate the number of experimental runs required for the precise estimation of β_0. From Eq. (3.126), β_0 is determined from the total measured phase Φ_T using the relation

$$\beta_0 = \frac{3}{4\kappa'\lambda_0^4}\left(\frac{\Phi_T}{N_p^3}\right) - \frac{3}{2\kappa'\lambda_0^2 N_p^2} + \frac{3k^3\lambda_0}{2\kappa'}N_p - \frac{105k^4\lambda_0^2}{4\kappa'}N_p^2 + \frac{3k^5\lambda_0^3}{\kappa'}N_p^3 \tag{3.127}$$

for

$$\kappa' := \frac{\hbar m\omega}{M_p c}. \tag{3.128}$$

The uncertainty in β_0 for one run of the experiment is given by

$$\begin{aligned}(\Delta\beta_0)^2 = \Bigg(&-\frac{9\Phi_T}{4\kappa\lambda_0^4 N_p^4} + \frac{3}{\kappa'\lambda_0^2 N_p^3} + \frac{3k^3\lambda_0}{2\kappa'} \\ &-\frac{105k^4\lambda_0^2 N_p}{2\kappa'}\Bigg)^2 (\Delta N_p)^2 + \left(\frac{3}{4\kappa\lambda_0^4 N_p^3}\right)^2 (\Delta\Phi_T)^2\end{aligned} \tag{3.129}$$

With the following experimental parameters, as suggested in [3]

$$N_p = 10^{14},$$

$$m = 10^{-7}\,\text{kg},$$

$$F = 4\times 10^5,$$

$$\lambda_L = 532\,\text{nm},$$

we obtain $(\Delta\beta_0)^2 = 10^{18}$ (10^{24}) in the quantum-noise-limited (classical-noise-limited) scheme. Thus, by performing 10^4 runs of the quantum-noise-limited experiment, an upper bound of $\beta + \Delta\beta < 10^7$ can be attained, which is still 26 orders of magnitude better than present bounds. As will be described in Section 4.1, the state undergoes possible distortion because of the nonlinear (in n) terms in the unitary operator, but this distortion is expected to be insignificant for current experimental parameters. Assuming that the distortion does not significantly affect the phase statistics, we see that if we also have squeezing with $r = 3$, we get $(\Delta\beta_0)^2 = 10^{15}$ (10^{21}).

We now calculate the number of runs if we use the four-loop path of Fig. 3.2. Performing similar calculations, we get number of runs to be $N_r = 10^{16}$ (10^{22}). As expected, the precision is higher in this case but the accuracy is possibly lower because of the uncontrolled approximation. Using a squeezing parameter $r = 3$, we can further reduce the number of runs by three orders of magnitude; $N_r = 10^{13}$ (10^{19}).

μ_0 case

In the μ_0 case, the largest quantum mechanical term cannot be removed from the total phase. So, the path in phase space is just a rectangular loop like the original path [3]. However, choosing a different starting point leads to smaller quantum mechanical terms in total. The optimal path is effected by the unitary operator

$$U_{\mu_0} = \mathrm{e}^{-iH_X}\mathrm{e}^{-iH_P}\mathrm{e}^{iH_X}\mathrm{e}^{iH_P} \tag{3.130}$$

and is depicted in Fig. 3.8.

Performing calculations similar to the γ_0 and β_0 cases, the total phase Φ_T is given by

$$\Phi_T = 2\mu\lambda_0^2 N_p + 2\lambda_0^2 N_p - 2k^3\lambda_0^5 N_p^4 + 35k^4\lambda_0^6 N_p^5. \tag{3.131}$$

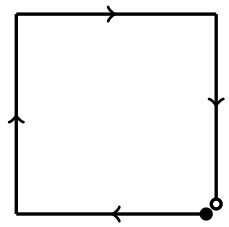

Figure 3.8: U_{μ_0}: The shape of the path to reduce QM contribution for the μ commutator. Figure reproduced from Ref [1].

Here, as in the second β_0 case, the largest contribution to the quantum mechanical phase remains the same. However, choosing a different starting point in the loop reduces the second-largest term by seven orders of magnitude. This leads to a marginal improvement in the number of runs with no extra experimental cost.

From Eq. (3.131), the value of μ_0 is estimated as

$$\mu_0 = \frac{1}{2\kappa''\lambda_0^2}\left(\frac{\Phi_T}{N_p}\right) - \frac{1}{\kappa''} + \frac{k^3\lambda_0^3 N_p^3}{\kappa''} - \frac{35k^4\lambda_0^4 N_p^4}{2\kappa''} \tag{3.132}$$

for

$$\kappa'' := \frac{m^2}{M_p^2}. \tag{3.133}$$

The variance in μ_0 is therefore given by

$$\begin{aligned}(\Delta\mu_0)^2 = &\left(\frac{1}{2\kappa''\lambda_0^2 N_p}\right)^2 (\Delta\Phi_T)^2 + \left(-\frac{\Phi_T}{2\kappa''\lambda_0^2 N_p^2}\right. \\ &\left. + \frac{3k^3\lambda_0^3}{\kappa''}N_p^2 - \frac{70k^4\lambda_0^4}{\kappa''}N_p^3\right)^2 (\Delta N_p)^2\end{aligned} \tag{3.134}$$

for one run of the experiment.

We evaluate the expression first for coherent states of light. For the same experimental parameters in the original proposal, we evaluate $(\Delta\mu_0)^2 = 10^5$ in both cases, which is the same as before because the path is almost the same. However we note that the error decreases monotonically with N_p, with m and with F, hence

the highest possible value of these parameters should be chosen for the experiment. Keeping the parameters

$$\lambda_L = 1064\,\text{nm} \tag{3.135}$$

$$L = 4\,\mu\text{m} \tag{3.136}$$

$$\omega_m = 2\pi \times 10^5 \tag{3.137}$$

$$F = 10^5 \tag{3.138}$$

fixed and changing the mean photon number and the oscillator mass to

$$N_p = 10^9, \tag{3.139}$$

$$m = 10^{-10}\,\text{kg}, \tag{3.140}$$

we obtain $(\Delta\mu_0)^2 = 2.2\ (22)$ for a single run of the experiment in the quantum-noise-limited (classical-noise-limited) scheme. If we also include using squeezed light with the squeezing parameter $r = -3$, the variance in the quantum-noise-limited scheme further reduces to $(\Delta\mu_0)^2 = 10^{-3}$. We can further increase the signal to noise ratio by increasing the mass of the oscillator.

To summarise this chapter, we have shown that the experimental scheme suggested in Ref. [3] is not experimentally feasible and we suggested modifications to this scheme to render it feasible.

More specifically, we show in Section 3.1 that the proposed experiment is not accurate when higher order corrections of the cavity Hamiltonian are considered, and in Section 3.2, show that it is not precise when accounting for non-zero uncertainty in mean photon number. We show in Table 3.2 that the required number of experimental runs is much larger when these sources of error are considered, thus making the scheme experimentally infeasible.

We suggest modifications to the scheme to improve the precision in Section 3.3 and Section 3.4. We suggest new paths in phase space which improve the precision by many orders of magnitude by improving the signal to noise ration. One such new path is illustrated in Fig. 3.2. We further show that using squeezed states of light can further improve the precision by around an order of magnitude as shown in Fig. 3.6. Finally, in Section 3.5, we list the results obtained by using new paths and using squeezed light for the other models of deformed commutators.

Chapter 4

Results: Effect of imperfections and assumptions

In Chapter 3, we proposed a new experimental scheme that improves the precision by many orders of magnitude. In this chapter, we check the robustness of this new scheme to experimental imperfections and assumptions made in the calculations.

In calculating the uncertainty in phase and photon number in Section 3.4, we assumed that the only effect of the unitary operator is a rotation in the coherent state. In Section 4.1, we go beyond this assumption and consider the effect of distortion in the coherent state on the variances of phase and mean photon number of the coherent state. In Section 4.2, we study the effects of imperfect implementation of the phase-space loops. Specifically, we consider area-preserving fluctuations in the loops and quantify the deviation in the acquired phase under these fluctuations. The third imperfection that we consider is in the imperfect preparation of the initial state of the oscillator. In Section 4.3, we detail the phase deviation due to small non-zero off-diagonal terms in the density matrix of the prepared thermal state corresponding to unintended coherences in the system. Finally, in Section 4.4, we discuss the assumptions made in the calculations of Chapter 3, especially regarding

uncontrolled truncation of terms while calculating the unitary operator.

4.1 State distortion

The experimental proposal considered in Section 3.3 assumes that the state of light that is initially in a coherent state remains in such a state under the unitary transformation describing the action of the pulsed laser sequences. However, this is not true when the unitary operator such as the one in Eq. (3.64) has terms that are non-linear in photon number n. In this case, the coherent states are distorted along with being rotated. The distortion of the coherent state due to nonlinear n terms keeps the variance in mean photon number unchanged but the variance in the phase, $(\Delta\Phi)^2$, changes. In this section, we calculate the value of $\Delta\Phi$ for this distorted state.

The outline of the calculations is as follows. The initial state of light is in a coherent state $|\alpha\rangle$ for real α with average photon number $N_p = |\alpha|^2$. The unitary operator that acts on the state during the experiment is given by $\mathrm{e}^{if(n)}$ and we assume $f(n)$ to be a polynomial in n. If $f(n)$ is not linear in n, the coherent state is distorted in addition to being rotated. To calculate the distortion, we bring the state back to the X axis and calculate the spread in P which we denote by ΔP. We assume that $\Delta\Phi \approx \frac{\Delta P}{\sqrt{N_p}}$.

The calculations are detailed here. To bring the state back to the X axis, we calculate the phase $\Phi(N_p)$ of the state $\mathrm{e}^{if(n)}|\alpha\rangle$ and rotate the state back by angle $\Phi(N_p)$. The state on the X axis is given by

$$|\xi\rangle = \mathrm{e}^{i\{f(n)-\Phi(N_p)n\}}|\alpha\rangle =: U|\alpha\rangle\,. \tag{4.1}$$

Here, the function $\Phi(n)$ is calculated from $f(n)$ by replacing n^m by $(n+1)^m - n^m$

for all non-zero m.

The variance $(\Delta P)^2$ is calculated by

$$(\Delta P)^2 = \langle P^2 \rangle_\xi - \langle P \rangle_\xi^2 . \tag{4.2}$$

We first calculate $\langle P \rangle_\xi$ which in terms of a and $a^\dagger$ is

$$\langle P \rangle_\xi = \frac{1}{2i} \langle a - a^\dagger \rangle_\xi . \tag{4.3}$$

Writing in terms of the initial coherent state, we have

$$\langle P \rangle_\xi = \frac{1}{2i} \left(\langle \alpha | U^\dagger a U | \alpha \rangle - \langle \alpha | U^\dagger a^\dagger U | \alpha \rangle \right) . \tag{4.4}$$

We can show that

$$U^\dagger a U = \mathrm{e}^{i\{\Phi(n) - \Phi(N_p)\}} a \tag{4.5}$$

and making the saddle point approximation, we can approximate

$$\langle \alpha | \mathrm{e}^{i\Phi(n)} | \alpha \rangle \approx \mathrm{e}^{i\Phi(N_p)}. \tag{4.6}$$

Therefore,

$$\langle P \rangle_\xi = \frac{1}{2i} (\alpha - \alpha^*) \tag{4.7}$$

which for real α gives

$$\langle P \rangle_\xi = 0. \tag{4.8}$$

To calculate the variance in Φ and therefore in P, we now evaluate $\langle P^2 \rangle_\xi$:

$$\begin{aligned} \langle P^2 \rangle_\xi = & -\frac{1}{4} \langle a^2 + a^{\dagger 2} - 2a^\dagger a - 1 \rangle_\xi \\ = & -\frac{1}{4} \left(\langle \alpha | U^\dagger a^2 U | \alpha \rangle + \langle \alpha | U^\dagger a^{\dagger 2} U | \alpha \rangle \right. \\ & \left. -2 \langle \alpha | U^\dagger a^\dagger a U | \alpha \rangle - 1 \right) . \end{aligned} \tag{4.9}$$

U commutes with $a^\dagger a = n$, so $U^\dagger a^\dagger a U = a^\dagger a$ and therefore $\langle\alpha|U^\dagger a^\dagger a U|\alpha\rangle = N_p$. We now evaluate $U^\dagger a^2 U$. We observe

$$\begin{aligned} U^\dagger a^2 U &= \left(U^\dagger a U\right)^2 \\ &= \mathrm{e}^{i\{\Phi(n)-\Phi(N_p)\}} a\, \mathrm{e}^{i\{\Phi(n)-\Phi(N_p)\}} a \\ &= \mathrm{e}^{2i\{\Phi(n)-\Phi(N_p)\}} \mathrm{e}^{i\Theta(n)} a^2 \end{aligned} \tag{4.10}$$

where the function $\Theta(n)$ is calculated from $\Phi(n)$ by replacing n^m by $(n+1)^m - n^m$ for all non-zero m. Therefore

$$\begin{aligned} \langle P^2\rangle_\xi &= -\frac{1}{4}\left(N_p \mathrm{e}^{i\Theta(N_p)} + N_p \mathrm{e}^{-i\Theta(N_p)} - 2N_p - 1\right) \\ &= \frac{1}{4}\left(1 + 4N_p \sin^2\frac{\Theta(N_p)}{2}\right). \end{aligned} \tag{4.11}$$

This leads to

$$(\Delta\Phi)^2 = \frac{1}{4N_p} + \sin^2\frac{\Theta(N_p)}{2} \tag{4.12}$$

which is the expression that has been used in Eq. (3.71) of Section 3.3. We also note that for the given experimental parameters, the correction due to distortion is negligible.

4.2 Area preserving fluctuations

In this section, we calculate the phase acquired by light when the paths in phase space described in Section 3.3 are imperfect. Specifically, we assume that state of the mechanical resonator undergoes area-preserving fluctuations in phase space. Here, we provide sufficient conditions for these deformations to have a negligible effect on the estimation of the quantum gravity signal.

Different kinds of area-preserving deformations are analyzed and are depicted in Fig. 4.1. The deformations have a magnitude of ϵ for loops whose dimensions

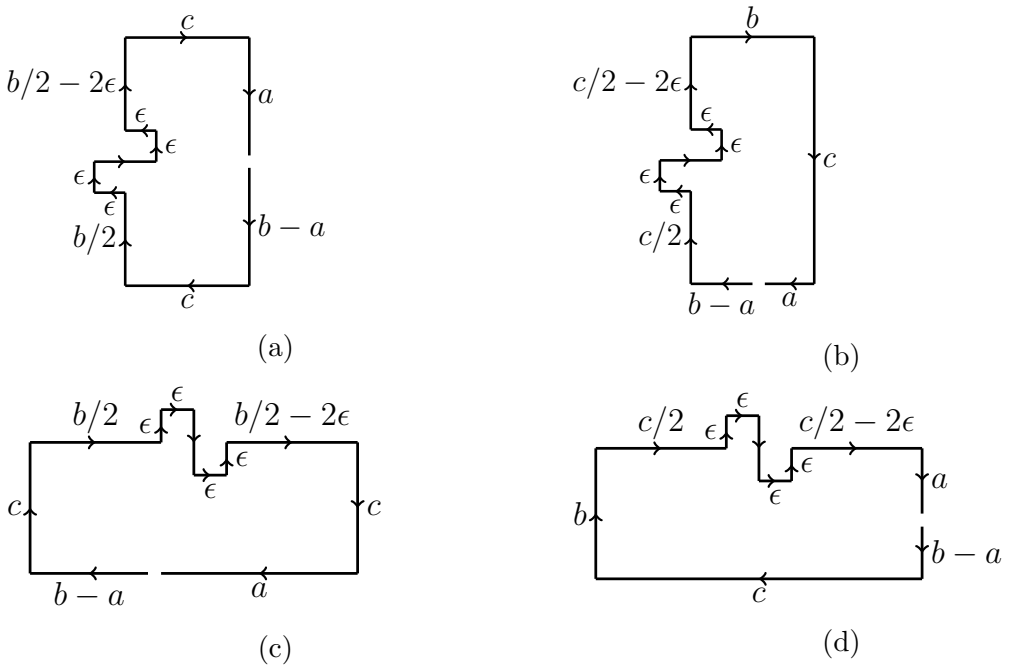

Figure 4.1: Figure showing different kinds of are-preserving fluctuations. (a) Loop starting from an arbitrary point along X with fluctuations along the opposite X side (b) Loop starting from an arbitrary point along P with fluctuations along the adjacent X side (c) Loop starting from an arbitrary point along P with fluctuations along the opposite P side (d) Loop starting from an arbitrary point along X with fluctuations along the P side. Figure reproduced from Ref [1]. ©2018 APS

are of order 1. We calculate the deviation from a perfect loop to leading order in ϵ for all kinds of deformations and tabulate the results in Table 4.1. The calculations are similar to those shown in the previous sections and are hence not detailed here.

In the remainder of the section, we provide conditions for the deformations to be negligible compared to the quantum gravity signal.

In the γ_0 case, we consider different instances of some or all of the four loops undergoing area-preserving deformations in one of the edges. Among the different deformations, we choose the case with the largest contribution to the phase. Under this deformation, the experimental requirements for this contribution to be less

Final path composed of	Leading order term in ϵ (γ case)	Leading order term in ϵ (β case)	Leading order term in ϵ (μ case)
Only one out of four loops deformed as depicted in Fig. 4.1a	$4kn^3\lambda_0^3\epsilon^3$	$4kn^3\lambda_0^3\epsilon^3$	$4kn^3\lambda_0^3\epsilon^3$
Only one out of four loops deformed as depicted in 4.1c respectively	$k^2n^4\lambda_0^4\epsilon^3$	$3k^2n^4\lambda_0^4\epsilon^3$	$3k^2n^4\lambda_0^4\epsilon^3$
Each of the four loops is deformed with identical ϵ along the edge opposite to the starting edge. Deformations depicted in Figs. 4.1a and 4.1c	$\frac{16}{3}k^2n^4\lambda_0^4\epsilon^3$		
Each of the four loops is deformed but deformations arise only on the edges parallel to X-axis, i.e., Figs. 4.1a and 4.1b	$\frac{842}{9}k^5n^7\lambda_0^7\epsilon^3$		
Each of the four loops is deformed but deformations arise only on the edges parallel to P-axis, i.e., Figs. 4.1c and 4.1d	$\frac{4}{3}k^2n^4\lambda_0^4\epsilon^3$		
In comparison, the magnitude of the signal term:	$\gamma_0\frac{\sqrt{\hbar m\omega_m}}{3M_pc}\lambda_0 n^3$	$\beta_0\frac{\hbar\omega_m m}{3M_pc}\lambda_0^4 n^4$	$\mu_0\frac{m^2}{M_p^2}\lambda_0^2 n^2$

Table 4.1: Summary of the leading order terms (in ϵ) in the phase for different kinds of deformations. Reproduced from Ref [1]. ©2018 APS

than the quantum gravity signal is

$$12N_p^2\lambda_0^3 k\epsilon^3 < \gamma_0 \frac{\sqrt{\hbar m\omega_m}}{M_p c}\lambda_0 N_p^2 \tag{4.13}$$

$$\epsilon^3 < \gamma_0 \frac{m\omega_m L}{12M_p c}. \tag{4.14}$$

Numerically, this translates to $\epsilon < 10^{-4}$ for $\gamma_0 \sim 1$.

In the β_0 case, the corresponding requirement is

$$12N_p^2\lambda_0^3 k\epsilon^3 < \beta_0 \frac{4\hbar\omega_m m}{3M_p c}\lambda_0^4 N_p^3 \tag{4.15}$$

$$\epsilon^3 < \beta_0 \frac{\sqrt{\hbar m^3 w_m^3}L}{9M_p c}\lambda_0 N_p \tag{4.16}$$

which numerically means that $\epsilon < 10^{-6}$ for reasonable experimental parameters for this proposal. Finally, the μ_0 case requires that

$$12N_p^2\lambda_0^3 k\epsilon^3 < 2\mu_0 \frac{m^2}{M_p^2}\lambda_0^2 N_p \tag{4.17}$$

$$\epsilon^3 < \mu_0 \frac{L\sqrt{m^3\omega_m}}{6M_p^2\lambda_0 N_p\sqrt{\hbar}}, \tag{4.18}$$

which leads to the condition that $\epsilon < 10^2$ or 10^3 depending on the choice of reasonable experimental parameters. This completes our analysis of the fluctuations in the phase-space paths and gives us an estimate of how well the experiment should be performed to circumvent errors from imperfect loops.

4.3 Imperfect thermal state

The proposed scheme of Section 3.3 assumes that the mechanical oscillator is in a thermal state with low phonon number. In this section, we calculate the resultant phase of light for an imperfectly prepared initial thermal state of the mechanical

resonator and present conditions for which imperfect state preparation does not affect the quantum gravity signal.

For this calculation, we consider a state that is a mixture of a thermal state and a pure state

$$\rho = \frac{1}{1+\epsilon}\rho_{th} + \frac{\epsilon}{1+\epsilon}\left|\psi\right\rangle\left\langle\psi\right| \tag{4.19}$$

where $\left|\psi\right\rangle = \frac{1}{\sqrt{2}}\left(\left|0\right\rangle + \left|1\right\rangle\right)$, which models unwanted off-diagonal terms in the density matrix. As usual, we evaluate the mean optical field

$$\left\langle a\right\rangle = \mathrm{Tr}\left(U^{\dagger}aU\left|\alpha\right\rangle\left\langle\alpha\right| \otimes \rho\right). \tag{4.20}$$

to estimate the measured phase in the different quantum gravity cases.

At the end of this section, we present the required condition for the β_0 and μ_0 cases. The detailed calculations in the γ_0 case are as follows.

4.3.1 Calculations in the γ_0 case

The unitary operator U for the γ_0 case is given by

$$U = \exp\left\{-iw(n) + \left(x^{*}n^{3} + y^{*}n^{4}\right)a_{m}^{\dagger} - \left(xn^{3} + yn^{4}\right)a_{m}\right\} \tag{4.21}$$

where

$$w(n) = -\frac{40}{3}k^{3}\lambda_{0}^{5}n^{5} + 24k^{4}\lambda_{0}^{6}n^{6} \tag{4.22}$$

$$x = (1-i)\,\frac{\sqrt{2}}{3}k^{2}\lambda_{0}^{3} \tag{4.23}$$

$$y = (-26+10i)\,\frac{\sqrt{2}}{3}k^{3}\lambda_{0}^{4}. \tag{4.24}$$

The final state of light is given by the expression for the thermal state followed by the contribution from the pure state as follows:

$$\left\langle a\right\rangle = \frac{1}{1+\epsilon}\alpha' \mathrm{e}^{-i\Phi_{QM}} + \frac{\epsilon}{1+\epsilon}\mathrm{Tr}\left(U^{\dagger}aU\left|\alpha\right\rangle\left\langle\alpha\right| \otimes \left|\psi\right\rangle\left\langle\psi\right|\right). \tag{4.25}$$

Here, the results from the thermal state are known, that is,

$$\begin{aligned}\alpha' = &\alpha \mathrm{e}^{-\frac{1}{2}\left(9|x|^2N_p^4+16|y|^2N_p^6\right)} \\ &\times \mathrm{e}^{-\left(9|x|^2N_p^4+16|y|^2N_p^6+12(xy^*+x^*y)N_p^5\right)\bar{n}}\end{aligned} \tag{4.26}$$

and

$$\Phi_{QM} = \frac{1}{2i}\left(x^*y - xy^*\right)N_p^6 - \frac{200}{3}k^3\lambda_0^5N_p^4 + 144k^4\lambda_0^6N_p^5 \tag{4.27}$$

as can be seen from calculations in Section 3.1.1.

We now evaluate the second part of the expression $\langle a_0\rangle = \mathrm{Tr}\left(U^\dagger aU\left|\alpha\right\rangle\left\langle\alpha\right|\otimes\left|\psi\right\rangle\left\langle\psi\right|\right)$. Performing calculations similar to that in Section 3.1.1 we see that

$$\begin{aligned}U^\dagger aU = &\mathrm{e}^{-\frac{1}{2}(x^*y-xy^*)\left(n^6+15n^5+33n^4+35n^3+21n^2+7n+1\right)} \\ &\times \mathrm{e}^{i\frac{40}{3}k^3\lambda_0^5\left(5n^4+10n^3+10n^2+5n+1\right)} \\ &\times \mathrm{e}^{-i24k^4\lambda_0^6\left(6n^5+15n^4+20n^3+15n^2+6n+1\right)} \\ &\times \mathrm{e}^{\left(x^*a_m^\dagger-xa_m\right)\left(3n^2+3n+1\right)} \\ &\times \mathrm{e}^{\left(y^*a_m^\dagger-ya_m\right)\left(4n^3+6n^2+4n+1\right)}a.\end{aligned} \tag{4.28}$$

Therefore,

$$\begin{aligned}\langle a_0\rangle = &\sum_{n=0}^{\infty}\alpha\left\langle\alpha|n\right\rangle\left\langle n|\alpha\right\rangle\mathrm{e}^{i\frac{40}{3}k^3\lambda_0^5\left(5n^4+10n^3+10n^2+5n+1\right)} \\ &\times \mathrm{e}^{-i24k^4\lambda_0^6\left(6n^5+15n^4+20n^3+15n^2+6n+1\right)} \\ &\times \mathrm{e}^{-\frac{1}{2}(x^*y-xy^*)\left(n^6+15n^5+33n^4+35n^3+21n^2+7n+1\right)} \\ &\times \left\langle\psi\right|\mathrm{e}^{\left(x^*a_m^\dagger-xa_m\right)\left(3n^2+3n+1\right)} \\ &\times \mathrm{e}^{\left(y^*a_m^\dagger-ya_m\right)\left(4n^3+6n^2+4n+1\right)}\left|\psi\right\rangle.\end{aligned} \tag{4.29}$$

To simplify the evaluation of the above expression, we define the variables

$$\upsilon = y\left(4n^3+6n^2+4n+1\right) \tag{4.30}$$

$$\chi = x\left(3n^2+3n+1\right) \tag{4.31}$$

and denote the displaced Fock state $\mathrm{e}^{\left(\upsilon^* a_m^\dagger - \upsilon a_m\right)}|m\rangle$ as $|\upsilon^*, m\rangle$. We rewrite

$$\langle\psi|\,\mathrm{e}^{\left(x^* a_m^\dagger - x a_m\right)\left(3n^2+3n+1\right)}\mathrm{e}^{\left(y^* a_m^\dagger - y a_m\right)\left(4n^3+6n^2+4n+1\right)}\,|\psi\rangle$$

as

$$\begin{aligned}\langle\psi|\,\mathrm{e}^{\left(\chi^* a_m^\dagger - \chi a_m\right)}\mathrm{e}^{\left(\upsilon^* a_m^\dagger - \upsilon a_m\right)}\,|\psi\rangle = \frac{1}{2}\{&\langle-\chi^*,0|\upsilon^*,0\rangle + \langle-\chi^*,0|\upsilon^*,1\rangle \\ &+\langle-\chi^*,1|\upsilon^*,0\rangle + \langle-\chi^*,1|\upsilon^*,1\rangle\}\,.\end{aligned} \tag{4.32}$$

Using the formula for the overlap of two displaced Fock states from [44]

$$\begin{aligned}\langle-\chi^*,m|\upsilon^*,n\rangle = &\langle-\chi^*|\upsilon^*\rangle\sqrt{m!n!} \\ &\times\sum_{j=0}^{\min(m,n)}\frac{\left(\upsilon^*+\chi^*\right)^{m-j}\left(-\chi-\upsilon\right)^{n-j}}{j!\,(m-j)!\,(n-j)!}\end{aligned} \tag{4.33}$$

where

$$\langle-\chi^*|\upsilon^*\rangle = \exp\left\{-\chi\upsilon^* - \frac{1}{2}\left(|\chi|^2+|\upsilon|^2\right)\right\} \tag{4.34}$$

we can evaluate the expression to find

$$\begin{aligned}\langle\psi|\,\mathrm{e}^{\left(\chi^* a_m^\dagger - \chi a_m\right)}\mathrm{e}^{\left(\upsilon^* a_m^\dagger - \upsilon a_m\right)}\,|\psi\rangle = \frac{1}{2}\langle-\chi^*|\upsilon^*\rangle\{&1+\chi^*+\upsilon^*-\chi-\upsilon \\ &+1-|\chi|^2-|\upsilon|^2-\chi\upsilon^*-\chi^*\upsilon\}\,.\end{aligned} \tag{4.35}$$

Also note that the remaining terms that are in the expression for $\langle a\rangle$ are given by

$$\langle\alpha|n\rangle\langle n|\alpha\rangle = \mathrm{e}^{-|\alpha|^2}\frac{|\alpha|^{2n}}{n!}. \tag{4.36}$$

Substituting all the above expressions in the expression for $\langle a_0 \rangle$, we get

$$\begin{aligned}
\langle a_0 \rangle = \sum_{n=0}^{\infty} & \alpha \mathrm{e}^{-|\alpha|^2} \frac{|\alpha|^{2n}}{n!} \mathrm{e}^{i\frac{40}{3}k^3\lambda_0^5\left(5n^4+10n^3+10n^2+5n+1\right)} \\
& \times \mathrm{e}^{-i24k^4\lambda_0^6\left(6n^5+15n^4+20n^3+15n^2+6n+1\right)} \\
& \times \mathrm{e}^{-\frac{1}{2}(x^*y-xy^*)\left(n^6+15n^5+33n^4+35n^3+21n^2+7n+1\right)} \\
& \times \mathrm{e}^{-xy^*\left(3n^2+3n+1\right)\left(4n^3+6n^2+4n+1\right)} \\
& \times \mathrm{e}^{-\frac{1}{2}\left(|x|^2\left(3n^2+3n+1\right)^2+|y|^2\left(4n^3+6n^2+4n+1\right)^2\right)} \\
& \times \frac{1}{2}\left\{1+(x^*-x)\left(3n^2+3n+1\right)\right. \\
& +(y^*-y)\left(4n^3+6n^2+4n+1\right)+1 \\
& -|x|^2\left(3n^2+3n+1\right)^2-|y|^2\left(4n^3+6n^2+4n+1\right)^2 \\
& -(x^*y+xy^*)\left(12n^5+30n^4+34n^3\right. \\
& \left.\left.+21n^2+12n+1\right)\right\}. \qquad (4.37)
\end{aligned}$$

The expression can be approximated (to leading order in N_p) to be

$$\begin{aligned}
\langle a_0 \rangle = & \alpha \mathrm{e}^{-\frac{1}{2}\left(9|x|^2N_p^4+16|y|^2N_p^6\right)} \\
& \times \mathrm{e}^{-\frac{1}{2}(x^*y-xy^*)N_p^6+i\frac{200}{3}k^3\lambda_0^5N_p^4-i144k^4\lambda_0^6N_p^5} \\
& \times \frac{1}{2}\left\{1+3\left(x^*-x\right)N_p^2+4\left(y^*-y\right)N_p^3-9|x|^2N_p^4\right. \\
& \left.+1-16|y|^2N_p^6-12\left(x^*y+xy^*\right)N_p^5\right\}. \qquad (4.38)
\end{aligned}$$

If we express $\langle a_0 \rangle$ in the form

$$\langle a_0 \rangle = \alpha_0 \mathrm{e}^{-i\Theta_0}, \qquad (4.39)$$

the new amplitude is

$$\alpha_0 \approx \alpha \mathrm{e}^{-\left(9|x|^2N_p^4+16|y|^2N_p^6+6(x^*y+xy^*)N_p^5\right)} \qquad (4.40)$$

and the new phase is

$$\begin{aligned}\Theta_0 \approx & \frac{1}{2i}\left(x^* y - x y^*\right) N_p^6 - \frac{200}{3} k^3 \lambda_0^5 N_p^4 + 144 k^4 \lambda_0^6 N_p^5 \\ & - \frac{1}{2i}\left\{3\left(x^* - x\right) N_p^2 + 4\left(y^* - y\right) N_p^3\right\} \end{aligned} \tag{4.41}$$

which on substituting with x and y gives

$$\begin{aligned}\Theta_0 \approx & -\frac{32}{9} k^5 \lambda_0^7 N_p^6 - \frac{200}{3} k^3 \lambda_0^5 N_p^4 + 144 k^4 \lambda_0^6 N_p^5 \\ & - \sqrt{2} k^2 \lambda_0^3 N_p^2 + \frac{40\sqrt{2}}{3} k^3 \lambda_0^4 N_p^3. \end{aligned} \tag{4.42}$$

Putting the two equations together, the final state of light is given by

$$\langle a \rangle = \frac{1}{1+\epsilon} \alpha' \mathrm{e}^{-i\Phi_{QM}} + \frac{\epsilon}{1+\epsilon} \alpha_0 \mathrm{e}^{-i\Theta_0}. \tag{4.43}$$

In the remainder of this section, we calculate the effective amplitude and phase of the light. The mean field is simplified to

$$\langle a \rangle = \frac{1}{1+\epsilon} \alpha' \mathrm{e}^{-i\Phi_{QM}} \left(1 + \epsilon \frac{\alpha_0}{\alpha'} \mathrm{e}^{-i\left(\Theta_0 - \Phi_{QM}\right)}\right). \tag{4.44}$$

Define

$$\epsilon \frac{\alpha_0}{\alpha'} \mathrm{e}^{-i\left(\Theta_0 - \Phi_{QM}\right)} = r \mathrm{e}^{i\phi}. \tag{4.45}$$

Expressing $1 + r\mathrm{e}^{i\phi}$ in the polar form, we have

$$1 + r\mathrm{e}^{i\phi} = \sqrt{1 + r^2 + 2r\cos\phi}\, \mathrm{e}^{i \tan^{-1}\left(\frac{r \sin\phi}{1 + r\cos\phi}\right)} \tag{4.46}$$

which to first order in r is (first order in ϵ)

$$1 + r\mathrm{e}^{i\phi} = \left(1 + r\cos\phi\right) \mathrm{e}^{ir\sin\phi}. \tag{4.47}$$

Therefore, the mean field is given by

$$\begin{aligned}\langle a \rangle = & \frac{1}{1+\epsilon} \alpha' \left(1 + \epsilon \frac{\alpha_0}{\alpha'} \cos\left(\Theta_0 - \Phi_{QM}\right)\right) \mathrm{e}^{-i\Phi_{QM}} \\ & \mathrm{e}^{-i\epsilon \frac{\alpha_0}{\alpha'} \sin\left(\Theta_0 - \Phi_{QM}\right)}, \end{aligned} \tag{4.48}$$

where the respective amplitude and phase of the output light are given by

$$\begin{aligned}\alpha' =& \alpha \mathrm{e}^{-\frac{1}{2}\left(9|x|^2N_p^4+16|y|^2N_p^6\right)} \\ & \times \mathrm{e}^{-\left(9|x|^2N_p^4+16|y|^2N_p^6+12(xy^*+x^*y)N_p^5\right)\bar{n}},\end{aligned} \tag{4.49}$$

$$\frac{\alpha_0}{\alpha'} = \mathrm{e}^{\left(9|x|^2N_p^4+16|y|^2N_p^6+12(xy^*+x^*y)N_p^5\right)\left(\bar{n}-\frac{1}{2}\right)} \tag{4.50}$$

and

$$\Phi_{QM} = -\frac{200}{3}k^3\lambda_0^5N_p^4 + 144k^4\lambda_0^6N_p^5 - \frac{32}{9}k^5\lambda_0^7N_p^6, \tag{4.51}$$

$$\Theta_0 - \Phi_{QM} = -\sqrt{2}k^2\lambda_0^3N_p^2 + \frac{40}{3}\sqrt{2}k^3\lambda_0^4N_p^3. \tag{4.52}$$

Note that the correction to the phase is given by $\epsilon\frac{\alpha_0}{\alpha'}\sin\left(\Theta_0 - \Phi_{QM}\right)$. Thus, for imperfect preparation to have no significant impact on the results, we require

$$\epsilon\frac{\alpha_0}{\alpha'}\sin\left(\Theta_0 - \Phi_{QM}\right) < \Phi_{QG}. \tag{4.53}$$

4.3.2 Results in the μ_0 case

Calculating similar quantities for the μ_0 case yields

$$\begin{aligned}\alpha' =& \alpha \mathrm{e}^{-\frac{1}{2}\left(4|x|^2N_p^2+9|y|^2N_p^4\right)} \\ & \mathrm{e}^{-\left(4|x|^2N_p^2+9|y|^2N_p^4+6(xy^*+x^*y)N_p^3\right)\bar{n}},\end{aligned} \tag{4.54}$$

$$\Phi_{QM} = 2\lambda_0^2N_p - 2k^3\lambda_0^5N_p^4, \tag{4.55}$$

$$\frac{\alpha_0}{\alpha'} = \mathrm{e}^{\left(4|x|^2N_p^2+9|y|^2N_p^4+6(xy^*+x^*y)N_p^3\right)\left(\bar{n}-\frac{1}{2}\right)}, \tag{4.56}$$

and

$$\Theta_0 - \Phi_{QM} = -2\sqrt{2}k\lambda_0^2N_p + \frac{3}{\sqrt{2}}k^2\lambda_0^3N_p^2 \tag{4.57}$$

for

$$x = (-1-i)\sqrt{2}k\lambda_0^2 \tag{4.58}$$

$$y = (-1+i)\frac{1}{\sqrt{2}}k^2\lambda_0^3. \tag{4.59}$$

4.3.3 Results in the β_0 case

Similarly for the β_0 case, we obtain

$$\begin{aligned}\alpha' =& \alpha \exp\left\{-\frac{1}{2}\left(4|x|^2N_p^2+9|y|^2N_p^4+16|z|^2N_p^6\right)\right\}\\ &\times\exp\left\{-\left(4|x|^2N_p^2+9|y|^2N_p^4+16|z|^2N_p^6\right.\right.\\ &+6\left(xy^*+x^*y\right)N_p^3+12\left(yz^*+y^*z\right)N_p^5\\ &\left.\left.+8\left(xz^*+x^*z\right)N_p^4\right)\bar{n}\right\},\end{aligned} \tag{4.60}$$

$$\Phi_{QM} = 2\lambda_0^2N_p+6k^2\lambda_0^2N_p-2k^3\lambda_0^5N_p^4-4k^5\lambda_0^7N_p^6. \tag{4.61}$$

$$\begin{aligned}\frac{\alpha_0}{\alpha'} =& \exp\left\{\left(4|x|^2N_p^2+9|y|^2N_p^4+16|z|^2N_p^6\right.\right.\\ &+6\left(xy^*+x^*y\right)N_p^3+12\left(yz^*+y^*z\right)N_p^5\\ &\left.\left.+8\left(xz^*+x^*z\right)N_p^4\right)\left(\bar{n}-\frac{1}{2}\right)\right\},\end{aligned} \tag{4.62}$$

and

$$\Theta_0-\Phi_{QM} = -2\sqrt{2}k\lambda_0^2N_p+\frac{3}{\sqrt{2}}k^2\lambda_0^3N_p^2+8\sqrt{2}k^3\lambda_0^4N_p^3 \tag{4.63}$$

for

$$x = (-1-i)\sqrt{2}k\lambda_0^2 \tag{4.64}$$

$$y = (-1+i)\frac{1}{\sqrt{2}}k^2\lambda_0^3 \tag{4.65}$$

$$z = (1+i)\,2\sqrt{2}k^3\lambda_0^4. \tag{4.66}$$

In summary, the state preparation should be such that the phase contribution of the off-diagonal terms is less than the quantum gravity signal, i.e.,

$$\epsilon\frac{\alpha_0}{\alpha'}\sin\left(\Theta_0-\Phi_{QM}\right) < \Phi_{QG}. \tag{4.67}$$

The expressions for $\frac{\alpha_0}{\alpha'}$ and $\Theta_0-\Phi_{QM}$ have been derived here for different models of deformed commutators.

4.4 Open problem: Accuracy of the assumptions made in the calculations

In Section 3.3 we calculated the phase acquired by light after the action of the suggested operator Eq. (3.60). Similar calculations are detailed in Section 3.1.1. In the calculation of the phase, we make several approximations. We note that this is not a deficiency of our approach but also arises implicitly in Ref. [3] where the effect of the truncation was however not estimated. In this section, we describe the approximations made and discuss their validity.

First, we recall the assumptions made in simplifying the unitary operator. In order to calculate the phase, we first need to express the unitary operator, which is a product (Eq. (3.4)) of exponentials of operators, as a single exponential of operators that is not truncated like Eq. (3.5). This simplification cannot be performed exactly for an arbitrary Hamiltonian. So, we need to truncate the Hamiltonian (Eq. (3.3)) to a finite order in k. This is our first approximation. The second approximation is choosing a finite order in BCH formula based on available computation resources. The unitary operator thus calculated has many terms in the exponent. We calculate the phase contribution from only the terms larger than the minimum uncertainty and ignore the rest to obtain the approximate unitary operator Eq. (3.12), thus making our third approximation. The final approximation made is the saddle-point approximation, which is employed in going from Eq. (3.46) to Eq. (3.47).

The exact (or general) form of the phase from the unitary operator calculated to an arbitrary order of BCH formula or k is not known. So, it is difficult to prove convergence of the phase rigorously. We, therefore, try to check the validity of the assumptions heuristically. One approach to check the validity of truncation

in the BCH order is to fix a specific order in k (like $k = 2$) and calculate the phase contribution from each order in BCH. A condition for the validity of our assumptions is that these phase contributions fall off quickly with increasing BCH order. However, we were not able to calculate the phase for each BCH order exactly. This is because even for a finite number of terms in each BCH order, there can be infinitely many phase terms. This is illustrated in the Section 4.4.1 below. Checking the validity of truncation in the k order has the same challenge of not being able to calculate the phase. Also, since the phase cannot be calculated exactly even for a few terms in the unitary operator for a given BCH and k order, we cannot comment on the validity of truncating the unitary operator. We leave a proof of the validity of these assumptions as an open problem.

We instead give heuristic evidence to the validity of the approximations of calculating the unitary operator to a given BCH and k order. We give evidence that the term with the largest phase contribution from each BCH order drops off geometrically, even though we can make no statement about the sum of all terms from that BCH order. Consider simplifying the expression $\mathrm{e}^{iH_X}\mathrm{e}^{iH_P}$ for

$$\begin{aligned} H_X &= n\lambda_0 \left(X - kX^2 + k^2X^3 - \dots\right) \\ H_P &= n\lambda_0 \left(P - kP^2 + k^2P^3 - \dots\right). \end{aligned} \tag{4.68}$$

In the final simplification, we see that the phase contribution from the terms constant in X and P is larger than the phase contribution from the non-constant terms. This is because the terms dependent on the mechanical modes (terms with X and P) only contribute through their commutators while the constant terms contribute directly as can be seen in the calculations in Section 3.1.1. So, for small coefficients ($kn\lambda_0 < 1$), the largest contribution is from the constant term.

The constant term from first order in BCH, $[H_X, H_P]$, comes from $[X, P]$ and is therefore of the order $n^2\lambda_0^2$. The constant term from second order comes from terms like $[X, [X, P^2]]$ and $[P, [P, X^2]]$. We see that these terms have coefficients of the order of $kn^3\lambda_0^3$. Similarly, the constant term from BCH order m is of the order of $k^{m-2}n^m\lambda_0^m$. So, the largest term in each BCH order falls of geometrically. The phase contribution from such a term is of the order of $k^{m-2}\lambda_0^m N_p^{m-1}$. If we assume that the sum of the rest of the terms is negligible, we need only to calculate up to BCH order m such that the phase is less than the minimum uncertainty $\Delta\Phi_T$. That is,

$$k^{m-2}\lambda_0^m N_p^{m-1} < \frac{1}{2\sqrt{N_p N_r}}. \tag{4.69}$$

For the γ_0 experimental parameters, we estimate that this condition is satisfied for $m = 6$. So we need to calculate up to BCH order 6 and k order 4. Similarly, $m = 28$ in the β_0 case and $m = 5$ in the μ_0 case suffice.

4.4.1 Example: infinite number of phase terms from unitary operator

Consider the case when the unitary operator is given by

$$U = \mathrm{e}^{\chi n^2 + \upsilon n^3} \tag{4.70}$$

where χ is linear and υ quadratic in a_m and $a_m^\dagger$. For example

$$\begin{aligned} \chi &= x^* a_m^\dagger - x a_m \\ \upsilon &= y^* a_m^{\dagger 2} - y a_m^2. \end{aligned} \tag{4.71}$$

The final quantity to be calculated is the mean field of light which is

$$\langle a \rangle = \mathrm{Tr}\left(U^\dagger a U \left|\alpha\right\rangle \left\langle\alpha\right| \otimes \rho_m^{th}\right). \tag{4.72}$$

The first step in this calculation is to simplify $U^\dagger a U$ and express it as Oa where O is an operator only dependent on n. a acts on $|\alpha\rangle$ to give $\alpha\,|\alpha\rangle$. The operator a can then be removed from the trace. The mean field is then given by

$$\langle a\rangle = \alpha \mathrm{Tr}\left(O\,|\alpha\rangle\,\langle\alpha|\otimes\rho_m^{th}\right). \tag{4.73}$$

Here we show that the approach that works in simplifying $U^\dagger a U$ used in the calculations of Section 3.1.1 does not work in the case where the unitary operator is of the form given by Eqs. (4.70) and (4.71). This approach relies on splitting U into a product of exponentials each containing one power of n as is done while going from Eq. (3.13) to Eq. (3.14). Using the Zassenhaus formula

$$\begin{aligned} \mathrm{e}^{(\chi+\upsilon)} = &\mathrm{e}^{\chi}\ \mathrm{e}^{\upsilon}\ \mathrm{e}^{-\frac{1}{2}[\chi,\upsilon]}\ \mathrm{e}^{\frac{1}{6}(2[\upsilon,[\chi,\upsilon]]+[\chi,[\chi,\upsilon]])} \\ &\times\ \mathrm{e}^{-\frac{1}{24}([[[\chi,\upsilon],\chi],\chi]+3[[[\chi,\upsilon],\chi],\upsilon]+3[[[\chi,\upsilon],\upsilon],\upsilon])}\ldots \end{aligned} \tag{4.74}$$

we see that the expansion does not truncate due to υ being quadratic in a_m and $a_m^\dagger$. Terms of the form $[\upsilon,\chi]$, $[\upsilon,[\upsilon,\chi]]$, $[\upsilon,[\upsilon,[\upsilon,\chi]]]$ and so on are non-zero and linear functions of a_m and $a_m^\dagger$. Terms of the form $[\chi,[\upsilon,\chi]]$, $[\chi,[\upsilon,[\upsilon,\chi]]]$, $[\chi,[\upsilon,[\upsilon,[\upsilon,\chi]]]]$ are non-zero and functions of n alone, not a_m or $a_m^\dagger$. So, even with a small number of terms in the unitary operator, we cannot calculate the phase of the state of light exactly.

In summary of this chapter, we have calculated the effects of many experimental imperfections and theoretical assumptions in the calculation of the measurable phase in Chapter 3. In Section 4.1, we calculate the variance in the phase due to distortions of the coherent state to obtain the result Eq. (4.12). The error that arises in the phase of light due to area-preserving imperfections in implementing the phase space loops are tabulated in Table 4.1 of Section 4.2. We have also

estimated how small these imperfections can be for the scheme to still be meaningful. In Section 4.3, we calculated the deviation in phase due to imperfections in the initial state preparation and obtained conditions for the imperfections to have no significant impact on the results in Eq. (4.53). Finally, in Section 4.4, we list all the assumptions made in the calculations, including truncation of terms and using a finite order of the BCH formula, and give heuristic arguments for these assumptions.

Chapter 5

Results: Correction to time period of a pendulum

As we have shown in Section 2.2, one of the effects of quantum gravity is that the time period of a harmonic oscillator is modified. The quantum gravity parameters can be determined or at least bounded by measuring the time period of such oscillators precisely. Experiments have been performed using oscillators in the quantum regime to bound the quantum gravity parameters [4, 11], but strictly speaking, the formalism used in these works is only valid for single particles. One of the main contributions in this thesis is the introduction of a new parametrisation for deformations involving composite particels. This formalism, introduced in Eq. (1.15) of Chapter 1, allows us to use macroscopic systems to test for these deformations. In this chapter and the next, we exploit this formalism for such tests.

Specifically, we extend the calculations of corrections to the time period of a harmonic oscillator to that of a pendulum. To make the calculations simpler, in Section 5.1, we perform these calculations using classical mechanics. We derive the results by assuming that the Poisson brackets are deformed [32–34] in the same way that the commutators are deformed due to quantum gravity. To ensure that these

results are not a consequence of using classical mechanics, in Section 5.2 we show that the Poisson equation approach and a fully quantum mechanical calculation yield the same result for the time period of a harmonic oscillator. This shows that the expression for the time period calculated using classical mechanics also extends to the quantum regime and thus provides further evidence for the correctness of our approach.

As a side remark we note that these matching results also connects two different approaches to studying deformed commutators, namely modifying the Poisson bracket [32–34] and modifying the commutator [16, 35, 36]. These two approaches have so far been thought to be separate [37].

5.1 Classical calculations based on deformed Poisson bracket

Here we calculate the corrections to the time period of a pendulum due to quantum gravity deformations of the canonical commutation relations so that it can then be compared against experimental data. We consider a pendulum of mass m and length L. To find the Hamiltonian of a pendulum in terms of its x coordinates, we begin by expressing it in angular coordinates. The Hamiltonian is

$$H = \frac{1}{2}mL^2\dot{\theta}^2 + mgL\left(1 - \cos\theta\right). \tag{5.1}$$

where θ is the angle between the pendulum string and the vertical. However, there are no quantum-mechanical uncertainty relations for θ and p_θ since they are not Hermitian variables. So, we rewrite the energy in terms of x and p_x using the

relation $x = L\sin\theta$. The Lagrangian, after ignoring constants, is

$$\mathcal{L} = \frac{1}{2}mL^2\dot{\theta}^2 + mgL\cos\theta \tag{5.2}$$

$$= \frac{m\dot{x}^2}{2\cos^2\theta} + mgL\cos\theta. \tag{5.3}$$

The momentum p_x, conjugate to the coordinate x, is defined as

$$p_x = \frac{\partial\mathcal{L}}{\partial\dot{x}} = \frac{m\dot{x}}{\cos^2\theta} = \frac{mL^2\dot{x}}{L^2 - x^2}. \tag{5.4}$$

For ease of notation, we express x in terms of θ. The Hamiltonian can be calculated from the Lagrangian to obtain

$$H = p_x\dot{x} - \mathcal{L} \tag{5.5}$$

$$= \frac{p_x^2}{2m}\cos^2\theta - mgL\cos\theta. \tag{5.6}$$

From here on, we drop the subscript x in p_x.

The time period can be obtained from the Hamiltonian in two ways. Here, we take the approach that defines a new momentum operator which satisfies the standard canonical commutation relations and hence the standard Heisenberg equations of motion. In this approach the Hamiltonian is modified as was discussed in Section 2.2. In an alternative, equivalent, approach the Hamiltonian can be left unchanged while the equations of motion are modified due to the deformed commutator [48]. Here we follow the first method due to ease of calculation.

For illustrative purposes, we perform the calculations using classical mechanics but in Section 5.2, we show that the results hold even by performing quantum calculations with deformed commutators. Here, we deform the standard Poisson brackets in analogy to the deformation of the canonical commutation relation due to quantum gravity [32–34], i.e.,

$$\{x, p\} = 1 + \beta p^2 \tag{5.7}$$

where

$$\beta = \frac{\beta_0}{N^{\alpha_0}(M_p c)^2}. \tag{5.8}$$

To ensure that the equations of motion are unchanged, a new momentum operator $\tilde{p}$ is defined such that we recover the standard Poisson bracket, i.e.,

$$\{x, \tilde{p}\} = 1. \tag{5.9}$$

We now express the Hamiltonian in terms of this modified momentum $\tilde{p}$ in order to solve for the time-evolution of the pendulum.

To find the relation between p and $\tilde{p}$, we write $p = f(\tilde{p})$. The deformed Poisson bracket therefore becomes

$$\{x, f(\tilde{p})\} = 1 + \beta f(\tilde{p})^2. \tag{5.10}$$

Since $\{x, \tilde{p}\} = 1$ as in regular classical mechanics, the relation

$$\{x, f(\tilde{p})\} = \frac{\mathrm{d}f(\tilde{p})}{\mathrm{d}\tilde{p}} \tag{5.11}$$

holds. From Eq. (5.10) and Eq. (5.11), we obtain the differential equation

$$\frac{\mathrm{d}f(\tilde{p})}{\mathrm{d}\tilde{p}} = 1 + \beta f(\tilde{p})^2 \tag{5.12}$$

which can be solved with the condition that $p = 0$ when $\tilde{p} = 0$. Therefore, we obtain the relation between p and $\tilde{p}$

$$p = f(\tilde{p}) = \frac{\tan\left(\sqrt{\beta}\tilde{p}\right)}{\sqrt{\beta}} \tag{5.13}$$

which on inverting is

$$\tilde{p} = \frac{\tan^{-1}\left(\sqrt{\beta}p\right)}{\sqrt{\beta}}. \tag{5.14}$$

This result does not make the small momentum assumption of Refs. [4, 11].

Writing the Hamiltonian in terms of the new momentum operator $\tilde{p}$, we note that it is modified to

$$H = \frac{1}{2m\beta}\tan^2\left(\sqrt{\beta}\tilde{p}\right)\cos^2\theta - mgL\cos\theta. \tag{5.15}$$

This modification of the Hamiltonian compared to Eq. (5.6) ensures that the equations of motion remain unchanged with respect to x and $\tilde{p}$, i.e.,

$$\dot{x} = \frac{\partial H}{\partial \tilde{p}} = \frac{\cos^2\theta}{m\sqrt{\beta}}\tan\left(\sqrt{\beta}\tilde{p}\right)\sec^2\left(\sqrt{\beta}\tilde{p}\right). \tag{5.16}$$

To solve this equation of motion, we express the momentum $\tilde{p}$ in terms of a constant of motion, the total energy of the system. From the expression for the energy in Eq. (5.15), note that the total energy in the system is $E = -mgL\cos\phi$ (when $\tilde{p} = 0$), where ϕ is the angular amplitude. Substituting for total energy in Eq. (5.15), the redefined momentum $\tilde{p}$ (Eq. (5.14)) can be expressed in terms of the angular displacement θ and amplitude ϕ as

$$\tilde{p} = -\frac{1}{\sqrt{\beta}}\tan^{-1}\left(\sqrt{2m^2gLf(\theta)\beta}\right) \tag{5.17}$$

where

$$f(\theta) := \frac{\cos\theta - \cos\phi}{\cos^2\theta}. \tag{5.18}$$

Therefore, in terms of the angular variable θ, the equation of motion Eq. (5.16) can be rewritten as

$$\dot{\theta}L\cos\theta = -\frac{\cos^2\theta}{m\sqrt{\beta}}\sqrt{2m^2gLf(\theta)\beta}\left(1 + 2m^2gLf(\theta)\beta\right) \tag{5.19}$$

and simplified to

$$\dot{\theta} = \frac{\mathrm{d}\theta}{\mathrm{d}t} = -\cos\theta\sqrt{2\frac{g}{L}f(\theta)}\left(1 + 2m^2gLf(\theta)\beta\right). \tag{5.20}$$

Separating variables and integrating over half a cycle, we obtain the time period for half an oscillation

$$\frac{T_{2\pi}}{2} = \int_{-\phi}^{\phi} \mathrm{d}\theta \frac{1}{\cos\theta\sqrt{2\frac{g}{L}f(\theta)}\,(1+2m^2gLf(\theta)\beta)}. \tag{5.21}$$

Since $\beta \ll 1$, as can be numerically verified from the above equation, the expression can be simplified to

$$T_{2\pi} \approx \sqrt{\frac{2L}{g}} \int_{-\phi}^{\phi} \mathrm{d}\theta \left\{ \frac{1}{\sqrt{\cos\theta - \cos\phi}} - \frac{\beta 2m^2gL\sqrt{\cos\theta - \cos\phi}}{\cos^2\theta} \right\}. \tag{5.22}$$

Furthermore, for small amplitudes, we can approximate the time-period to

$$T_{2\pi} \approx 2\pi\sqrt{\frac{L}{g}}\left(1 + \frac{\phi^2}{16} - \frac{\beta}{2}m^2gL\phi^2\right) \tag{5.23}$$

and in terms of the amplitude A, where $A = \phi L$, it can be expressed as

$$T_{2\pi} \approx 2\pi\sqrt{\frac{L}{g}}\left(1 + \frac{A^2}{16L^2} - \frac{\beta_0 m^2 g}{2N^{\alpha_0}(M_p c)^2 L}A^2\right). \tag{5.24}$$

Here, we note that the time period of a pendulum is modified by a term proportional to the quantum gravity parameters. Hence by measuring the amplitude-dependence of the the time period very precisely, we can bound the quantum gravity parameters. This is done by using measured experimental data in Section 6.1.

5.2 Full quantum mechanical calculations based on deformed canonical commutators

In Section 5.1, we found that the time period of a pendulum is modified by quantum gravity effects. Since the calculations were based on classical mechanics, it could happen that these results are a consequence of using classical mechanics. In this section, we refute this argument by performing calculations in a quantum

mechanical framework and obtaining the same results. However, finding the time period of a quantum pendulum modified due to quantum gravity is very involved. So here we instead compare the time period of a harmonic oscillator obtained using classical and quantum mechanics and show that they match, thereby validating our results.

An outline of the calculations is as follows: We start with the eigenvalues and eigenfunctions of the quantum harmonic oscillator derived in Refs. [16, 49]. Since ladder operators are defined differently due to commutator deformation, we use a generalised Heisenberg algebra [50] to find the action of the ladder operators on the eigenstates. Using this algebra, we derive the expressions for the position and momentum operators in terms of the ladder operators. With this, the operators are well defined. In order to choose the most classical pure state in our calculations, we choose a definition of coherent states, the Gazeau-Klauder states [39], such that the states remain coherent states during the evolution under this Hamiltonian. Calculating the expectation value of the position operator with respect to these Gazeau-Klauder coherent states, we recover the classical calculations. The calculations are detailed in the remainder of this section.

5.2.1 Formalism

In this section, we work in the momentum basis where the operators $\hat{x}$ and $\hat{p}$ are defined by their action on the momentum wave-functions as

$$\hat{x}\psi(p) = i\hbar(1+\beta p^2)\frac{\partial\psi(p)}{\partial p} \tag{5.25}$$

$$\hat{p}\psi(p) = p\psi(p). \tag{5.26}$$

These definitions of $\hat{x}$ and $\hat{p}$ allow us to write the harmonic oscillator Hamiltonian as

$$\hat{H} = -\frac{\hbar^2 m\omega^2}{2}\left((1+\beta p^2)\frac{\partial}{\partial p}\right)^2 + \frac{p^2}{2m}. \tag{5.27}$$

Solving the Schrödinger equation $\hat{H}\psi_n(p) = E_n\psi_n(p)$, the energy eigenvalues are found to be [16]

$$E_n = \hbar\omega\left(n+\frac{1}{2}\right)\left(\sqrt{1+\frac{1}{16r}}+\frac{1}{4\sqrt{r}}\right) + \frac{\hbar\omega}{4\sqrt{r}}n^2 \tag{5.28}$$

for $1/r = (2\beta m\hbar\omega)^2$ and the eigenfunctions in the momentum basis are [49]

$$\begin{aligned}\psi_n(p) &= (-i)^n 2^\lambda \Gamma(\lambda)\sqrt{\frac{n!(n+\lambda)\sqrt{\beta}}{2\pi\Gamma(n+2\lambda)}}(1-s^2)^{\lambda/2}C_n^\lambda(s)\\ &=: z_n(1-s^2)^{\lambda/2}C_n^\lambda(s)\end{aligned} \tag{5.29}$$

where $C_n^\lambda(s)$ are Gegenbauer polynomials and

$$s = \frac{\sqrt{\beta}p}{\sqrt{1+\beta p^2}} \tag{5.30}$$

$$\lambda = \frac{1}{2}+\sqrt{\frac{1}{4}+\frac{1}{(m\hbar\omega\beta)^2}}. \tag{5.31}$$

The phase $(-i)^n$ in Eq. (5.29) has been introduced so that in the limit $\beta \to 0$, we recover results from quantum mechanics, namely $\hat{a} = \sqrt{\frac{m\omega}{2\hbar}}\hat{x} + \frac{i}{\sqrt{2m\hbar\omega}}\hat{p}$. The eigenvalues Eq. (5.28) and eigenfunctions Eq. (5.29) so obtained are useful in defining the Fock basis $\{|n\rangle\}$, which is used in the calculations in the rest of this section. The eigenfunctions are defined by $\psi_n(p) = \langle p|n\rangle$ and the number operator $\hat{n}$ is defined such that $\hat{n}\,|n\rangle = n\,|n\rangle$. So, in the Fock basis, the Hamiltonian is

$$H = \hbar\omega\left(\hat{n}+\frac{1}{2}\right)\left(\sqrt{1+\frac{1}{16r}}+\frac{1}{4\sqrt{r}}\right) + \frac{\hbar\omega}{4\sqrt{r}}\hat{n}^2 \tag{5.32}$$

which we use in the rest of this section.

5.2.2 Generalised Heisenberg algebra

Due to the quantum gravitational modifications of the canonical commutator, the ladder operators and their commutation relations also would be modified. Here, we find the commutator between the ladder operators based on their action on an energy eigenstate. Using the version of generalised Heisenberg algebra used in Ref. [50], we find the action of the annihilation operator on state $|n\rangle$ to be

$$\hat{a}\,|n\rangle = \sqrt{n\,(1+\nu+\nu n)}\,|n-1\rangle \tag{5.33}$$

for $\nu = \beta m\hbar\omega/2$. Similarly, the action of the creation operator on a Fock state is [50]

$$\hat{a}^\dagger\,|n\rangle = \sqrt{(n+1)\,(1+\nu+\nu(n+1))}\,|n+1\rangle\,. \tag{5.34}$$

Therefore, the number operator is related to the ladder operators as

$$\hat{a}^\dagger\hat{a} = \hat{n}\,(1+\nu+\nu\hat{n}) \tag{5.35}$$

and the commutator is derived to be

$$\left[\hat{a},\hat{a}^\dagger\right] \approx 1 + 2\nu(1+\hat{a}^\dagger\hat{a}) \tag{5.36}$$

to first order in ν (or equivalently first order in β).

5.2.3 Calculating position and momentum in terms of ladder operators

The relation between the canonical operators $\hat{x}$ and $\hat{p}$ and the ladder operators $\hat{a}$ and $\hat{a}^\dagger$ is modified due to deformed commutators. In this section, we derive the modified expression for the position and momentum operators in terms of the ladder operators. The outline of the calculations is as follows: We start with Eq. (5.33) in

the momentum basis and use recursion relations of the eigenfunctions to express $\psi_{n-1}(p)$ in terms of $\psi_n(p)$. This gives us the operator $\hat{a}$ in the momentum basis which can be expressed in terms of the operators $\hat{x}$ and $\hat{p}$. This relation is then inverted to obtain $\hat{x}$ in terms of the ladder operators.

The calculations are detailed below. Eq. (5.33) in the momentum basis is

$$\hat{a}\psi_n(p) = \sqrt{n\,(1+\nu+\nu n)}\psi_{n-1}(p). \tag{5.37}$$

Using the following recursion relations of Gegenbauer polynomials

$$(n+2\lambda)C_n^\lambda(s) = \frac{\mathrm{d}}{\mathrm{d}s}C_{n+1}^\lambda(s) - s\frac{\mathrm{d}}{\mathrm{d}s}C_n^\lambda(s) \tag{5.38}$$

$$(1-s^2)\frac{\mathrm{d}}{\mathrm{d}s}C_n^\lambda(s) = (n+2\lambda)sC_n^\lambda(s) - (n+1)C_{n+1}^\lambda(s) \tag{5.39}$$

$\psi_{n-1}(p)$ can be expressed in terms of $\psi_n(p)$ and its derivatives. Therefore, we obtain the action of the annihilation operators on the wavefunction to be

$$\hat{a}\psi_n = i\sqrt{\frac{(1+\nu+\nu n)\,(n+\lambda-1)(\lambda+n)\beta}{(n+2\lambda-1)(1+\beta p^2)}}\left\{\frac{1+\beta p^2}{\beta(\lambda+n)}\frac{\mathrm{d}}{\mathrm{d}p}+p\right\}\psi_n. \tag{5.40}$$

Since the ψ_ns form a complete basis [16], Eq. (5.40) can be written in operator form. In the limit of $\beta \ll 1$ and using the definitions of the position and momentum operators in Eq. (5.25) and Eq. (5.26), we obtain

$$\begin{aligned}\hat{a} = &\sqrt{\frac{m\omega}{2\hbar}}\left[\hat{x} - \beta\left\{\frac{1}{2}\hat{p}^2\hat{x} + \frac{m\hbar\omega}{4}\hat{x}\right\}\right] \\ &+ \frac{i}{\sqrt{2m\hbar\omega}}\left[\hat{p} + \frac{\beta}{4}\left\{-2\hat{p}^3 + \hbar m\omega\hat{p}(1+4\hat{n})\right\}\right].\end{aligned} \tag{5.41}$$

A similar expression for the creation operator $\hat{a}^\dagger$ is

$$\begin{aligned}\hat{a}^\dagger = &\sqrt{\frac{m\omega}{2\hbar}}\left[\hat{x} - \beta\left\{\frac{1}{2}\hat{x}\hat{p}^2 + \frac{m\hbar\omega}{4}\hat{x}\right\}\right] \\ &- \frac{i}{\sqrt{2m\hbar\omega}}\left[\hat{p} + \frac{\beta}{4}\left\{-2\hat{p}^3 + \hbar m\omega(1+4\hat{n})\hat{p}\right\}\right].\end{aligned} \tag{5.42}$$

The relations Eq. (5.41) and Eq. (5.42) can be inverted to find the expressions for $\hat{x}$

$$\hat{x} = \sqrt{\frac{\hbar}{2m\omega}}\left(\hat{a}+\hat{a}^\dagger\right) + \frac{\beta}{4}\sqrt{\frac{\hbar^3 m\omega}{2}}\left(\hat{a}^\dagger\hat{a}^2 + \hat{a}^{\dagger 2}\hat{a} - \hat{a}^3 - \hat{a}^{\dagger 3}\right) \tag{5.43}$$

and similarly $\hat{p}$

$$\hat{p} = i\sqrt{\frac{\hbar m\omega}{2}}\left(\hat{a}^\dagger - \hat{a}\right) + i\beta\frac{(\hbar m\omega)^{3/2}}{4\sqrt{2}}\left(\hat{a}^\dagger\hat{a}^2 - \hat{a}^{\dagger 2}\hat{a} + \hat{a}^3 - \hat{a}^{\dagger 3} + 2\hat{a} - 2\hat{a}^\dagger\right) \tag{5.44}$$

in terms of the ladder operators. Most of the calculations in this section were performed using Mathematica.

Here, we have defined the position operator in terms of the ladder operators, whose action on the Fock states is known. In the next section, we find the trajectory of the oscillator by finding the expectation value of the position operator with respect to some generalised coherent state.

5.2.4 Trajectory of the pendulum

To compare the result ultimately with that obtained from classical mechanics in Section 5.1, we consider the most classical pure state as the initial state. So, we choose the generalised coherent states, the Gazeau-Klauder states, that were defined in Section 2.3. The Hamiltonian in this case can be rewritten from Eq. (5.28) as

$$H = \hbar\omega\left(n + \nu n + \nu n^2 + \frac{1}{2}(1+\nu)\right) \tag{5.45}$$

and therefore

$$e_n = n\left(1 + \nu + \nu n\right). \tag{5.46}$$

To recap, the Gazeau-Klauder coherent states [39], are

$$|J,\gamma\rangle = \frac{1}{N(J)}\sum_n \frac{J^{n/2}\mathrm{e}^{-i\gamma e_n}}{\sqrt{\rho_n}}|n\rangle \tag{5.47}$$

where $\rho_n = \prod_{k=1}^{n} e_k$ and $N(J)^2 = \sum_n \frac{J^n}{\rho_n}$.

Using the rules of the generalised Heisenberg algebra (Eqs. (5.33) and (5.34)), and the expressions for the position (Eq. (5.43)) and momentum (Eq. (5.44)) operators derived in the above section, we calculate the expectation value of position and momentum in this state. For illustration, we calculate the expectation value of the annihilation operator $\hat{a}$. Writing the state $|J,\gamma\rangle$ explicitly in terms of the Fock states and using Eq. (5.33) and simplifying, we obtain

$$\begin{aligned}\langle J,\gamma|\hat{a}|J,\gamma\rangle &= \sum_{n,m} \frac{J^{(m+n)/2}\mathrm{e}^{-i\gamma(e_n-e_m)}\sqrt{e_n}}{N^2\sqrt{\rho_m\rho_n}}\delta_{n-1,m} \\ &= \frac{\sqrt{J}}{N^2}\sum_n \frac{J^{n-1}}{\rho_{n-1}}\mathrm{e}^{-i\gamma(1+2n\nu)} \\ &\approx \frac{\sqrt{J}}{N^2}\mathrm{e}^{-i\gamma}\left(N^2 - i\gamma 2\nu\sum_n n\frac{J^{n-1}}{\rho_{n-1}}\right).\end{aligned} \tag{5.48}$$

We now evaluate the second term considering that $e_{n-1} = n-1+O(\beta)$. Since this term is already of order β (or equivalently ν) and we neglect second order terms, we can assume that $e_{n-1} \approx n-1$ for this calculation. Hence, this term can be evaluated as follows:

$$\begin{aligned}\sum_n n\frac{J^{n-1}}{\rho_{n-1}} &\approx \sum_n e_{n-1}\frac{J^{n-1}}{\rho_{n-1}} + \sum_n \frac{J^{n-1}}{\rho_{n-1}} \\ &= \sum_n \frac{J^{n-1}}{\rho_{n-2}} + \sum_n \frac{J^{n-1}}{\rho_{n-1}} \\ &= N^2(J+1).\end{aligned} \tag{5.49}$$

Putting the equations together, we obtain the expected value of the annihilation operator

$$\langle J,\gamma|\hat{a}|J,\gamma\rangle = \sqrt{J}\mathrm{e}^{-i\gamma}\left(1 - i\gamma 2\nu\ (J+1)\right). \tag{5.50}$$

The expectation values of other functions of $\hat{a}$ and $\hat{a}^\dagger$ can be similarly evaluated to obtain the expectation values of $\hat{x}$ and $\hat{p}$, which, up to first order in β are given by

$$\begin{aligned}\langle J,\gamma|\hat{x}|J,\gamma\rangle =&\sqrt{\frac{2\hbar J}{m\omega}}\cos\gamma+\beta\sqrt{2\hbar^3 m\omega}\left\{\frac{J^{3/2}}{4}\cos\gamma\right.\\&\left.-\frac{J^{3/2}}{4}\cos 3\gamma-\sqrt{J}(1+J)\gamma\sin\gamma\right\}\end{aligned}\tag{5.51}$$

and

$$\begin{aligned}\langle J,\gamma|\hat{p}|J,\gamma\rangle =&-\sqrt{2\hbar m\omega J}\sin\gamma+\beta\frac{(\hbar m\omega)^{3/2}}{2\sqrt{2}}\left\{J^{3/2}\sin\gamma+J^{3/2}\sin 3\gamma\right.\\&\left.+2J^{1/2}\sin\gamma-4\gamma\sqrt{J}(1+J)\cos\gamma\right\}.\end{aligned}\tag{5.52}$$

Since these states satisfy the relation $\mathrm{e}^{-iHt/\hbar}\,|J,\gamma\rangle = |J,\gamma+\omega t\rangle$, the time-evolved expectation values are easily obtained by replacing γ with $\gamma+\omega t$. In these calculations, we have assumed not only that $\beta \ll 1$ but also $\beta\gamma \ll 1$ and $\beta\omega t \ll 1$.

To evaluate the position of the oscillator as a function of time in terms of measurable quantities, we choose the initial state $|J,\gamma\rangle$ such that the oscillator starts at rest with non-zero amplitude, i.e., $\langle p(0)\rangle = 0$ and $\langle x(0)\rangle = A$. This condition is satisfied when $\gamma = 0$ and $J = \frac{m\omega A^2}{2\hbar}$, as can be seen from Eqs. (5.51) and (5.52). Therefore, for this initial state, the expectation value of position in terms of its amplitude is

$$\langle x(t)\rangle = A\cos\omega t+\beta\frac{m^2\omega^2A^3}{2}\sin\omega t\left\{\cos\omega t\sin\omega t-\omega t\left(1+\frac{2\hbar}{m\omega A^2}\right)\right\}.\tag{5.53}$$

We now compare the time-dependent position thus obtained with that obtained from the classical calculations. Since we are comparing quantum harmonic oscillator calculations with that of classical pendulum calculations, we compare the classical limit of Eq. (5.53) to the solution of the low amplitude limit of the differential equation Eq. (5.16). We can verify that the classical limit ($\hbar \to 0$) of Eq. (5.53)

$$\langle x(t)\rangle = A\cos\omega t+\beta\frac{m^2\omega^2A^3}{2}\sin\omega t\,(\cos\omega t\sin\omega t-\omega t)\tag{5.54}$$

satisfies the differential equation

$$\dot{x} = -\omega\sqrt{(A^2 - x^2)}\left\{1 + \beta m^2\omega^2\left(A^2 - x^2\right)\right\}, \tag{5.55}$$

which is the low amplitude limit of the differential equation Eq. (5.16) with $\omega = \sqrt{g/L}$. This shows that the two approaches match, thereby validating the easier, classical approach.

In summary, we have shown that one of the effects of the deformed commutators is an observed change in time period of a pendulum. This modification to the time period is calculated in Section 5.1 using classical mechanics by assuming deformed Poisson brackets to obtain Eqs. (5.21) and (5.24). In Section 5.2, we also calculate the modification to the time period of a harmonic oscillator using a fully quantum mechanical approach, where the canonical commutators are deformed, to obtain the trajectory of the oscillator in Eq. (5.53). We then show that the two approaches yield the same modification to the time period of a harmonic oscillator, thereby validating our results. We also note that the two approaches of modifying Poisson brackets and modifying commutators had so far thought to be separate and our results connects them. In the next chapter, we use experimental data of measured time period of a pendulum to place bounds on the quantum gravity parameters.

Chapter 6

Results: Obtaining experimental bounds on quantum gravity parameters

As we show in Section 2.2, there are two arbitrary parameters in the models of deformed commutators: α_0, which determines the scaling of the deformations with particle number, and β_0, which determines the magnitude of the deformations. The best experiments so far could only place negative bounds on α_0 when $\beta_0 = 1$. In this chapter, we consider experiments to place better bounds on these quantum gravity parameters.

In Chapter 5, we calculated the corrections to the time period of a pendulum due to quantum gravitational effects. With precise measurements of the pendulum time period as a function of its amplitude, bounds can be placed on the parameters. Precise time period measurements of a pendulum have been performed for many decades now. Using data from one such experiment [51], we provide the first positive bound on α_0 in Section 6.1. To substantially improve the bounds, we suggest an experiment using levitated diamagnetic spheres in Section 6.2. Furthermore, in Section 6.3, we show that even the existing experimental scheme based on

optomechanics can be slightly modified to obtain better bounds on α_0.

6.1 Pendulum experiment to bound quantum gravity parameters

In this section, we use experimental data from precise measurements of the time period of a pendulum to place bounds on the quantum gravity parameters α_0 and β_0 using Eq. (5.24). From Eq. (5.24), we see that the quantum gravitational corrections to the time period are amplitude dependent. Hence, we consider an experiment [51] which measures the time-period as a function of its amplitude.

The experimental data is represented in Fig.(3) of Ref. [51], which plots the measured time-period as a function of the square of the amplitude. From Eq. (5.24), we see that the intercept T_0 of this line is

$$T_0 = 2\pi\sqrt{\frac{L}{g}} \tag{6.1}$$

and the slope s is

$$s = 2\pi\sqrt{\frac{L}{g}}\left(\frac{1}{16L^2} - \frac{\beta_0 m^2 g}{2N^{\alpha_0}(M_p c)^2 L}\right). \tag{6.2}$$

Since the expression for the slope of this plot includes corrections from quantum gravity, we calculate the slope from Fig.(3) to compare with theory.

We extracted the data from Fig.(3) of the paper by magnifying it and determining the central positions of the data points. This data is used to calculate the slope and intercept. Table 6.1 contains the data extracted from the experimental results obtained in Ref. [51]. We use this extracted data to perform a linear fit using the reported error of 2% in amplitude measurement and negligible error in

$A^2(\mathrm{cm}^2)$	$T_{2\pi}(\mathrm{s})$	$A^2(\mathrm{cm}^2)$	$T_{2\pi}(\mathrm{s})$
43	3.47315	578	3.47438
52	3.47308	709	3.47468
132	3.47341	837	3.47498
168	3.47342	1020	3.47538
204	3.47351	1228	3.47583
244	3.47363	1404	3.47633
293	3.47373	1760	3.47705
360	3.47396	1850	3.47736
387	3.47394	2115	3.47801
443	3.47409	2160	3.47798

Table 6.1: Measured data of the time-period of a pendulum as a function of its amplitude extracted from Smith (1964). Reproduced from Ref [2], CC BY 4.0, https://creativecommons.org/licenses/by/4.0/

time-period measurement [51]. From this fit we obtain the value of the intercept

$$T_0 = 3.473\,010(4)\,\mathrm{s}. \tag{6.3}$$

Using this value and following the analysis of Ref. [51], we can precisely infer the effective length of the pendulum to be

$$L = g\left(\frac{T_0}{2\pi}\right)^2 = 2.995\,384(6)\,\mathrm{m}. \tag{6.4}$$

In this calculation, the local value of acceleration due to gravity $g = 9.803\,93\,\mathrm{m\,s^{-2}}$ has been used [51]. The pendulum is an iron cylinder of radius 2.54 cm and height 5.08 cm and therefore a mass of approximately 1.22 kg.

Using the obtained value of the length L and mass m, the expected slope is numerically evaluated to be

$$2\pi\sqrt{\frac{L}{g}}\left(\frac{1}{16L^2} - \frac{\beta_0 m^2 g}{2N^{\alpha_0}(M_p c)^2 L}\right) = 0.0242 - 0.20\frac{\beta_0}{N^{\alpha_0}}. \tag{6.5}$$

From the linear fit of the data (Table 6.1), the slope of the line is obtained to be 0.0246 ± 0.0005 (95% confidence interval). We see that for the fit and Eq. (6.5) to be consistent, we obtain $-0.005 < \frac{\beta_0}{N^{\alpha_0}} < 0.0005$. For β_0 positive, the condition becomes

$$\beta_0 N^{-\alpha_0} < 5 \times 10^{-4}. \tag{6.6}$$

For the determination of N we assume that the nucleons form the elementary particles. Since the mass of one nucleon is 1 a.m.u $= 1.66 \times 10^{-27}$ kg, the number of nucleons in the iron cylinder is

$$\begin{aligned} N &= \frac{1.22}{1.66 \times 10^{-27}} \\ &= 7.32 \times 10^{26}. \end{aligned} \tag{6.7}$$

For this value of N, we obtain $\alpha_0 > 0.12$ for $\beta_0 = 1$. Note that the bound on α_0 is quite insensitive to the precise number of nucleons. The region excluded by Eq. (6.6) in the α_0, β_0 plane is plotted in Fig. 6.1.

Recent experiment using oscillators in the quantum regime have been used to provide bounds on β_0 under the assumption that $\alpha_0 = 0$. We argue however that any test of consequences of deformed canonical commutation relations due to quantum gravity need to account for both α_0 and β_0. So we calculate the bounds on α_0 for the value of $\beta_0 \sim 1$ that is expected from quantum gravity models [19]. The best bound on α_0 from the experiments of Ref. [4] is $\alpha_0 > -0.33$ for $\beta_0 = 1$. Similarly, from Ref. [11] we obtain $\alpha_0 > -0.25$. Note that these bounds are significantly worse than those obtained in the present work using the data from [51]. In Fig. 6.1 we present the parameter ranges that have been excluded in the α_0, β_0-plane in the three experiments discussed here.

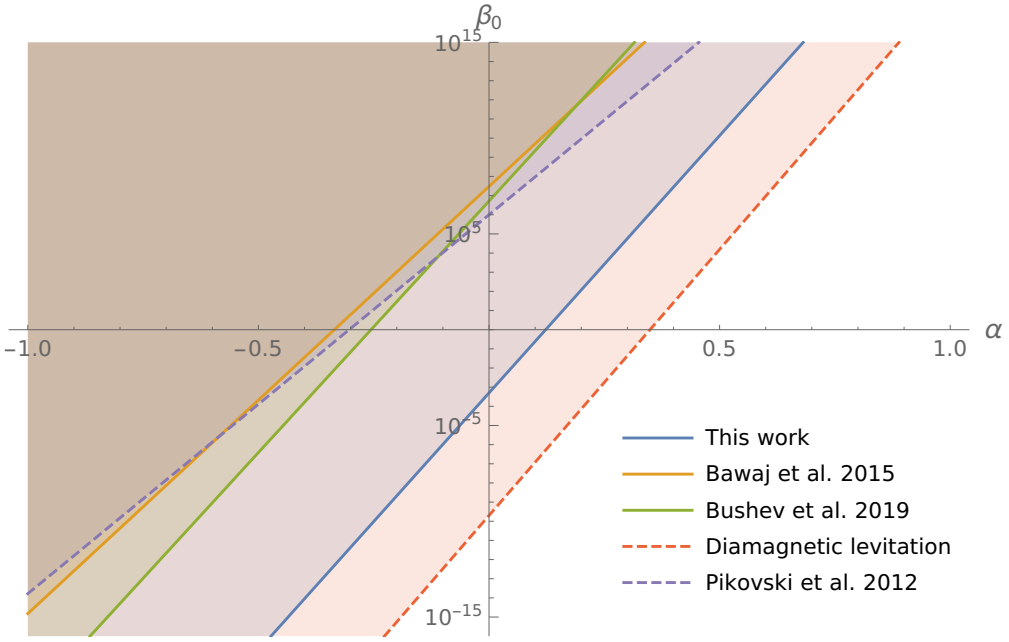

Figure 6.1: **Excluded regions of parameter space from different experiments.** Solid lines represent bounds obtained from experimental data and dashed lines represent expected bounds from proposed experiments. The shaded areas represents the region excluded by these experiments. The present work based on Smith (1964) provides the largest excluded region of parameters which, in particular, excludes the point $\beta_0 = 1, \alpha_0 = 0$, thereby showing that suppression of quantum gravity deformations should be accounted for if $\beta_0 \sim 1$ as expected from quantum gravity models. The proposal to use massive levitated diamagnetic objects promises significant improvement in bounds. A modified version of this figure is already published in Ref. [2], CC BY 4.0, https://creativecommons.org/licenses/by/4.0/

Quantum gravity suggests corrections to the canonical commutation relations that are proportional to a parameter β_0. This parameter is expected to be of order of unity if physics exhibits a minimum length of order of the Planck length but is also expected to scale as $N^{-\alpha_0}$ where N is the number of constituent particles of the test mass – a consequence of the soccer ball problem of quantum gravity. We strongly argue that any test of such physics needs to account for both parameters α_0 *and* β_0 in its analysis. We perform an analysis of several quantum regime

experiments in those terms to show that they cannot provide positive bounds on α_0 while we find that a macroscopic pendulum can provide the first positive bound on α_0 assuming $\beta_0 = 1$. This shows that the suppressions with the number of particles cannot be ignored in tests of quantum gravity and that entering the deep quantum regime is not essential for the observation of quantum gravity corrections to physical dynamics. We discuss possible advanced experimental designs and the parameter requirements to allow for entering tests in the $\alpha_0 > 1$ regime that is suggested by various models of quantum gravity.

6.2 Diamagnetic levitation for enhanced tests of quantum gravity

In order to explore how far we can possibly bound the α_0-parameter, here we propose an experiment that relies on the precise measurement of the oscillation frequency of a diamagnetic levitated particle to obtain enhanced bounds on the quantum gravity parameters.

In an experiment on a space probe, such as LISA pathfinder, one could imagine to levitate a particle in a uniform magnetic field gradient. In this case the frequency of oscillation would be [52]

$$\omega = \sqrt{\frac{1}{\rho\mu_0}\chi_V \left(\frac{dB}{dx}\right)^2} \tag{6.8}$$

where ρ is the mass density of the object, μ_0 is the vacuum permeability, χ_V is the magnetic volume susceptibility of the material and we assume a constant magnetic field gradient $\frac{dB}{dx}$. Since the oscillations can be approximated as harmonic, the change in frequency resulting from deformed commutators can be obtained from

Eq. (5.24) by identifying that $\omega = \sqrt{g/L}$. The change in frequency is therefore

$$\Delta\omega = \frac{\beta_0 m^2 \omega^3 A^2}{2N^{\alpha_0}(M_p c)^2}. \tag{6.9}$$

The oscillation frequency of levitated objects can be measured very precisely due to very low damping rates. Here we assume, optimistically, that the damping rate is the only source of error in frequency measurement. At low pressures of 266×10^{-10} Pa, the damping rate is expected to be $\gamma = 1.2 \times 10^{-7}$ Hz [53, 54]. If, in the experiment, no deviation from the expected frequency is observed, then $\Delta\omega \lesssim \gamma/\sqrt{M}$ where M is the number of measurements taken.

We calculate the bounds that one would obtain if such an experiment can be performed. We consider optimistic parameters of a gold sphere of diameter 10 cm that is levitated in a uniform magnetic field gradient of 10^3 T/m^3 that is initially displaced with an amplitude of 10 cm. The density and magnetic volume susceptibility of gold are $\rho = 19300\,\mathrm{kg/m^3}$ and $\chi_V = 3.287 \times 10^{-5}$ [55] respectively. From these parameters, we estimate that for $\beta_0 = 1$, we obtain $\alpha_0 > 0.35$ for $M = 1$, which is a much better bound than the one obtained with a pendulum in Section 6.1. The region of parameter space that can be excluded from such an experiment is shown in Fig. 6.1. This bound may be further improved by performing the experiment in space, where the pressure is about 2000 times lower which leads to a further reduction in γ.

6.3 Other experiments to bound the parameters

Experiments to place bounds on quantum gravity parameters are not restricted to the framework of measuring the change in frequency of oscillators. Here we show

that the other existing optomechanical scheme can also be used to placed stringent bounds on α_0 if an appropriate initial state is considered.

Specifically, we consider the optomechanical scheme of Refs. [3, 9] that is described in Section 2.1. To recap, in this scheme, the mechanical resonator is initially in a thermal state very close to the ground state. After interacting with the resonator, the field of the light pulse is [3]

$$\langle a_\ell \rangle \approx \xi \mathrm{e}^{-i2\lambda^2 N_p - i(4/3)\beta\hbar m\omega\lambda^4 N_p^3} \tag{6.10}$$

where ξ is the amplitude of the coherent state $|\xi\rangle$ of light, as derived in Eqs. (2.17) and (2.18). Using the experimental parameters of Ref. [3] (Table 2.1) and the error analysis detailed in Section 3.2 and assuming that experiment returns a null result, we obtain the bound $\beta_0 N^{-\alpha_0} < 10^6$ which leads to $\alpha_0 > -0.3$ for $\beta_0 = 1$. The excluded parameter range is presented in Fig. 6.1.

This bound can be improved if, instead of the ground state, the resonator is initially in a coherent state with a large enough momentum. In this case, the output field is given by

$$\langle a_\ell \rangle \approx \xi \mathrm{e}^{-i2\lambda^2 N_p - i(4/3)\beta\hbar m\omega\lambda^4 N_p^3 + i\beta\lambda^2 N_p 2\langle p\rangle^2} \tag{6.11}$$

for the initial state of the oscillator in a coherent state with mean initial momentum $\langle p \rangle$. We see that the extra term arising from a non-zero initial momentum can, in principle, be made very large by choosing a more massive oscillator. If we make the optimistic assumption that all other parameters remain the same but the mass is increased to $10^{-3}\,\mathrm{kg}$, we can achieve a a positive bound on α_0. While such a large mass is likely to reduce the optomechanical coupling it nevertheless suggests that the measurement of the phase of the output light for macroscopic systems may provide another method to obtain a good bound on the deformation parameters.

To summarise, in this chapter, we have discussed the experimental bounding of the quantum gravity parameters. Using data of measured time period of a pendulum in Ref. [51], we obtain the bound $\alpha_0 > 0.12$ in Section 6.1, which is the first positive bound on the parameter α_0 for $\beta_0 = 1$. We have also suggested experiments using levitated diamagnetic spheres in Section 6.2 and phase measurement of light in pulsed optomechanics in Section 6.3 to also obtain positive bounds on α_0 and also to possibly improve the bounds substantially. Using these experiments, we argue that we need to consider both parameters α_0 and β_0 to place reasonable bounds on the parameters. Hence, we have introduced the α_0, β_0 phase space and plotted the regions on phase space exclude by different experiments in Fig. 6.1.

Chapter 7

Summary and Outlook

7.1 Summary

To summarise this thesis, we have addressed two key challenges faced by tabletop experiments to test for deformations in canonical commutators.

First, in Ref. [1], we address the challenge of improving the accuracy and precision of cavity-optomechanical tests of quantum gravity as shown in Chapter 3. On one hand, unaccounted-for mean photon number uncertainty and quantum mechanical contributions to the phase lead to low precision (Section 3.2), while on the other, higher order terms of cavity Hamiltonian lead to low accuracy via unaccounted phase (Section 3.1). We account for the higher-order terms and develop sophisticated paths in phase-space to obtain experimentally feasible accuracy and precision (Section 3.3), and we suggest the use of squeezed light to further improve precision (Section 3.4).

Considering the quantum-noise-limited scheme, where the intensity is measured throughout the experiment, our proposed phase-space paths and rigorous analysis reduces the number of experimental runs from 10^{14} to 10^5 for the case of the γ_0 model for the same experimental parameters as in the original proposal (Sections 3.3

and 3.4). Similarly, considering the classical-noise-limited scheme, where the intensity is measured precisely at the beginning of the experiment, the required number of experimental runs reduces from 10^{16} to 10^5.

For the β_0 and μ_0 models, our suggested paths are similar to the original path (Section 3.5). However, our refined analysis can help us choose better experimental parameters. With these parameters, the required number of experimental runs decreases by three and five orders of magnitude for the β_0 and μ_0 cases respectively.

We also test the robustness of our scheme to experimental imperfections in Chapter 4, including the effects of distortion from the unitary operator on the light state (Section 4.1), imperfect implementation of the laser pulses (Section 4.2), and the imperfect preparation of the initial thermal state of the resonator (Section 4.3). In Section 4.4, we discuss the assumptions made in the calculations of Chapter 3.

By improving the accuracy and the required number of runs, and by accounting for experimental imperfections, our work opens the way for tests of quantum gravity with near-future optomechanical technology.

The second key problem that we address in Ref. [2] is the use of composite macroscopic systems to test for deformed commutators. There are four main contributions in this work. Firstly, we introduce a new phenomenological parameter, which we call α_0, to the models of deformed commutators in order to take into account the so-called soccer ball problem. The idea is to replace the quantum gravity parameter β_0 with β_0/N^{α_0} and instead of placing bounds on only β_0, one must exclude regions in a 2D plane of β_0 and α_0. This is presented in Chapter 1 and exploited in the analysis of Section 6.1. This new parameterization enables comprehensive tests of quantum gravity using composite particles. Secondly, in Section 6.1, we use the results of an old experiment that measures the time period

of a pendulum precisely to obtain more stringent bounds on the parameters β_0 and α_0 than those obtained from other experiments. To obtain the bound, we first calculate the modifications to the time period of a pendulum due to quantum gravity (Section 5.1). Third, we show that the results obtained were not only a consequence of using classical mechanics by showing the equivalence of a classical treatment using deformed Poisson brackets and a quantum treatment using deformed commutators (Section 5.2). Finally, we also discuss other possible experiments that promise even more stringent bounds in Sections 6.2 and 6.3.

These four improvements together bring rigorous and well-controlled tests of quantum gravity closer to reality.

7.2 Open problems

The open problems and potential future directions are as follows.

- As described in Section 4.4, there are numerous theoretical approximations in calculating the phase acquired by light after the optomechanical interaction in Chapter 3. These errors mainly arise from the truncation of terms in the Hamiltonian and the resulting unitary. The errors from these approximations might be small, but perhaps not negligible compared to the phase from quantum gravity. Hence, it is relevant to quantify the error from all the approximations.

- In Eq. (3.2), we have accounted for the higher order terms of the optomechanical Hamiltonian. However, this expansion is not strictly correct and to perform a more accurate estimation of the quantum gravity parameters, one

could use a more rigorous expression for the non-linearities, for example that in Ref. [40].

- In calculating the effect of the light pulses on the mechanical oscillator and phase of light in Chapter 3, we have not included the effects of dissipation. These could have a large effect on the small quantum gravity parameters, and should therefore be quantised.

- In Section 5.2, we have calculated the change in time period of a quantum harmonic oscillator under deformed commutators. To more rigorously compare with the classical calculations, time period calculations for a quantum pendulum can be performed.

- In Section 5.2, we have chosen the initial state of the pendulum to be a generalised coherent state. A more realistic initial state would be a thermal state. However, it is not clear how to define a thermal state in the presence of deformed commutators. Hence, it would also be a useful contribution to be able to consistently define a thermal state when the commutators are deformed.

- Another potential future direction to understand deformed commutators could be to connect our formalism, which is based on the Gazeau-Klauder coherent states (Section 2.3), with that of Ref. [56], which starts with a somewhat different definition of creation and annihilation operators.

- The bounds placed on the quantum gravity parameters from the old pendulum experiment in Section 6.1 does not consider the effect of dissipation on the change in frequency of a pendulum. Future experiments could measure the

amount of dissipation and include its effect on the slope and intercept of the T versus A^2 plot in order for the bounds to be more precise.

This completes the list of suggested open problems to bring tabletop tests of quantum gravity closer to reality.

Bibliography

[1] S. P. Kumar and M. B. Plenio. Quantum-optical tests of Planck-scale physics. *Phys. Rev. A*, 97(6):63855, 2018.

[2] S. P. Kumar and M. B. Plenio. On quantum gravity tests with composite particles. *Nat. Commun.*, 11(1):3900, 2020.

[3] I. Pikovski, M. R. Vanner, M. Aspelmeyer, and M. S. Kim. Probing Planck-scale physics with quantum optics. *Nat. Phys.*, 8(March):393–398, 2012.

[4] M. Bawaj, C. Biancofiore, M. Bonaldi, F. Bonfigli, A. Borrielli, G. Di Giuseppe, L. Marconi, F. Marino, R. Natali, A. Pontin, G. A. Prodi, E. Serra, D. Vitali, and F. Marin. Probing deformed commutators with macroscopic harmonic oscillators. *Nat. Commun.*, 6(May):1–7, 2015.

[5] S. Carlip. Quantum gravity: a progress report. *Reports Prog. Phys.*, 64(8):885–942, 2001.

[6] L. J. Garay. Quantum gravity and minimum length. *Int. J. Mod. Phys. A*, 10(02):145–165, 1995.

[7] G. Amelino-Camelia, J. Ellis, N. E. Mavromatos, D. V. Nanopoulos, and S. Sarkar. Tests of quantum gravity from observations of γ-ray bursts. *Nature*, 393(6687):763–765, 1998.

[8] G. Amelino-Camelia. Quantum-spacetime phenomenology. *Living Rev. Relativ.*, 16(1):5, 2013.

[9] P. Bosso, S. Das, I. Pikovski, and M. R. Vanner. Amplified transduction of Planck-scale effects using quantum optics. *Phys. Rev. A*, 96(2):23849, 2017.

[10] A. Albrecht, A. Retzker, and M. B. Plenio. Testing quantum gravity by nanodiamond interferometry with nitrogen-vacancy centers. *Phys. Rev. A*, 90:033834, 2014.

[11] P. Bushev, J. Bourhill, M. Goryachev, N. Kukharchyk, E. Ivanov, S. Galliou, M. Tobar, and S. Danilishin. Testing of Quantum Gravity With Sub-Kilogram Acoustic Resonators. 2019, arXiv:1903.03346v1.

[12] M. Maggiore. A generalized uncertainty principle in quantum gravity. *Phys. Lett. B*, 304(1-2):65–69, 1993.

[13] F. Scardigli. Generalized uncertainty principle in quantum gravity from micro-black hole gedanken experiment. *Phys. Lett. B*, 452(1-2):39–44, 1999.

[14] R. J. Adler and D. I. Santiago. On gravity and the uncertainty principle. *Mod. Phys. Lett. A*, 14(20):1371–1381, 1999.

[15] D. V. Ahluwalia. Wave-Particle duality at the Planck scale: Freezing of neutrino oscillations. *Phys. Lett. A*, 275(1-2):31–35, 2000.

[16] A. Kempf, G. Mangano, and R. B. Mann. Hilbert space representation of the minimal length uncertainty relation. *Phys. Rev. D*, 52(2):1108–1118, 1995.

[17] M. Maggiore. The algebraic structure of the generalized uncertainty principle. *Phys. Lett. B*, 319(1-3):83–86, 1993.

[18] A. F. Ali, S. Das, and E. C. Vagenas. Discreteness of space from the generalized uncertainty principle. *Phys. Lett. B*, 678(5):497–499, 2009.

[19] A. Plato, C. Hughes, and M. Kim. Gravitational effects in quantum mechanics. *Contemp. Phys.*, 57(4):477–495, 2016.

[20] C. A. Mead. Possible connection between gravitation and fundamental length. *Phys. Rev.*, 135:B849–B862, 1964.

[21] D. Amati, M. Ciafaloni, and G. Veneziano. Can spacetime be probed below the string size? *Phys. Lett. B*, 216(1):41 – 47, 1989.

[22] S. Das and E. C. Vagenas. Universality of quantum gravity corrections. *Phys. Rev. Lett.*, 101:221301, 2008.

[23] F. Marin, F. Marino, M. Bonaldi, M. Cerdonio, L. Conti, P. Falferi, R. Mezzena, A. Ortolan, G. A. Prodi, L. Taffarello, G. Vedovato, A. Vinante, and J.-P. Zendri. Gravitational bar detectors set limits to Planck-scale physics on macroscopic variables. *Nat. Phys.*, 9:71, 2012.

[24] C. Villalpando and S. K. Modak. Probing Quantum Gravity with Large Molecular Wave-packets. 2019, arXiv:1901.09696.

[25] G. Amelino-Camelia. Challenge to Macroscopic Probes of Quantum Spacetime Based on Noncommutative Geometry. *Phys. Rev. Lett.*, 111(10):101301, 2013.

[26] J. Magueijo and L. Smolin. Generalized Lorentz invariance with an invariant energy scale. *Phys. Rev. D*, 67(4):44017, 2003.

[27] G. Amelino-Camelia, L. Freidel, J. Kowalski-Glikman, and L. Smolin. Relative locality and the soccer ball problem. *Phys. Rev. D*, 84(8):87702, 2011.

[28] S. Hossenfelder. The Soccer-Ball Problem. *Symmetry, Integr. Geom. Methods Appl.*, 10:1–8, 2014.

[29] G. Amelino-Camelia. Planck-Scale Soccer-Ball Problem: A Case of Mistaken Identity. *Entropy*, 19(8):400, 2017.

[30] M. Bhattacharya, A. N. Vamivakas, and P. Barker. Levitated optomechanics: introduction. *J. Opt. Soc. Am. B*, 34(6):LO1–LO2, 2017.

[31] D. Zheng, Y. Leng, X. Kong, R. Li, Z. Wang, X. Luo, J. Zhao, C.-K. Duan, P. Huang, and J. Du. Room temperature test of wave-function collapse using a levitated micro-oscillator. 2019, arXiv:1907.06896.

[32] S. Benczik, L. N. Chang, D. Minic, N. Okamura, S. Rayyan, and T. Takeuchi. Short distance versus long distance physics: The classical limit of the minimal length uncertainty relation. *Phys. Rev. D*, 66(2):26003, 2002.

[33] K. Nozari and S. Akhshabi. Noncommutative geometry and the stability of circular orbits in a central force potential. *Chaos Soliton. Fract.*, 37(2):324–331, 2008.

[34] P. Pedram. A higher order GUP with minimal length uncertainty and maximal momentum II: Applications. *Phys. Lett. B*, 718(2):638–645, 2012.

[35] A. F. Ali, S. Das, and E. C. Vagenas. Proposal for testing quantum gravity in the lab. *Phys. Rev. D*, 84(4):44013, 2011.

[36] F. Brau. Minimal length uncertainty relation and the hydrogen atom. *J. Phys. A. Math. Gen.*, 32(44):7691–7696, 1999.

[37] F. Scardigli and R. Casadio. Gravitational tests of the generalized uncertainty principle. *Eur. Phys. J. C*, 75(9):425, 2015.

[38] M. R. Vanner, I. Pikovski, G. D. Cole, M. Kim, Č. Brukner, K. Hammerer, G. J. Milburn, and M. Aspelmeyer. Pulsed quantum optomechanics. *Proc. Natl. Acad. Sci. U. S. A.*, 108(39):16182–16187, 2011.

[39] J. P. Gazeau and J. R. Klauder. Coherent states for systems with discrete and continuous spectrum. *J. Phys. A. Math. Gen.*, 32(1):123–132, 1999.

[40] C. K. Law. Interaction between a moving mirror and radiation pressure: A hamiltonian formulation. *Phys. Rev. A*, 51:2537–2541, 1995.

[41] L. Latmiral, F. Armata, M. G. Genoni, I. Pikovski, and M. S. Kim. Probing anharmonicity of a quantum oscillator in an optomechanical cavity. *Phys. Rev. A*, 93:052306, 2016.

[42] S. Machnes. *Qlib package*. (unpublished). 2017.

[43] F. Casas, A. Murua, and M. Nadinic. Efficient computation of the zassenhaus formula. *Comput. Phys. Commun.*, 183(11):2386 – 2391, 2012.

[44] A. Wunsche. Displaced fock states and their connection to quasiprobabilities. *Quant. Semiclass. Opt. Euro. Opt. Soc. B.*, 3(6):359, 1991.

[45] H. H. Ku. Notes on the Use of Propagation of Error Formulas. *J. Res. Natl. Stand. Sec. C*, 70C(4):75–79, 1966.

[46] A. Schreiber, A. Gábris, P. P. Rohde, K. Laiho, M. Štefaňák, V. Potoček, C. Hamilton, I. Jex, and C. Silberhorn. A 2d quantum walk simulation of two-particle dynamics. *Science*, 336(6077):55–58, 2012.

[47] M. S. Kim, F. A. M. de Oliveira, and P. L. Knight. Properties of squeezed number states and squeezed thermal states. *Phys. Rev. A*, 40(5):2494–2503, 1989.

[48] K. Nozari and T. Azizi. Coherent States of Harmonic Oscillator and Generalized Uncertainty Principle. 2005, arXiv:gr-qc/0504090.

[49] L. N. Chang, D. Minic, N. Okamura, and T. Takeuchi. Exact solution of the harmonic oscillator in arbitrary dimensions with minimal length uncertainty relations. *Phys. Rev. D*, 65(12):125027, 2002.

[50] P. Pedram. Coherent States in Gravitational Quantum Mechanics. *Int. J. Mod. Phys. D*, 22(02):1350004, 2013.

[51] M. K. Smith. Precision Measurement of Period vs Amplitude for a Pendulum. *Am. J. Phys.*, 32(8):632–633, 1964.

[52] J. S. Pedernales, G. W. Morley, and M. B. Plenio. Motional Dynamical Decoupling for Matter-Wave Interferometry. 2019, arXiv:1906.00835.

[53] P. S. Epstein. On the resistance experienced by spheres in their motion through gases. *Phys. Rev.*, 23:710–733, 1924.

[54] B. R. Slezak, C. W. Lewandowski, J.-F. Hsu, and B. D'Urso. Cooling the motion of a silica microsphere in a magneto-gravitational trap in ultra-high vacuum. *New J. Phys.*, 20(6):063028, 2018.

[55] R. Dupree and C. J. Ford. Magnetic susceptibility of the noble metals around their melting points. *Phys. Rev. B*, 8:1780–1782, 1973.

[56] P. Bosso, S. Das, and R. B. Mann. Planck scale corrections to the harmonic oscillator, coherent, and squeezed states. *Phys. Rev. D*, 96(6):1–12, 2017.

Copyright notice

scopic harmonic oscillators. *Nat Commun.*, 6(1), 7503, 2015.

DOI: https://doi.org/10.1038/ncomms8503

CV was removed for data privacy protection reasons.

CV was removed for data privacy protection reasons.